URBAN FORM, URBAN HEAT ISLAND EFFECT, AND ENERGY DEMAND :INSIGHTS FROM SEOUL, SOUTH KOREA

Master Graduation Thesis Report

by Geunchan Song

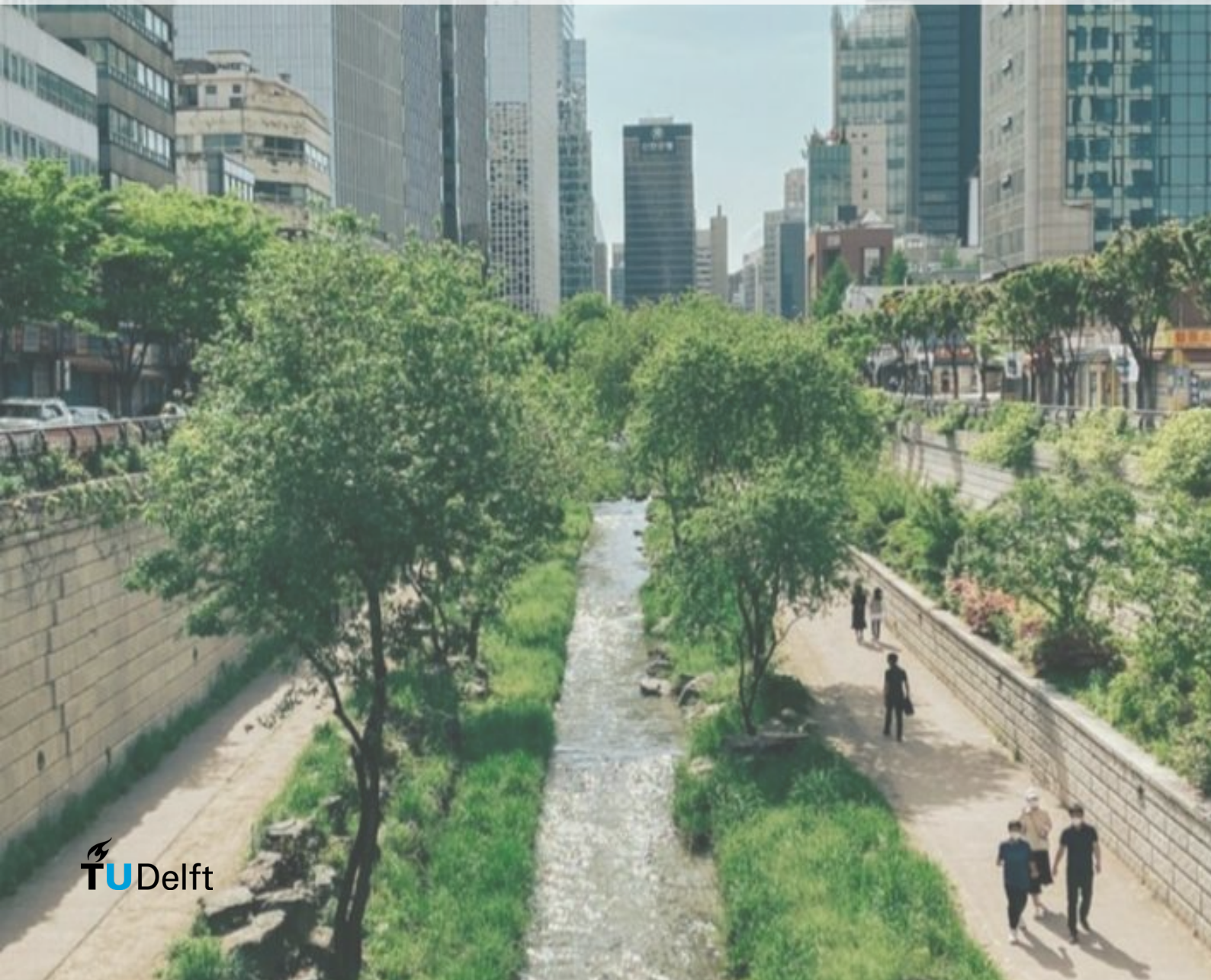

TU Delft

URBAN FORM, URBAN HEAT ISLAND EFFECT, AND ENERGY DEMAND :INSIGHTS FROM SEOUL, SOUTH KOREA

Geunchan Song
4806115

Date:
29th of October, 2025

University:
Delft University of Technology
Faculty of Architecture and the Built Environment
Building Technology

Master Graduation Thesis

1st Mentor	Martín Mosteiro Romero	Building Techonology
2nd Mentor	Azarakhsh Rafiee	Geomatics
Delegate Examiner	Marlon Boeve	Management in the Built Environment

Table of Contents

Abstract

This study investigates the relationships between urban form elements (UFEs), Urban Heat Island (UHI) effects, and building energy consumption in Heukseok-dong, Seoul, South Korea. Using 10 years of satellite imagery, air temperature measurements, and energy consumption data, the research examines how six UFEs (NDVI, building ratio, building height, building volume, FSI, and GSI) influence air temperatures and building energy consumption across multiple spatial scales and seasons.

A Multi-Layer Perceptron (MLP) neural network was developed to convert satellite-derived Land Surface Temperature (LST) to air temperature, achieving an R^2 of 0.9684 and tested with independent S-DoT sensors. The independent testing was conducted in two phases: for May-August 2020, the mean temperature difference was 1.84°C, remarkably close to the known systematic temperature difference of 1.8°C between S-DoT sensors and AWS. When extended to 2020-2024, the mean difference was 0.98°C with an R^2 of 0.807, confirming the model successfully predicts actual air temperatures rather than sensor-specific values.

The Genizi method and partial correlation analysis were combined to address multicollinearity while revealing both relative importance and directional effects of UFEs. This complementary approach provides more comprehensive insights than traditional regression methods alone. Key findings reveal that NDVI dominates temperature variance in spring (79.3%), fall (64.7%), and winter (71.6%), but building characteristics become more important in summer, with building ratio contributing 71.8% at pixel scale. Scale-dependent patterns emerged, with energy consumption best captured at 100m scale (R^2 up to 0.378) while temperature variations appeared more clearly at 300m scale (R^2 up to 0.328). The cascade relationship from UFE through air temperature to energy consumption showed air temperature driving 54.3% of electricity variance in summer, while building volume consistently influenced both electricity and gas consumption despite EUI normalization.

A decade-long analysis of District 3's transformation from 478 low-rise buildings to 28 high-rise apartments confirmed the statistical findings. Despite a 2,112.6% increase in building volume and 168% improvement in NDVI, temperature trends showed 0.10-0.16°C/year increases, which are approximately half of Heukseok-dong's 0.17-0.32°C/year rates, demonstrating that urban design can partially mitigate but not eliminate warming effects.

The moderate R^2 values (0.067-0.378) indicate that urban form elements explain only a portion of variance, partly reflecting the temporal limitation of correlating single hourly satellite observations with monthly energy totals. The research provides evidence-based recommendations for urban planning policies, including maintaining GSI below 0.55, achieving NDVI above 0.15, and implementing seasonal strategies for temperature mitigation and energy management.

Acknowledgements

I would like to express my deepest gratitude to my mentors, Martín Mosteiro Romero and Azarakhsh Rafiee, for their invaluable guidance throughout this research. I am particularly grateful to Martín for his active involvement and rich insights that shaped the direction of this work, and to Azarakhsh for her detailed methodological guidance and for suggesting me with various analytical options that strengthened the research approach.

I extend my sincere thanks to Professors Yeonsook Heo (Korea University), Yujin Park (Chung-Ang University), and Steven Jige Quan (Seoul National University) for their valuable discussions and feedback during the early stages of this project. Their expertise on Seoul's urban environment provided crucial context for this research.

Finally, I am deeply grateful to my family and friends for their unwavering support and encouragement throughout this challenging journey. Their belief in me has been a constant source of strength and motivation.

Lexicon

Air temperature	Measure of how hot or cold the air is in a specific location, typically measured with a thermometer a 1.5-2 meters above the ground.
Energy use intensity	A measurement of a building's energy efficiency calculated by dividing total energy consumption by the building's gross floor area, typically expressed in kWh/m^2 per month or year.
Floor space index	Measurement that shows the total floor area of buildings compared to the land area they sit on. Higher FSI means more densely built areas with taller or larger buildings.
Genizi method	A statistical technique that decomposes R^2 values to determine the relative importance of correlated predictor variables by properly allocating shared variance among them.
Ground space index	Ratio of building footprint area to the total land area. It shows how much of the ground is covered by buildings, with higher values indicating more densely built areas.
Land surface temperature	Temperature of the Earth's surface as measured from above (often by satellites), reflecting how hot the actual ground or roof surfaces are rather than the surrounding air.
Multi layer perceptron	Basic type of artificial neural network with multiple layers of connected nodes that can learn to recognize patterns in data and make predictions.
Normalized vegetation difference index	Measurement that uses satellite imagery to determine the amount and health of vegetation in an area. Higher values indicate more vegetation.
Partial correlation	A statistical measure that determines the strength and direction of the relationship between two variables while controlling for the effects of other variables.
Urban heat island effect	Phenomenon where urban areas are significantly warmer than surrounding rural areas due to human activities, buildings, roads, and reduced vegetation, creating "islands" of higher temperatures.

Acronyms

AT	Air temperature
AWS	Automatic weather station
DEM	Digital elevation model
EUI	Energy use intensity
FSI	Floor space index
GSI	Ground space index
LST	Land surface temperature
MLP	Multi layer perceptron
NDVI	Normalized difference vegetation index
SZA	Solar zenith angle
UFE	Urban form element
UHI	Urban heat island

01
Introduction

01 Introduction

1.1 Problem statement

In recent years, rapid urbanization and industrialization have intensified the challenges posed by global warming. As number of population in cities increases, urban areas have become significant contributors to greenhouse gas emissions while simultaneously experiencing the adverse effects of climate change. Among these effects, the **Urban Heat Island (UHI)** phenomenon becomes a critical concern for urban planners, policymakers, and researchers. The UHI effect, defined as "a phenomenon involving increased air temperature of a city compared to the surrounding rural area" (Oh et al., 2020), which exacerbates global warming by amplifying energy demands and deteriorating air quality.

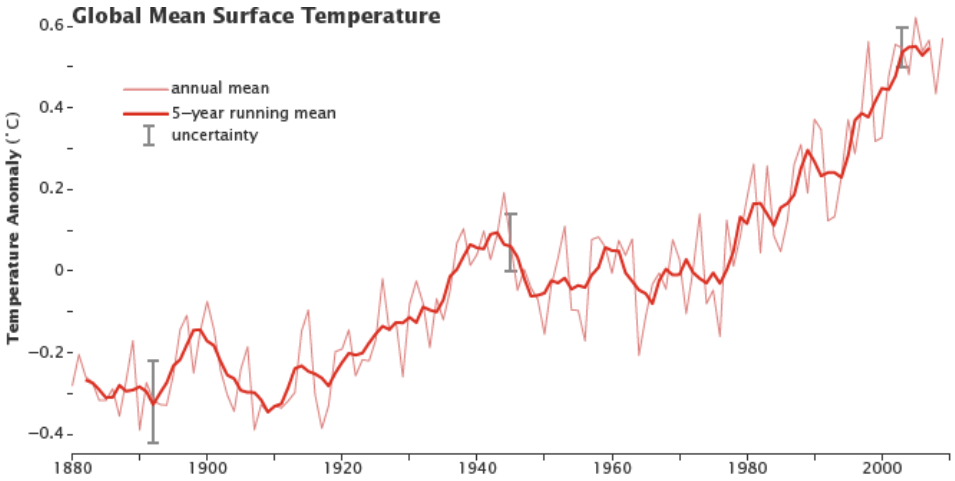

Figure 1.1 *Annual global mean surface temperature (NASA, 2020)*

The implications of the UHI effect extend beyond simple temperature increases. As urban temperatures increase, buildings require significantly more energy for cooling during summer months, leading to increased electricity consumption. Moreover, the interaction between urban form elements (UFEs) and the UHI effect is complex. While green spaces can mitigate heat through shading and evaporative cooling, the density and configuration of buildings, road networks, and other impervious surfaces contribute to heat accumulation and reduced ventilation.

Understanding these relationships becomes even more critical as big cities face pressure to accommodate growing populations. United Nations (UN) expected the world's population lives in urban areas is expected to increase by 68% by 2050, making it essential to develop evidence-based strategies that balance development needs with environmental sustainability. However, existing approaches to analyze and mitigate the UHI effect face several limitations. Most studies examined these phenomena over short time periods, failing to capture long-term urban transformations. Research typically investigated temperature-energy or urban form-energy relationships in isolation, missing the cascading effects among all three elements. Additionally, the statistical challenges posed by correlated urban variables often led to oversimplified or misleading conclusions about which factors truly drive urban temperatures and energy consumption.

Seoul, South Korea, presents an ideal case study for investigating these complex relationships. As one of the world's most densely populated cities, Seoul has experienced rapid urban development over several decades while facing increasing urban temperatures. The city's diverse urban morphology, ranging from traditional low-rise neighborhoods to modern high-rise apartments, provides a good example for examining how different UFEs influence temperature and energy patterns. Furthermore, Seoul's comprehensive data infrastructure, including weather stations, energy consumption history, and satellite coverage, enables detailed analysis of urban environmental conditions.

This research focuses on one of the districts in Seoul, Heukseok-dong, which underwent significant transformation from low-rise residential areas to high-rise developments. By analyzing the relationships between UFEs, the UHI effect, and building energy consumption over a decade, this study aims to provide quantitative evidence for sustainable urban development strategies. The research aims to address critical questions about how physical characteristics of the urban environment influence local climate conditions and energy use patterns.

1.2 Research Context and Gaps

While many studies have examined the UHI effect and building energy consumption, there are some significant gaps remain in current approaches. Most research including Liao et al. (2021) analyzes these phenomena over short periods, missing long-term urban transformations and their cumulative impacts. While Raj and Yun (2024) analyzed UHI effect in Seoul over 20 years, it only analyzed how the temperature changed but did not include energy consumption relationships and only focused on city-wide patterns. This temporal limitation is particularly problematic in rapidly developing cities where urban form can change dramatically within a decade. Studies typically examine either temperature-energy or urban form-energy relationships separately such as S. Peng et al. (2011) and Su et al. (2021)'s works, failing to capture the cascade effects among all three elements. The complex interactions between urban morphology, local climate, and energy demand remain poorly understood due to this fragmented approach.

The multicollinearity between UFEs, such as the negative correlation between vegetation coverage and building density is often inadequately addressed or simply ignored. Traditional regression approaches struggle with these correlated predictors, leading to potentially misleading results about which factors actually drive temperature and energy patterns. Many studies report simple correlations without considering the relative importance of different variables when they interact, making it difficult to prioritize urban planning interventions. Furthermore, there are limited validations with independent datasets, relying solely on the same data used for model development, which limits confidence in the generalizability of findings.

Methodological limitations extend to data collection and analysis approaches. Satellite-based studies, including this research, face temporal resolution constraints, capturing only single daily observations that miss diurnal temperature variations. While this limitation affects all satellite-based approaches, many existing studies failed to acknowledge or address this constraint in their analysis. This research explicitly recognizes this temporal limitation and addresses it by focusing on correlations at the specific satellite overpass time (11:12 AM) rather than attempting to generalize to full diurnal patterns.

Additionally, the testing with dense Seoul Data of Things (S-DoT) sensor networks and the decade-long analysis partially compensates for the temporal resolution constraints by providing spatial density and long-term trends that snapshot studies miss. Ground-based studies, while offering better temporal resolution, often suffer from sparse spatial coverage that cannot capture urban microclimate variations. The scale at which analysis is conducted varies widely across studies, with little understanding of how relationships between urban form, temperature, and energy might differ across spatial scales. Additionally, most research focused on modern buildings with comprehensive HVAC systems, overlooking the significant portion of urban building stock consisting of older residential structures that may have different building characteristics.

These limitations highlight the need for an integrated, long-term approach that can handle complex statistical relationships while providing practical insights for urban planning. A comprehensive understanding requires analyzing the cascade effects from urban form through temperature to energy consumption, employing methods that can properly account for multicollinearity while revealing both the importance and direction of relationships. Long-term analysis capturing actual urban transformations, rather than static snapshots, is essential for understanding how development patterns influence environmental outcomes. This research addresses these gaps by examining a decade of data from Heukseok-dong, employing complementary statistical methods, and validating findings through both independent sensor networks and real-world urban redevelopment outcomes.

1.3 Research Questions

This research examines the complicated nonlinear relationships between the urban form elements (UFEs), urban heat island (UHI) effects, and building energy consumption in one of the areas in Seoul, South Korea. The research aims to understand how changes in urban form elements affect local microclimate and influence energy consumption patterns. Through analysis of satellite imagery, air temperature measurements, and energy consumption data over 10 years, this research would answer the following main research question and sub-questions.

Main Research Question	**"How do urban form elements influence the Urban Heat Island (UHI) effect and building energy performance in a selected area of Seoul, South Korea?"**

The main research question examines the complex non-linear relationships between physical urban characteristics, local air temperature patterns, and energy consumption, providing insights for sustainable urban development for urbanized cities like Seoul.

Sub-question 1	**"How can land surface temperature (LST) from satellite imagery be converted to air temperature for urban climate analysis?"**

The 1st sub-question addresses the methodological challenge of using satellite data for urban temperature monitoring. By developing and testing a conversion of LST to air temperature, the research enables UHI analysis in cities with limited ground-based monitoring infrastructure.

Sub-question 2	**"How have urban form elements (UFEs) changed over the past decade, and what impact have these changes had on the UHI effect?"**

The sub-question 2 examines the temporal analysis on UFE and effects on air temperature. By analyzing a decade of data, the research captures how actual urban transformations influence air temperature patterns over time.

Sub-question 3	**"How do urban form elements affect air temperature, and how does this relationship influence energy consumption across different seasons and spatial scales?"**

This sub-question investigates the cascade effects from UFEs through air temperature to energy consumption. By examining both electricity and gas consumption separately across seasons and multiple spatial scales, the research reveals how these relationships vary temporally and spatially, providing potential guidance for energy management strategies.

Sub-question 4	**"How does combining the Genizi method with Partial correlation improve understanding of relationships between UFEs, air temperature, and energy consumption?"**

The last sub-question addresses the statistical challenge of multicollinearity in urban studies. By employing complementary analytical methods, this research separates relative importance from directional effects, providing more accurate insights than traditional regression approaches alone.

By answering these main research question and sub-questions, the research would provide a comprehensive understanding of urban heat island effects in Heukseok-dong, which can guide more climate responsive and energy efficient during urban development in dense urban environments.

02
Literature Review

02 Literature Review

2.1 Introduction

2.1.1 Literature Search

Multiple electronic research databases such as Scopus and TU Delft Research Portal were used to conduct a comprehensive literature search. Some main keywords were used for searching the literature such as "Urban heat island", "Building", "Urban element" and "Energy demand". These keywords were combined for advanced search in Scopus and TU Delft Research Portal along with a few synonyms for each keyword using appropriate Boolean operators (e.g., OR, AND).

2.1.2 Quality of Literature

To ensure the quality and validity of the literature, some modifications to the query were added and the search plan has been filtered. Urban heat island phenomenon has been actively researching from the last several decades ago. The quality of the literature was ensured with the number of reviews (peer-review) and citation numbers. Literature was excluded if they were review papers, editorials, or conference proceedings and only limited to final articles (publication stage), which were legally published by trustworthy sources.

2.2 Urban Heat Island (UHI) Effect

2.2.1 Definition and Fundamental Concepts

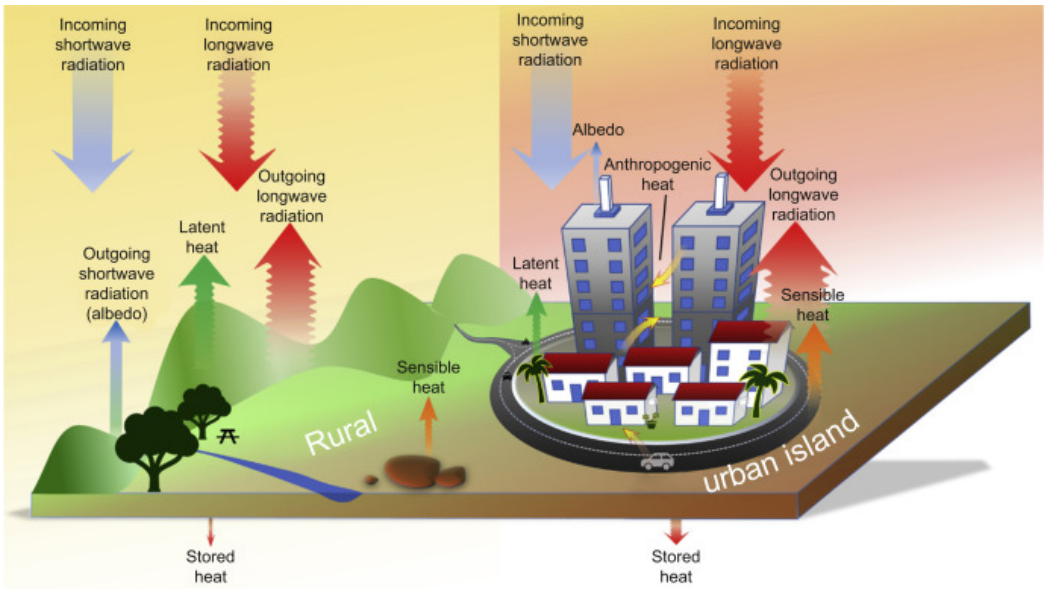

Figure 2.1 *Urban heat island effect by Jamei and Tapper (2018)*

The Urban Heat Island (UHI) effect is one of the most studied phenomena in urban climatology, defined as "a phenomenon involving increased air temperature of a city compared to the surrounding rural area" (Oh et al., 2020). UHI is fundamentally a heat accumulation phenomenon within urban areas resulting from urban construction and human activities, and the conversion of pervious surfaces to impervious surfaces significantly modifies local energy balance in urban areas and contributes to urban heat island formation, mainly in densely developed cities (Vujovic et al., 2021).

Multiple factors influence UHI intensity and characteristics. City size and morphology play crucial roles, with UHI being a major anthropogenic alteration on Earth's environments, and its geospatial pattern remains poorly understood over large areas (Zhou et al., 2014). The physical mechanisms underlying UHI formation were comprehensively explained by Oke (1982). The UHI phenomenon results from various interacting mechanisms, including modified surface properties where impervious surfaces replace natural surfaces, reduced evapotranspiration due to decreased vegetation coverage, anthropogenic heat emissions from vehicles and buildings, and urban geometry effects that trap heat radiation and reduce wind flow. The UHI index varies across cities due to different development levels and climatic conditions. A summary of studies on UHI in different cities in China is given in a review paper by Tian et al. (2021), which demonstrates the complexity of factors influencing the UHI phenomenon.

The global significance of UHI continues to grow with accelerating urbanization. Santamouris (2015) analyzed UHI effect in 101 Asian and Australian cities, indicating widespread prevalence across different climates. Of particular concern are synergies between UHI and climate change, and UHI and global warming increase significantly the ambient temperature (Santamouris et al., 2014). Higher temperatures have a serious impact on electricity consumption of the building sector, which increases considerably the peak and the total electricity demand.

This fundamental understanding of UHI mechanisms and characteristics provides the essential foundation for examining its relationships with urban form elements and building energy consumption, particularly in the context of one of the most urbanized cities, like Seoul.

2.2.2 UHI Measurement and Assessment Methods

Measuring the UHI effect requires two main approaches: Ground-based methods that measure air temperature and Satellite methods that measure surface temperature. Each method has its own strengths and limitations for understanding how cities become warmer than their surroundings.

Ground-Based Air Temperature Measurement

The most direct way to measure UHI is through weather stations that record air temperature at standard heights. According to the EPA guidelines, air temperatures important for assessing heat islands are those found within the urban canopy, from ground level to the tops of trees and buildings (Measuring Heat Islands | US EPA, 2025). These types of measurements represent the best that people actually experience. Traditional weather stations measure temperature at 1.5-2 meters height using shielded sensors, following World Meteorological Organization standards. However, weather stations have limited spatial coverage, which may miss important temperature variations across urban areas.

To address this limitation, researchers use mobile measurement where vehicles equipped with sensors traverse urban areas, recording temperatures. Stewart et al. (2021) reviewed various mobile traverse studies and found they effectively capture spatial temperature patterns, though they are limited to specific time periods. Another solution is adding low-cost weather sensors. Schatz and Kucharik (2015) installed 150 temperature and humidity sensors at 3.5 meters height on streetlights and utility poles in Madison to capture fine-scale temperature variations.

Muller et al. (2013) reviewed urban meteorological networks and found that highlighted the need for standardized approaches and better documentation of network characteristics. The selection of appropriate weather stations is critical to ensure temperature differences reflect urbanization effects rather than geographic factors.

Satellite-Based Land Surface Temperature Measurement

Satellites provide a very high spatial coverage of urban temperatures by measuring thermal radiation from surfaces compared to weather stations. Voogt and Oke (2003) confirmed that thermal remote sensing has been used for a few decades to assess the UHI, to perform land cover classifications, and as input for models of urban surface atmosphere exchange.

Different satellites offer various advantages for UHI studies. Landsat provides 30-100m thermal resolution every 16 days, suitable for detailed spatial analysis, while MODIS offers daily coverage at 1km resolution, which is better for temporal studies. As reported by Zhou et al. (2014), MODIS data effectively analyzed surface urban heat island (SUHI) across major Chinese cities.

Processing satellite thermal data requires several corrections. Atmospheric effects must be removed using radiative transfer models. Surface emissivity varies with material type, and without proper corrections, temperature error can exceed 2-3°C (Sobrino et al., 2004).

Key Measurement Challenges

Both methods face important challenges. For ground weather stations, main issues include ensuring spatial coverage across the areas, avoiding microclimate effects from nearby heat sources or shading, and maintaining consistent measurement protocols. On the other hand, satellite measurements face different challenges. Urban surfaces create complex 3D structures that affect thermal observations. As Voogt and Oke (2003) noted, viewing geometry significantly affects observed temperatures. Satellites primarily observe horizontal surfaces from above, missing vertical surfaces like walls that contribute to the complete urban thermal environment.

Stewart et al. (2021) highlighted that the diurnal cycles of atmospheric UHI are well known based on years of continuous measurements in cities, but it cannot be measured continuously or in situ. This fundamental difference between surface and atmospheric measurements creates challenges for integrated UHI assessment.

Despite these challenges, combining ground and satellite measurements provides the most comprehensive UHI assessment. Ground weather stations offer accurate point measurements, while satellites reveal spatial patterns across entire cities. This relationship between surface and air temperatures measured by different methods varies with surface properties, weather conditions, and time of the day, and combining these 2 methods would provide a comprehensive UHI assessment.

2.3 Land Surface Temperature (LST) vs Air Temperature

2.3.1 Fundamental Differences

Definitions and Measurements

Land surface temperature (LST) is the radiative skin temperature of the uppermost layer Earth's surface (Li et al., 2013). LST represents how hot the surface of the Earth would feel to touch in a particular location, which is usually measured remotely by satellites detecting thermal infrared radiation emitted by surfaces. Air temperature, in contrast, is the temperature of air at a specific height above the surface. Meteorological standards specify measurement at 1.5-2 meters height using thermometers sheltered from direct radiation. Most global temperature analyses are based on station air temperatures, which represent the atmospheric conditions humans directly experience (Mildrexler et al., 2011).

The fundamental distinction between LST and air temperature lies in their physical nature and behavior. The analysis of 17 years of satellite data notes that the relationship between satellite LST and ground-based observations of 2m air temperature (T2m) is characterized in space and time (Good et al., 2017). The study found that LST and air temperatures can differ by 10-20°C during daytime, particularly over dry surfaces.

Recent research by Naserikia et al. (2023) found that LST and air temperature have distinct spatiotemporal characteristics, and their relationship differs by season, ecological infrastructure, and building morphology. They mentioned that greater seasonal variability in LST compared to air temperature, along with more pronounced intra-urban spatial variability in LST.

2.3.2 Importance for Building Energy Analysis

While LST serves specific purposes in environmental monitoring by providing critical information on evapotranspiration (Li et al., 2013), air temperature, however, remains the standard for assessing human exposure and comfort.

Air temperature represents the fundamental driver of building energy consumption, particularly for heating and cooling demands. Building HVAC systems operate based on air temperature measurements. Thermostats monitor indoor air temperature and modulate heating or cooling output to maintain setpoint temperatures. The control logic responds to the temperature differential between indoor and outdoor air, not LST, as mentioned that "the indoor-outdoor temperature difference determines the load demands" by Xiong et al. (2023).

The empirical evidence by Su et al. (2021) strongly supports the primacy of air temperature in energy consumption. The paper confirmed that "outdoor air temperature shows strong positive correlations with cooling energy consumption". This correlation reflects the direct physical relationship where higher outdoor air temperatures increase cooling loads through conductive heat gain, increased ventilation loads, and greater infiltration heat gains. Similarly, lower air temperatures drive heating energy consumption through these same mechanisms operating in reverse.

Human comfort is highly related to building energy consumption. All standard thermal comfort indices, including Predicted Mean Vote (PMV) and Physiological Equivalent Temperature (PET), rely on air temperature measurements rather than surface temperature (Peng & Huang, 2022). Another work by Schultz and Svendsen (1998) also concluded that the thermal comfort assessment requires air temperature as a primary input parameter.

2.3.3 LST to Air Temperature Conversion Methods

Converting satellite-derived LST to air temperature has become a critical methodology in urban climate research due to fundamental differences in spatial data availability. Ground-based weather stations, while providing accurate point measurements, typically offer sparse spatial coverage in urban areas, often one station per several square kilometers. This spatial limitation makes it challenging to capture the fine-scale temperature variations essential for understanding urban heat island effects and their relationships with UFEs at the building or neighborhood scale.

Satellite thermal imagery offers complete spatial coverage at resolutions of 30-100m, providing temperature information for every pixel across entire cities. However, satellites measure surface temperature rather than air temperature, necessitating conversion methods to obtain the air temperature values required for building energy analysis and human comfort assessment. This conversion enables researchers to leverage the spatial completeness of satellite data while maintaining relevance to energy consumption patterns and urban planning applications.

The following review examines various LST to air temperature conversion methods that have been developed to bridge this gap between spatial coverage and measurement type, evaluating their performance and suitability for urban climate applications.

Linear and Statistical Methods

The most fundamental approach involves simple linear regression between LST and air temperature. Meyer et al. (2016) compared simple linear regression with machine learning algorithms for air temperature prediction in Antarctica using MODIS LST satellite data. Their linear regression model achieved an average R^2 of 0.78 and RMSE of 5.83°C, which demonstrates that simple approaches can also provide high R^2 values.

Multiple linear regression (MLR) incorporates additional predictor variables beyond LST to improve accuracy. Noi et al. (2017) employed MLR with MODIS LST data along with elevation and Julian day as auxiliary variables in mountainous regions of Northwest Vietnam. The results showed very high accuracy with R^2 values exceeding 0.93 for maximum temperature, 0.80 for minimum temperature, and 0.89 for mean temperature, with RMSE values around 1.5-2.0°C. This suggests that when auxiliary data was included, especially in distinctive areas, the improvements were substantial.

Chen et al. (2016) developed an enhanced empirical regression method that incorporated multiple predictors, including nighttime light data, LST, normalized difference vegetation index (NDVI), impervious surface area, albedo, elevation, and daylight duration. Their approach achieved satisfactory results with 98% of stations showing errors within ±2.5K, demonstrating the value of including diverse environmental variables.

Tree-based Approaches

Random Forest (RF) has emerged as a powerful method for air temperature estimation, which is one of the most common methods to convert LST to air temperature in recent studies. Tang et al. (2021) used RF to create temperature maps by building multiple decision trees using predictors (LST, NDVI, elevation) and aggregating their result. It achieved R^2 values between 0.96-0.98 with RMSE of 1.48-2.55°C.

Although the RF algorithm has a great ability to handle non-linear relationships and multiple variables, making it particularly suitable for complex urban environments, the paper noted an important limitation. RF can create artificial spatial patterns due to its tree-based structure, which may be problematic for continuous temperature mapping. Also, RF significantly understimates temperature extremes and struggles to recover finer scale spatial resolution. The author suggests that standard RF implementations miss important spatial context necessary for realistic temperature mapping, making it less suitable than other nethods like neural neworks.

Geostatistical Methods

Regression Kriging (RK) combines regression analysis with spatial interpolation. It applies regression to establish relationships between temperature and axuilary variables, which kriging to spatially interpolate based on their spatial structure. Ding et al. (2023) used regression kriging to analyze urban air temperature in Guangzhou city, China based on the weather stations. The final temperature map combines the regression-based trend surface with kriged residual surface, leveraging both the explanatory power of environmental covariates and the spatial dependence of temperature fields. Although the result show high R^2 of 0.95 with RMSE 0.92°C, the author mentioned that RK assumes linear relationships in trend, while temperature analysis have beyond non-lienar complicated relationships, which not be feasible to analyze the detail relationships.

Neural Network Methods

Muli-Layer Perceptron (MLP) neural networks have shown superior performance for air temperature estimation, particularly in challenging conditions. The Temperature Estimation with ML and Land Input (TEMLI) framework by Salih et al. (2025) mentioned that "Among the models tested within the TEMLI framework, the Multilayer Perceptron (MLP) demonstrated superior performance", by achieving R^2 of 0.91 and RMSE of 1.5°C. Apart from MLP, Choi et al. (2021) used Artificial Neural Networks (ANN) and achieved high accuracy with R^2 of 0.98 and RMSE of 2.19°C. However, they noted that model performance is highly dependent on input variables and network architecture.

The advantages of MLP for air temperature estimation are particularly relevant for complex urban environments. Unlike linear methods that assume constant relationships, MLP can capture the non-linear relationships between LST and air temperature that vary with surface types, time of day, and weather conditions. The ability to integrate multiple input variables simultaneously is another key strength. As Noi et al. (2017) demonstrated, MLP can effectively combine LST with auxiliary variables like NDVI, elevation, and solar angles to create comprehensive air temperature maps. Combining with multiple variables is crucial as air temperature in urban areas is highly influenced by numerous factors beyond surface temperature.

MLP also excels in maintaining spatial continuity, which is essential for urban climate applications. While Random Forest methods can achieve high point accuracy, they often create artificial spatial patterns or boundaries in temperature maps due to their tree-based structure. In contrast, MLP learns the underlying physical relationships between variables and produces smooth, continuous temperature surfaces that better represent the gradual transitions observed in real urban thermal environments. This spatial continuity is particularly important for building energy analysis, where temperature gradients between neighborhoods affect heating and cooling demands.

Comparative Performance

Category	Method	Study	R^2	RMSE (°C & K)	Key Advantage	Limitations
Statistical method	Linear Regression	*Meyer et al. (2016)*	0.78	5.83	Simple interpretable	Cannot handle nonlinear relationships
	Multiple Linear Regression	*Noi et al. (2017)*	0.93/0.80/0.89	1.5/2.0/1.6	Good baseline performance	Limited in spatial variations
Geostatistical method	Regression Kriging	*Ding et al. (2023)*	0.95	0.92	Smooth air temperature variation	Assumes linear relationships in trend
Tree-based methods	Random Forest	*Tang et al. (2021)*	0.96-0.98	1.48-2.55	Handles multiple variables	Creates artificial spatial patterns
Neural Network	MLP (TEMLI)	*Salih et al. (2025)*	0.91	1.5	Superior in extreme conditions	Requires substantial training data
	Artificial Neural Network (ANN)	*Choi et al. (2021)*	0.98	2.19	Capture complex relationships	Highly dependent on input variables

Table 2.1 *Comparative performance of methodologies to obtain air temperature*

Study	Application Purpose
Meyer et al. (2016)	Antarctic climate monitoring - General temperature distribution mapping for climate science, not urban or energy-specific applications
Noi et al. (2017)	Agricultural and environmental monitoring in Vietnam - Temperature mapping for vegetation phenology and agricultural planning, not urban heat island or energy analysis
Ding et al. (2023)	Urban climate adaptation - Specifically for urban heat mitigation strategies and climate-responsive urban planning in Guangzhou
Tang et al. (2021)	General temperature downscaling - Improving spatial resolution of temperature data for various applications, tested on mixed land cover types
Salih et al. (2025)	Climate monitoring across Morocco - Country-wide temperature estimation for climate assessment, including but not limited to urban areas
Choi et al. (2021)	Korean Peninsula weather forecasting - Operational weather prediction and monitoring, general purpose temperature retrieval

Table 2.2 *Air Temperature application purpose*

The application context significantly influences the suitability of each LST to air temperature conversion method. Studies focused on general climate monitoring or agricultural applications (Meyer et al., 2016; Noi et al., 2017) may tolerate different error patterns than those specifically targeting urban energy analysis. For instance, methods optimized for capturing spatial temperature patterns for agricultural planning may not adequately represent the peaked midday temperatures critical for cooling energy demand estimation.

Among the reviewed methods, the MLP approach (Salih et al., 2025) demonstrates particular advantages for urban applications despite being developed for country-wide climate monitoring in Morocco. The TEMLI framework's MLP architecture showed superior performance in handling extreme temperature conditions and complex terrain, which are analogous to the heterogeneous urban environment with varying building heights, materials, and land cover types found in Seoul. Importantly, MLP's ability to capture non-linear relationships between multiple input variables (LST, NDVI, elevation, solar angle) makes it well-suited for urban areas where temperature is influenced by numerous interacting factors. While Salih et al. (2025) applied this method across diverse Moroccan landscapes, the model's proven capability in areas with built environments and its high accuracy (R^2= 0.91) suggest strong transferability to dense urban contexts like Heukseok-dong.

Only Ding et al. (2023) specifically addressed urban applications, though their focus was on climate adaptation rather than energy consumption. This highlights a gap in the literature where most LST to air temperature conversion studies have not been specifically validated for building energy applications, which require accurate representation of temperature conditions during peak cooling and heating hours. The selection of MLP for this research addresses this gap by applying a method with proven non-linear modeling capabilities to the specific challenge of urban energy analysis.

Temperature Conversion Method Selection Considerations

The choice of conversion method depends critically on the specific application, available resources, and the trade-offs researchers are willing to accept. For building energy studies, ideally the method would capture temperature variations at both temporal and spatial scales. However, current data sources force a fundamental trade-off: ground-based stations provide excellent temporal resolution (hourly or sub-hourly) but sparse spatial coverage, while satellite data offers complete spatial coverage but is limited to snapshot observations at fixed overpass times.

Researchers using satellite-based methods, including this study, must acknowledge that they prioritize spatial completeness over temporal resolution. This means capturing temperature patterns across entire urban areas at building-level detail, but only at specific moments in time (11:12 AM for Landsat in Seoul). This temporal limitation is significant for energy analysis since building energy consumption varies throughout the day following occupancy patterns and diurnal temperature cycles. However, for studies examining spatial relationships between urban form and environmental conditions, or requiring temperature data for every building in a district, the spatial completeness of satellite data becomes essential despite its temporal constraints.

While simple regression might suffice when only LST data exists, the inclusion of auxiliary variables like vegetation indices, solar zenith angle, and elevation data significantly improves accuracy regardless of method choice. Computational resources also matter, particularly for operational systems that need to process daily satellite imagery across entire cities. The method must handle data gaps from cloud coverage while maintaining spatial and temporal consistency.

For urban heat island studies focusing on building energy impacts, MLP neural networks offer the optimal balance of accuracy, computational efficiency, and physical realism. The method's ability to learn complex non-linear relationships while producing spatially continuous temperature fields makes it particularly suitable for heterogeneous urban environments like Seoul. The seasonal variations and diverse urban forms in Seoul can create challenging conditions where temperature relationships vary significantly across space and time. Conditions where MLP's adaptive learning capabilities provide clear advantages over traditional statistical methods. This superiority in handling urban complexity, combined with proven performance metrics from recent studies, provides strong justification for adopting neural network approaches for converting satellite LST to air temperature in urban energy analysis applications, despite the inherent temporal limitations of satellite-based data.

2.3.4 Satellite Data for Temperature Estimation

Multiple satellite platforms provide thermal data for LST acquisition, each offering different trade-offs between spatial resolution, temporal frequency, and data availability. The selection of appropriate satellite data is crucial for UHI studies and temperature mapping.

Satellite	Exclusive Use		Combination	
	No. of Papers	%	No. of Papers	%
Landsat	317	54.75	396	68.39
MODIS	103	17.79	185	31.95
ASTER	15	2.59	36	6.22
NOAA/AVHRR	1	0.17	7	1.21
METEOSAT	-	-	3	0.52

Table 2.3 *Most used satellites/sensors to obtain LST data (De Almeida et al., 2021)*

De Almeida et al. (2021) reviewed the different platforms of remote sensing techniques (satellites) and summarized the use of each satellite platform. Landsat remains the most widely used platform for LST studies, with 54.75% of papers exclusively using Landsat data, while MODIS accounts for 17.79% of exclusive use. The combination of multiple sensors is less common, with only 7% of studies using Landsat with AVHRR and 3% using METEOSAT.

Satellite	Spatial Resolution	Temporal Resolution	Spectral Bands	Years of Operation
Landsat	30m	16 days	11 bands (2 thermal)	2013 - present
MODIS	1000m	Daily	36 bands (16 thermal)	1999 - present
ASTER	90m	16 days	14 bands (5 thermal)	1999 - present
Sentinel-3	1000m	2 days	11 bands (3 thermal)	2016 - present
ECOSTRESS	70m	5 days	6 bands (5 thermal)	2018 - present

Table 2.4 *Satellites' spatial, temporal resolution, spectral bands and years of operation*

Table 2.4 shows a comprehensive overview of commonly used satellite platforms with spatial/temporal resolution, spectral bands, and years of operations. **Landsat** has provided the longest continuous record of thermal observation (Landsat 4), and since 2013, Landsat 8 accessories the Thermal Infrared Sensor (TIRS) with 2 thermal bands. The thermal resolution is resampled to 30m, which provides sufficient detail for UHI studies. The 30m optical bands enable precise land cover classification to support emissivity estimation and urban form analysis. The 16-day revisit cycle, while limiting for some applications, provides consistent seasonal coverage. **MODIS** has been providing satellite imagery since 1999, which was designed for global environmental monitoring. It provides a very high temporal resolution with daily coverage and extensive spectral information with 36 bands. However, its 1000m spatial coverage limits its application in urban environments where temperature can vary significantly over short distances, especially in urban areas. **AESTER** was also launched in 1999, with 5 thermal bands at 90m resolution. It can provide detailed thermal information than most sensors through 14 total spectral bands. However, similar to Landsat, the 16-day revisit cycle has a limited acquisition schedule, making it challenging to obtain consistent time series data. **Sentinel-3**

and **ECOSTRESS** were launched in recent years, with higher temporal resolution of 2-day revisit and 5-day revisit. However, Sentinel provides 1000m spatial resolution, which is insufficient for detailed urban analysis where the areas of the building level variations are important. Although ECOSTRESS provides 70m of spatial resolution and high temporal resolution, there are limitations for historical archives for long-term studies.

For this research investigating Seoul's urban heat island effects on building energy consumption over a 10-year period, careful consideration of available platforms led to selecting Landsat as the primary data source. The 30m resolution effectively captures Seoul's urban morphology, distinguishing between high-rise residential complexes, commercial districts, and green spaces that influence local temperature patterns. The complete temporal coverage from 2013-2024 enables robust analysis of urban development impacts. Established processing methods, particularly the mono-window algorithm, validated for East Asian urban environments, ensure reliable LST retrieval. Most importantly, the extensive scientific validation of Landsat for urban heat island studies provides confidence in the results and enables comparison with the broader literature.

2.3.5 Limitations of Using Satellite Data

A fundamental limitation of using Landsat is its temporal resolution as it captures only 1-2 images per month at a fixed time of day, which can not represent the full diurnal temperature cycle. Li et al. (2022) acknowledged that single daily observations miss critical temperature extremes and diurnal variations essential for energy analysis. To address this limitation, some studies combined multiple satellite platforms. Weng et al. (2014) used MODIS's four daily observations to model diurnal temperature cycles and applied patterns to enhance Landsat's temporal resolution.

Zhou et al. (2014) noted in their analysis of Surface Urban Heat Island (SUHI) in Chinese cities that Landsat's temporal sampling 'represents a snapshot rather than a comprehensive thermal characterization,' but proceeded with analysis using only available images because their focus was on spatial patterns of SUHI intensity across cities. Similarly, Imhoff et al. (2009) acknowledged that MODIS captured only four moments in the diurnal cycle, potentially missing peak temperatures, yet concluded this was acceptable for their comparative UHI mapping objectives.

However, many studies have simply acknowledged these temporal limitations without attempting to overcome them. This research similarly accepts the temporal constraints of satellite data while focusing on spatial relationships between urban form, temperature, and energy consumption at the satellite overpass time. Rather than attempting to model full diurnal cycles, this study examines how urban form elements correlate with both temperature and energy consumption patterns specifically at 11:12 AM, acknowledging that this represents only one point in the daily energy consumption cycle.

2.4 Urban Form Elements (UFE) and Measurement

2.4.1 Urban Form Elements

Urban form elements (UFE) quantify the physical characteristics of cities that influence thermal behavior and energy consumption. One of the commonly mentioned UFEs in city studies is are Ground Space Index (GSI) and the Floor Space Index (FSI). GSI represents the ratio of building footprint to total land area, while FSI, also known as Floor Area Ratio (FAR), measures the total floor area relative to plot area, and these indicators provide essential metrics for understanding urban density patterns (Pont & Haupt, 2023). Building height and building footprints represent the 3-dimensional urban structure, while building volume provides a comprehensive measure of built mass that affects heat storage and shadow patterns.

Vegetation indicators play a crucial role in UHI studies. The Normalized Difference Vegetation Index (NDVI) is one of the most widely used metrics, which is calculated from red and near-infrared satellite bands to quantify vegetation abundance with values ranging from -1 to 1, with higher values indicating denser vegetation. S. Peng et al. (2011) evaluated that NDVI shows strong negative correlations with surface temperature, with correlation typically running from -0.4 to -0.7 in urban areas.

Liao et al. (2021) examined the spatial heterogeneity in London and Seoul with 10 UFEs, including canyon H/W ratio, building height, building ratio, street width, green space ratio, and analyzed the relative importance of variables on LST using Partial Correlation and Genizi Method. While their methodological approach was comprehensive, their analysis was limited to only four days of data, specifically two summer and two winter days, and focused solely on LST rather than air temperature.

This research builds upon Liao et al.'s methodological framework while addressing several of their limitations. Rather than analyzing isolated days, this study examines multiple satellite images across a full decade from 2015 to 2024, enabling the detection of long-term trends and actual urban transformations. The analysis converts LST to air temperature, providing more direct relevance to building energy consumption patterns. Additionally, this research investigates relationships across multiple spatial scales including pixel level, 100m buffers, and 300m buffers to understand how urban form effects vary with scale. The seasonal analysis incorporates multiple images per season across ten years rather than single representative days, providing more robust seasonal patterns. Most importantly, this study extends beyond temperature analysis alone to examine the complete cascade relationship from urban form through temperature to actual building energy consumption data, offering practical insights for urban planning and energy management strategies.

2.4.2 Scale of Analysis

Diverse spatial scales are used for understanding the relationship between UFE and temperature patterns in UHI studies. Buffer analysis is generally useful to study the influence area of spatial entities on their surroundings (Na et al., 2024). Many papers have employed various buffer distances to capture the temperature effects of urban green spaces and other UFEs. Dong et al. (2020) examined 100 m buffer zones to evaluate cooling effects from the green roof installation in Xiamen Island, which effectively captured immediate surroundings and local microclimate effects. The 100 m is also called as "characteristic cooling buffer zone", making it particularly valuable for analyzing building-level energy consumption patterns.

At larger scales, different buffer ranges affect the LST-distance fitting results of urban parks, and Cai et al. (2023) confirmed that a 300 m buffer zone is the optimal fitting interval for understanding neighborhood-level thermal dynamics. The cooling radiation range of urban green space (UGS) on the UHI effect is 300 m, and the cooling effect is most effective from 0 to 200 m (Na et al., 2024; Bhattarai et al., 2025). These findings support the use of both 100m and 300m buffer zones as they can capture different scales of urban thermal dynamics, where the 100m buffer can reveal immediate building-environment relationships for energy analysis, while the 300m buffer reveals neighborhood effects for understanding broader temperature patterns.

2.5 Building Energy Consumption

2.5.1 Energy Consumption Patterns

Residential energy consumption shows distinct seasonal patterns, which are driven by space conditioning and ambient temperature. M. Li et al. (2018) found that the household daily electrical consumption varies significantly between months, with mean electrical load, peak load, load factor, and timing of peak load all exhibiting significant monthly variations. In the summer season, average electricity consumption increases by around 5-7% for each degree Celsius increase in ambient temperature, while winter shows a similar magnitude of increase in gas consumption for each degree decrease in temperature (Fikru & Gautier, 2015). The temperature sensitivity varies significantly based on building uses, with energy-efficient buildings showing 40-50% less sensitivity to weather variations compared to conventional buildings.

Wang et al. (2023) found that for each 1°C of temperature increase, energy use intensity (EUI) experiences an average increase of approximately 14% for cooling and a decrease of 10% for heating. The electricity demand patterns show both peaks in summer and winter due to mixed use of electricity for both cooling and heating systems, while natural gas consumption for heating can range from more than 30 billion cubic feet per day in winter months, which is around ten times larger than in the summer season (Su et al., 2021).

2.5.2 Factors Affecting Building Energy Consumption

Building energy demand is influenced by a combination of the interplay of climate variables, building characteristics, occupant behavior, and urban context effects. Among many factors, there are six primary factors that affect building energy consumption: climate, building envelope, building equipment, operation and maintenance, indoor environmental conditions, and occupant behaviors (Yoshino et al., 2017).

Building characteristics play a crucial role in determining energy demand patterns, such as building size, envelope properties, and system efficiency. Building typology and floor area show strong correlations with energy demand, as larger buildings and those with poor thermal insulation require substantially more energy for space conditioning (Led, 2023). Led (2023) also found that building orientation, window-to-wall (WTW) ratio, and thermal mass characteristics can influence annual energy consumption by 15-40%, with these effects varying significantly across climate zones and building types.

Occupant behavior is one of the most influential factors, which can cause up to 300% variation between predicted and actual building energy consumption (Delzendeh et al., 2017). According to the World Business Council for Sustainable Development (WBCSD), wasteful behavior can add one-third to a building's designed energy performance, while conservation behavior can save a third (Bäcklund et al., 2023).

2.6 Relationships between UHI, UFE, and Energy

2.6.1 UHI Effect on Energy Consumption

The UHI effect significantly influences building energy consumption by elevating urban temperatures, which directly increases cooling demands in summer and reduces heating demands in winter. Li et al. (2019) examined a comprehensive review on UHI and building energy consumption, and found that UHI effects result in a median increase of 19.0% in cooling energy consumption and a median decrease of 18.7% in heating energy consumption, though with substantial spatial variations ranging from 10-120% increase in cooling and 3-45% decrease in heating across different cities. Yang et al. (2019) examined Local Climate Zone (LCZ) in Nanjing and concluded that heat islands in urban neighborhoods increased cooling demand by 12-24% for residential buildings, while reducing heating demand by 3-20%, resulting in a net annual energy increase of 2-6% for residential buildings.

The magnitude of UHI impacts on energy consumption varies significantly based on building type, urban morphology, and climate zones. Santamouris (2019) reported that the global energy penalty induced by UHI at the city scale averages 0.74 kWh/m^2/°C, translating to approximately 237 kWh per person annually, with peak electricity demand increasing by 21 W per degree of temperature rise. Another research by Su et al. (2021) provided empirical evidence showing that changes in average UHI intensity of 0.5K result in monthly cooling energy consumption increases from 0.17-1.84 kWh/m^2, with nocturnal UHI intensity correlating more strongly with energy consumption than daytime values. These effects are accelerated during heat wave events when regional climate extremes and local UHI can more than double the cooling energy penalty, which creates critical stress on urban electricity infrastructure and raises serious concerns during peak demand periods.

2.6.2 Urban Form Elements Impact on UHI

UFEs significantly influence the intensity and spatial distribution of UHI through their effects on energy balance, surface properties, and atmospheric dynamics. The NDVI demonstrates the strongest cooling effect among UFEs. Liao et al. (2021) found that the green space ratio was among the most influential factors affecting LST in London and Seoul, with NDVI showing negative correlations ranging from -0.415 to -0.688 with air temperature, depending on the season. Ziter et al. (2019) explained that tree canopy cover above 40% provides substantial cooling benefits, with scale-dependent interactions showing that cooling effects are most pronounced within 60-90m of vegetated areas.

Building density and morphology can influence temperature variations through radiation trapping, wind flow, and heat storage. Y. Li et al. (2020) showed that UHI intensity is directly related to a linear combination of city area and gross building volume, capturing the amplifying effects of building density on temperature. Horizontal density metrics such as GSI and building coverage ratio show a stronger correlation with LST than vertical metrics like building height.

The 3-dimensional configuration of UFEs introduces scale-dependent thermal impacts through a complex interplay between building morphology and atmospheric processes. 3D metrics performed better in predicting air temperature than 2D metrics at the 500m scale, while the influence of 2D features was stronger at the 1000m scale, with 3D features showing stronger correlations with average daily, daytime, and nighttime air temperatures, regardless of spatial scale (C. Yang et al., 2022). Fan et al. (2023) proposed that the correlation between building coverage ratio, FAR, and LST is largest at a 300m scale, while building height and sky view factor show the strongest correlations at a 400m scale. These scale-dependent relationships show that urban morphology shows stronger correlations with LST differences within built-up areas compared to entire cities, which indicates the critical importance of ventilation and solar radiation for urban thermal environments (Gao et al., 2020).

2.6.3 Urban Form Elements Impact on Energy

UFEs influence building energy consumption through both direct physical mechanisms and indirect microclimate variations, with impacts varying significantly across different climate and spatial variations. Vegetation shows consistent cooling effects through evapotranspiration, which can reduce energy consumption, particularly for summer cooling demands. Mostafavi et al. (2021) analyzed 12,700 buildings and found complex relationships between urban form factors and energy use. Surprisingly, their statistical analysis showed a 1 m^2 increase in tree-cover area associated with a 0.04% increase in EUI, though this minimal effect (less than 0.1%) may reflect correlation rather than causation, for instance, older neighborhoods with mature trees may also have less efficient buildings. More intuitively, they found that a one-unit increase in building count per hectare was associated with a 0.52% reduction in EUI, likely due to shared walls reducing heat loss and the efficiency benefits of compact development. The study emphasized that "form, through the layout and orientation of urban blocks, vegetation and high albedo materials, and the shading effect of surrounding blocks, changes the microclimate within building networks," with impacts varying between cities based on local climate and urban density patterns.

Building density and 3D morphology of buildings create complex energy impacts through natural ventilation and thermal mass. D. Wang et al. (2021) demonstrated that urban 3D form has a greater influence than 2D form when investigating building energy consumption, as higher 3D compactness may cause lower sky view factors, resulting in reduced air ventilation and hot air trapped between buildings, significantly increasing cooling energy demand. Song et al. (2020) analyzed 5 urban morphological parameters in China and found that higher aspect ratio (AR) and building height (BH) were associated with lower heating EUI, likely due to reduced surface area-to-volume ratios in taller buildings. However, they found that increasing building density (BD), floor area ratio (FAR), and shape factor (SF) led to increased heating EUI. This partially contradicts Mostafavi et al. (2021), who found building density reduced overall EUI. This discrepancy may reflect different climate contexts or different definitions of density metrics. In cold climates, the negative effects of reduced solar access in dense developments may outweigh the benefits of shared walls, while in mixed climates, the year-round benefits of compact development may dominate. A similar study conducted in China revealed that building density affects natural lighting and passive solar gains, causing energy use variations up to 30% in offices and 19% in residential areas (Cui et al., 2024).

2.7 Analytical Methods for Complex Urban Systems

2.7.1 Handling Multicollinearity

When analyzing UFEs in UHI studies, multicollinearity in UFEs can be found, which poses significant challenges. Traditional regression methods struggle with such correlated predictors because they cannot properly partition the shared variance among variables, such as high NDVI areas typically correspond with low building ratios, and building height strongly correlates with FSI, creating confounding effects that obscure the true contribution of each variable.

To address these multicollinearity challenges, specialized variance decomposition methods have been developed to quantify the effects of highly correlated spatial variables. Liao et al. (2021) applied the Genizi method in their study, which decomposes the total R^2 among predictors while accounting for shared variance between correlated variables, producing percentage contributions that sum to the total explained variance. The study mentioned that the Genizi method is particularly valuable when predictors show high correlations. While the Genizi method reveals relative importance percentages, it must be complemented with other correlation methods to determine the direction of relationships, as the variance decomposition does not show whether correlations are positive or negative. By complementing with other methods, it can make a comprehensive understanding of UFE impacts.

2.7.2 Feature Importance Methods

There are limitations to evaluating the feature importance of UFE with the Genizi method alone, as it does not show whether it increases or decreases the target variable. One of the common methods to complement the Genizi method is a Partial correlation. Partial correlation analysis complements the Genizi method by revealing the directional effects of each variable while controlling for all other variables in the system. The combination of these methods has proven particularly effective for urban climate study by Liao et al. (2021), which allows researchers to understand both the relative importance percentages from the Genizi method and the directional relationships from the Partial correlation coefficients.

Not only Partial correlation, but there are other comparative methods to show the directional analysis used in other UHI studies. Tong et al. (2017) used the Pearson correlation coefficient to analyze simple bivariate relationships between variables, but they failed to account for the confounding effects of other variables in the system, which restricts the predictors when they are correlated. The article by Song et al. (2020) used Multiple linear regression (MLR) coefficients to show directional effects, but the result became unstable and difficult to interpret when there is multicollinearity in variables. Spearman rank correlation also offers improvement by assessing monotonic relationships rather than strictly linear ones. However, it still only captures bivariate associations without controlling for other variables, which does not properly show linear relationships between environmental factors (Chaudhary et al., 2022).

03
Research Area

03 Research Area

3.1 Why Seoul as a Research Area

There are mainly three reasons why Seoul is chosen for the research area. Firstly, Seoul experienced rapid urbanization, and the city has been experiencing a significant UHI effect as a consequence (Hong et al., 2019). Secondly, which is also the main reason for choosing Seoul, is the exceptional data availability from both the Korean government and the Seoul municipality. Thirdly, Seoul has very diverse urban form elements from high-rise to low-rise buildings across the districts and several major urban parks and mountains, which will be interesting to analyze in relation to the UHI effect and energy consumption.

Regarding the data availability, the Korean government has been providing precise weather data through automatic weather stations (AWS) since 1997, with 554 AWSs throughout Korea. Among them, 39 AWSs are located within the Seoul boundary. These AWSs are well distributed across the districts and provide comprehensive meteorological data, including air temperature, humidity, wind speed, and air pressure (Hong et al., 2019). This extensive weather history from AWSs can facilitate accurate and precise modelling and validation for the UHI effect. The accessibility of the data helps to enhance the precision and reliability of the research methodology.

Moreover, the Seoul municipality has been providing a well-structured database for energy consumption. It provides a very precise and detailed energy consumption database of electricity and gas for buildings in Seoul. The energy demand has been recorded for more than a decade, which enables analysis of the correlation with urban heat patterns in Seoul (Korea Architecture Hub, 2024).

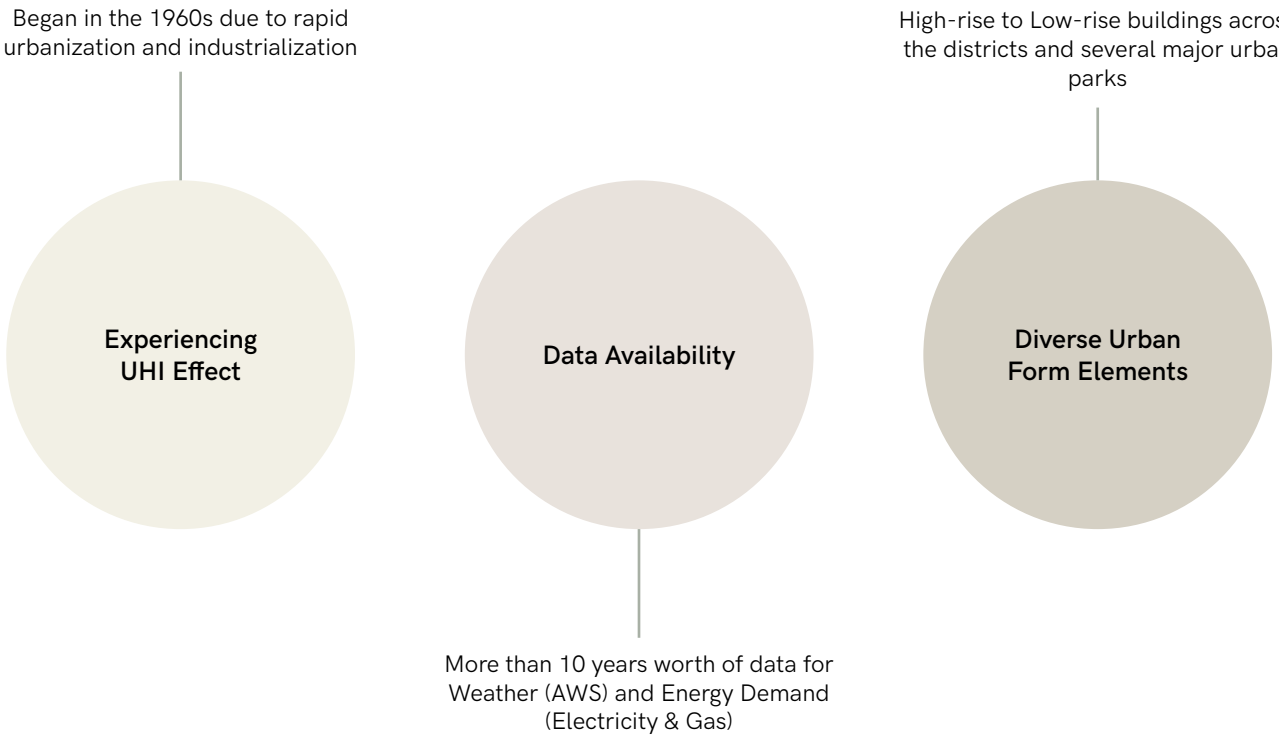

3.2 City Characteristic

The capital city of South Korea, Seoul, is one of the most urbanized and populated cities in the world, with a population of around 10 million in 2023. The total area of Seoul is approximately 605 km^2, with very dense urban infrastructure, high-rise buildings, and a very complex transportation system. Within Seoul, there are 25 Gu (boroughs) and 426 Dong (smaller units of boroughs). Each Gu has different characteristics, and Seoul is mainly divided into Northern and Southern Seoul, with the Han River running in the middle of the city.

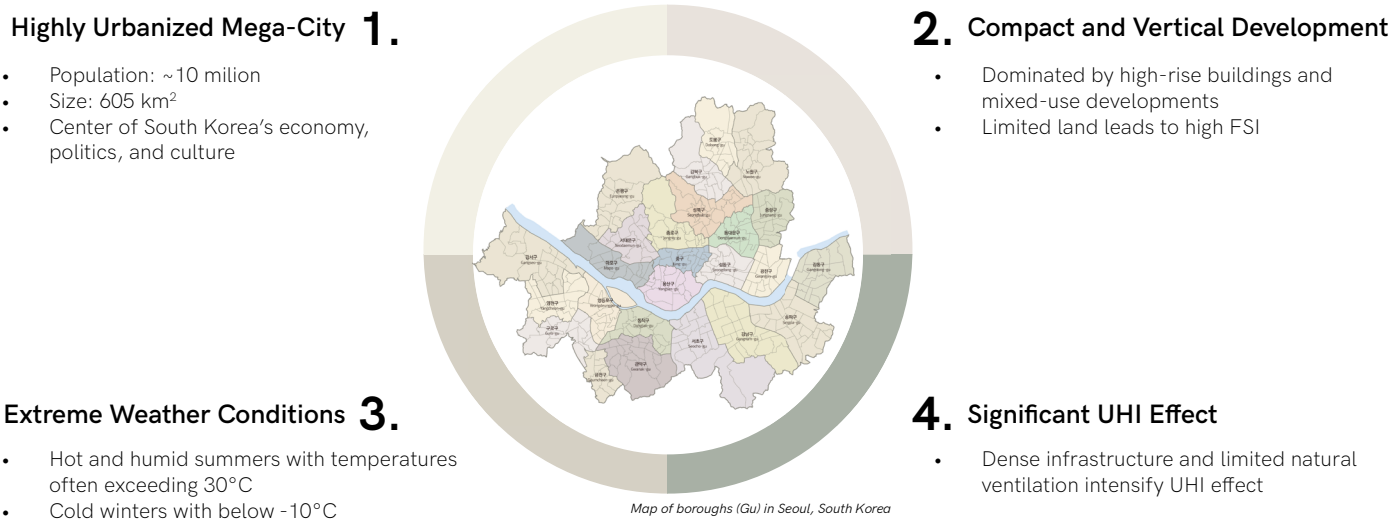

Figure 3.1 *4 major city characteristics in Seoul*

As one of the most urbanized and complex cities in the world, Seoul has a very diverse range of urban forms, from high-density business districts such as Gangnam to suburban residential areas. Due to a high number of residents, the city is characterized by extensive impervious surfaces, high buildings, and limited green spaces, which provide a rich context for studying how urban morphology influences UHI effect and energy consumption.

In addition, Seoul has implemented green roofs and developed urban parks to mitigate the effects of urbanization on the environment. The Seoul Metropolitan Government has introduced the concept of green infrastructure to solve urban problems such as the urban heat island phenomenon, fine dust, and localized heavy rains, with specific projects including support for roof greening and the creation of ecological trails (J. Choi & Kim, 2022).

3.3 Heukseok-dong

Seoul consists of 25 boroughs, where 14 boroughs are located on the north side and the other 11 boroughs are located on the south side of the Han River. Indeed, analyzing every single borough would require a significant amount of time and numerous datasets. To reduce the timeframe of the research, this paper focuses on one of the regions in Seoul. Since the research is aiming to find the correlation of UHI, energy demand, and urban form elements in the last decade, it is ideal to choose the region that has many changes in urban form elements in the last 10 years to analyze how the change in urban form affects the other parameters.

Figure 3.2 *Diverse urban form elements in Heukseok-dong*

One of the regions that fulfills these requirements is **Heukseok-dong**. Heukseok-dong is one of the districts in Dongjak-gu. Heukseok-dong covers an area of 1.67 km^2 and is a multi-generational area due to old buildings and a university campus. There are multiple reasons why Heukseok-dong is a good area to be researched. The area has very diverse urban form elements from the Chung-Ang University campus, a large park (Dalma park), and thousands of buildings, from old to new residential and multifunctional buildings. This would help to find how the different urban form elements are related to air temperature distribution.

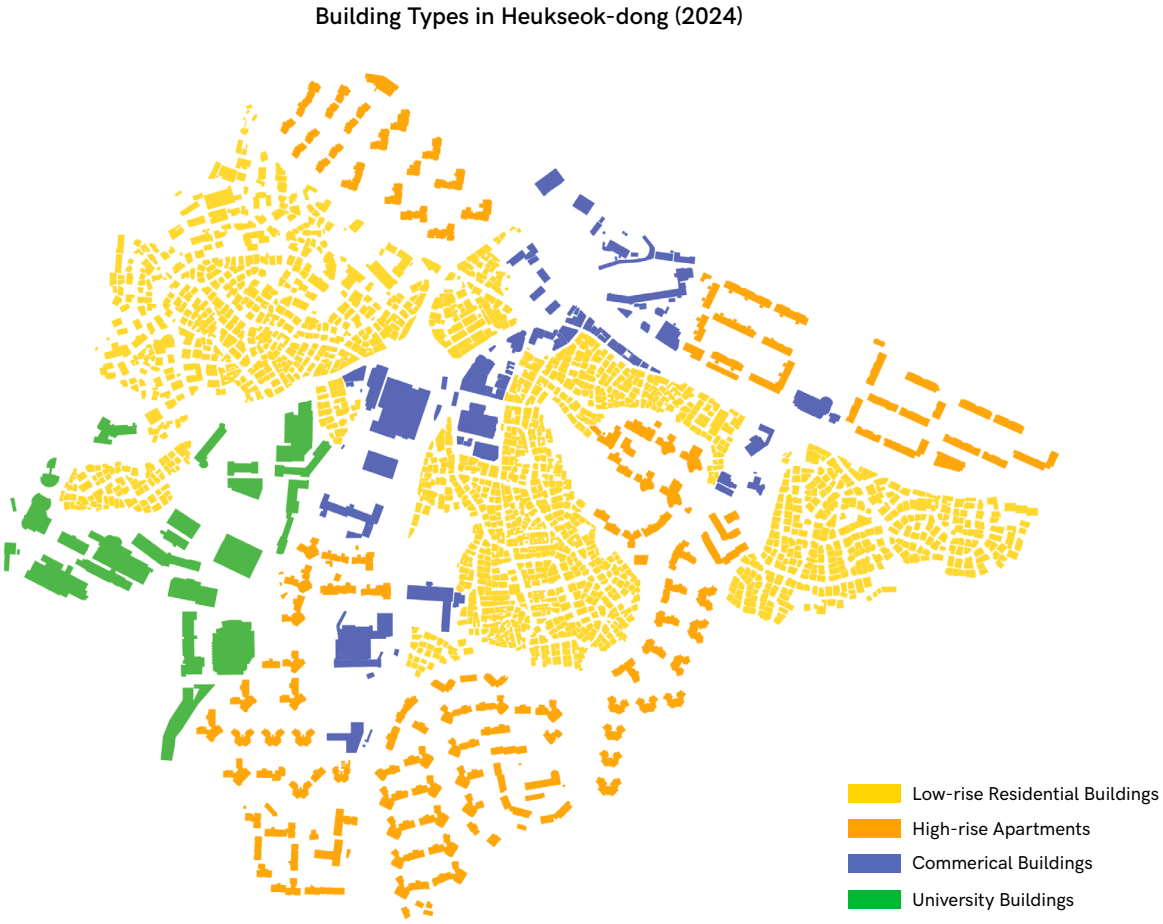

Figure 3.3 *Different building types in Heukseok-dong in 2024*

Despite ongoing redevelopment, Heukseok-dong in 2024 remains characterized by a huge number of low-rise residential structures. While certain districts have undergone transformation into high-rise apartment districts, the predominant building type continues to be low-rise residential building, which is almost 81% of the total buildings in Heukseok-dong. These buildings are densely packed with short distances between buildings, contrasting with other building types that have comparatively more open areas. This dense, compact arrangement of low-rise buildings represents a typical urban pattern throughout Seoul and it should be an important consideration for this research.

3.3.1 Heukseok New Town Project

There is also an ongoing redevelopment promotion project, which is called '**Heukseok New Town Project**'. Heuksoek-dong is one of the places where many refugees gathered together during and after the Korean War in 1950s. As a result, there are still many very old residential buildings, and the Seoul municipality started a redevelopment project in the early 2000s, which is still ongoing these days. This project has continuously changed the number and characteristics of buildings over the years in Heukseok-dong. The Seoul municipality classified 11 districts in Heukseok-dong, which are in need of redevelopment.

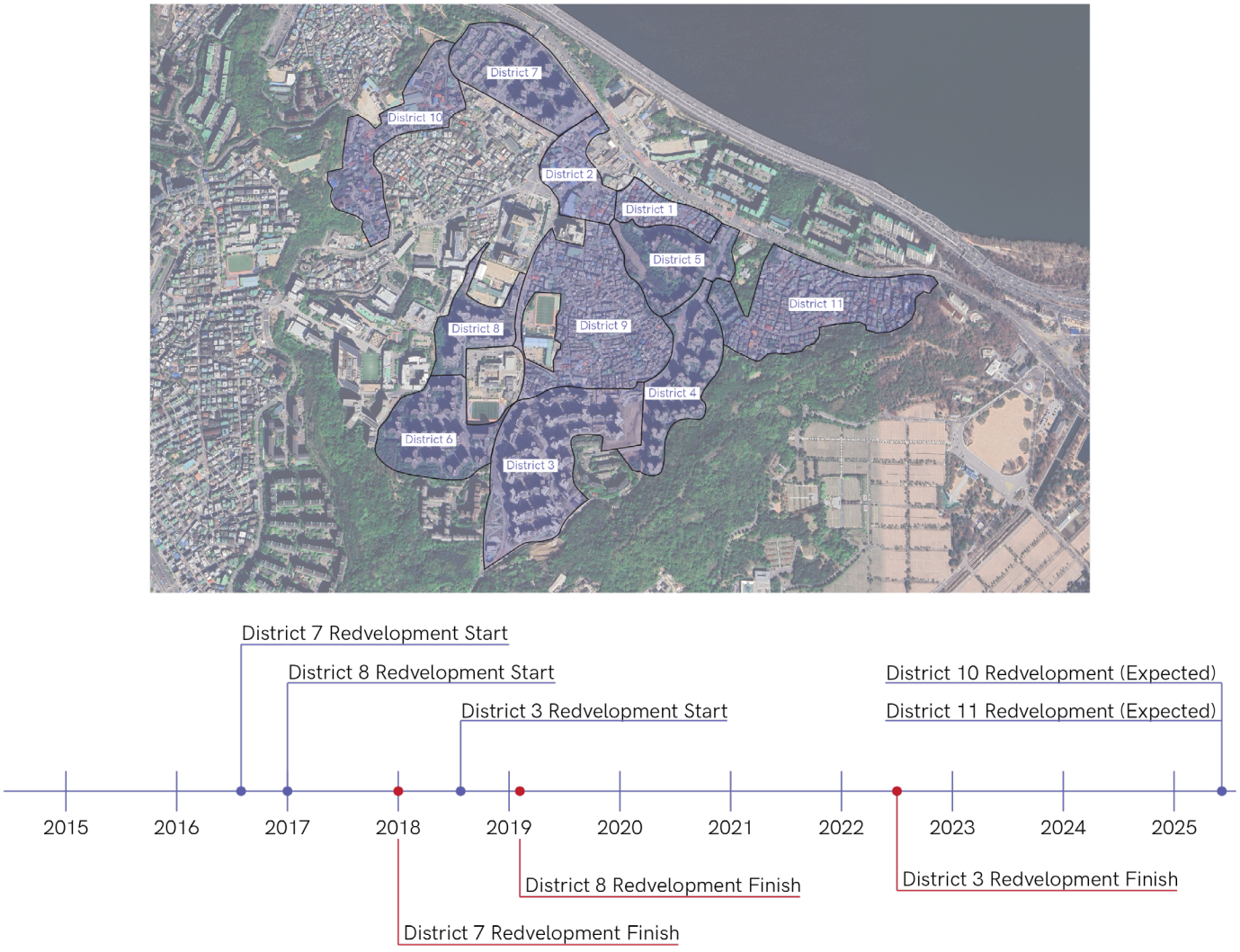

Figure 3.4 *Heukseok-dong redevelopment project timline between 2015 and 2025*

Heukseok-dong comprises 11 districts at various stages of urban transformation, with some already redeveloped and others awaiting renewal. Districts 3, 4, 5, 6, 7, and 8 have been transformed into high-rise residential complexes, replacing the original compact low-rise buildings. The primary purpose of this redevelopment is to transition from densely packed low-rise structures to modern high-rise apartments with increased open spaces, which would enhance residents' quality of life and improve environmental conditions.

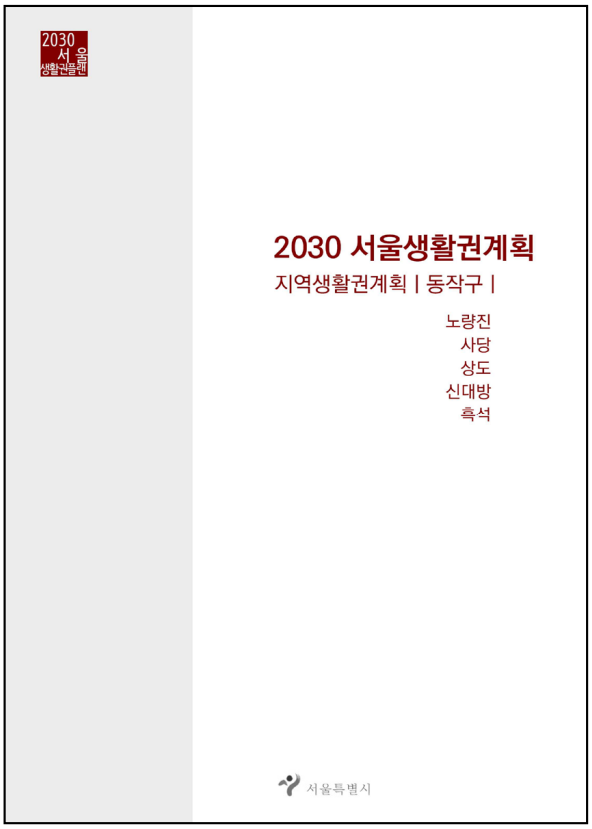

Figure 3.5 *2030 SeoulPlan cover page*

The Seoul municipality has published a comprehensive vision for Heukseok-dong's future through its "2030 SeoulPlan" report, which contains four main goals and ten strategic approaches for transforming the area. Goal 3 addresses residential area management and establishment, and Goal 4 focuses on expanding leisure spaces and developing green infrastructure networks. The report plans a mixed-use development approach, promoting single and double-household apartments alongside multifunctional complexes near Heukseok subway station. Additionally, the Seoul municipality aims to create an inner-city green space and establish connectivity between Dalma Park and the Han River through an integrated green network. This plan will significantly change the key urban form elements, especially vegetation coverage and building density ratios, which have direct implications for UHI effects in the area.

04

Data Collection

04 Data Collection

Data collection is a fundamental component of this research, providing the foundation for analyzing the relationship between UHI effects, energy consumption and UFE. This chapter shows the five primary data sources. Each data source contributes unique spatial and temporal information necessary for understanding the complex interactions between Heukseok-dong's urban morphology, microclimate effects, and energy consumption patterns.

4.1 Satellite Imgery

4.1.1 Landsat 8

One of the most widely used methods for obtaining precise temperature data in UHI studies is using satellite imagery. Although there are hundreds of satellites that capture the LST (land surface temperature) of the Earth, this research uses Landsat 8 due to its extensive temporal coverage of over 10 years and high spatial resolution of 30 by 30 meters. From Landsat 8, the digital elevation model (DEM) and solar zenith angle (SZA) can be acquired, while LST and normalized difference vegetation index (NDVI) can be calculated using 3 spectral bands.

Landsat-7 ETM+ Bands (µm)			Landsat-8 OLI and *TIRS* Bands (µm)		
			30 m Coastal/Aerosol	0.435 - 0.451	Band 1
Band 1	30 m Blue	0.441 - 0.514	30 m Blue	0.452 - 0.512	Band 2
Band 2	30 m Green	0.519 - 0.601	30 m Green	0.533 - 0.590	Band 3
Band 3	30 m Red	0.631 - 0.692	30 m Red	0.636 - 0.673	Band 4
Band 4	30 m NIR	0.772 - 0.898	30 m NIR	0.851 - 0.879	Band 5
Band 5	30 m SWIR-1	1.547 - 1.749	30 m SWIR-1	1.566 - 1.651	Band 6
Band 6	60 m TIR	10.31 - 12.36	*100 m TIR-1*	*10.60 – 11.19*	Band 10
			100 m TIR-2	*11.50 – 12.51*	Band 11
Band 7	30 m SWIR-2	2.064 - 2.345	30 m SWIR-2	2.107 - 2.294	Band 7
Band 8	15 m Pan	0.515 - 0.896	15 m Pan	0.503 - 0.676	Band 8
			30 m Cirrus	1.363 - 1.384	Band 9

Table 4.1 *Landsat band information by B. Markham (July 2013)*

To calculate LST and NDVI of the research area, 3 bands are required: Band 4 (RED), Band 5 (NIR), and Band 10 (TIR-1).

Band 4 (RED) - OLI Band

- It captures red light in the visible spectrum of 0.64-0.67 µm, which is the portion of light that human eyes perceive as red. This band is often used to assess vegetation health analysis, distinguishing vegetation from non-vegetated surfaces and urban area identification (Landsat NASA, 2023).

Band 5 (NIR) - OLI Band

- Band 5 captures near-infrared radiation (NIR), which is invisible to human eyes, that is wavelengths between 0.85-0.88 µm. Vegetations reflect strongly in NIR, as when there are healthier plants, the more complex the internal structure, the higher the reflectance can be captured (Landsat NASA, 2023).

Band 10 (Thermal Infrared) - TIRS Band

- This band captures thermal infrared radiation, which is also known as heat, by measuring emitted radiation (Landsat NASA, 2023).

These bands can be obtained from the various websites, but this research uses Google Earth Engine (GEE) as it can calculate the research area by itself and download all the required bands at once.

4.1.2 Calculating LST and NDVI

To calculate the LST and NDVI of the research area, a method, the 'Mono-window Algorithm' or "Single-channel Algorithm" should be used. This method is commonly used with Landsat data for LST and NDVI retrieval, which uses a systematic flowchart that includes calculating Top of Atmosphere (TOA) radiance, Proportion of Vegetation (PV), Brightness temperature (BT), and finally LST. This report follows the methodology that Sahani (2021) proposed in the published paper.

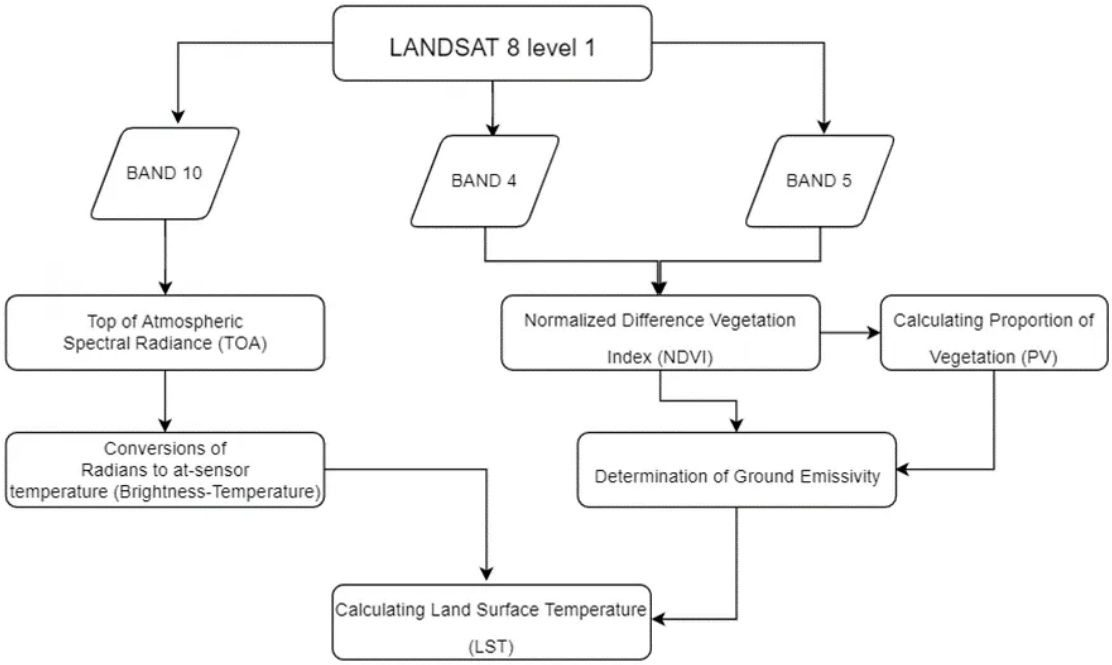

Figure 4.1 *Flowchart of calculating NDVI and LST from Landsat 8 by Sahani (2021)*

L. Wang et al. (2019) compared 3 algorithms for the retrieval of land surface temperature from the Landsat 8 images, and their report is well summarized for each step for calculating NDVI and LST. According to their research, it requires 6 steps to calculate NDVI and LST, which are interrelated.

Step 1 - Retrieval of TOA spectral radiance

- The first step is to convert Digital Number (DN) values from the Landsat 8 TIRS Band 101 to spectral radiance using the equation.

$$R\lambda = ML \times Qcal + AL$$

- Rλ is spectral radiance, ML is the radiance multiplicative scaling factor, Qcal is the DN value, and AL is the radiance additive scaling factor. These parameters can be found in the metadata (MTL) file that comes with Landsat imagery when downloading.

Step 2 - Transmission of spectral radiance to at-sensor brightness temperature

- Once the spectral radiance is calculated, it has to be converted to brightness temperature using Planck's function.

$$TB = K2 / \ln(K1/R\lambda + 1) - 273l.15$$

- TB is brightness temperature in Kelvin, K1 and K2 are calibration or thermal constants specific to Landsat 8 Band 10, where K1 = 774.8853 and K2 = 1321.0789. It is important to substitute 273.15 to convert Kelvin to degrees Celsius.

Step 3 - Calculation of NDVI

- NDVI (Normalized Vegetation Index) is one of the most widely used urban factors to examine environmental impacts, which can be calculated using the equation.

$$NDVI = (NIR - RED) / (NIR + RED)$$

- NIR is the value from Band 5, and RED can be derived from Band 4. NDVI values range from -1 to 1, with water typically below 0, soil between 0-0.2, and vegetation above 0.2.

Step 4 - Calculation of Proportion of Vegetation (Pv)

- The proportion of vegetation represents the fractional vegetation cover within a pixel. It can be calculated by using the fractions from NDVI values.

$$Pv = [(NDVI - NDVI_{min}) / (NDVI_{max} - NDVI_{min})]^2$$

- $NDVI_{min}$ is the minimum value of the NDVI, which is usually for bare soil (typically 0.2), and $NDVI_{max}$ is the NDVI for full vegetation. The range for Pv is from 0 (no vegetation) to 1 (full vegetation).

Step 5 - Calculation of Land Surface Emissivity (LSE)

- Land surface emissivity is the efficiency with which a surface emits thermal radiation compared to a perfect blackbody. It has to be determined to calculate the final LST using the proportion of vegetation (Suresh. S et al., 2016).

$$LSE = 0.004 \times Pv + 0.986$$

Step 6 - Calculation of Land Surface Temperature (LST)

- LST can be finally calculated using all the factors that are obtained.

$$LST = TB / [1 + (\lambda \times TB / p) * \ln(LSE)]$$

- λ represents the wavelength of emitted radiance, which can be used as 10.8, while p represents the radiation constants used in Planck's law. It consists of Planck's constant, speed of light, and Boltzmann constant, but it can be easily used as 14388 when calculating LST.

4.1.3 Data Quality

Satellite imagery can be obtained using the mono-window algorithm introduced in **Chapter 4.1.2**. However, when using the Google Earth Engine, it is much easier to obtain satellite imagery as it is published to anyone for free, and it can reduce time to calculate the NDVI and LST, as they can be calculated using the java script, which does not require manual work. However, not all satellite imageries are useful from the Landsat. Seoul is in continental climate, where the summers being long, warm, muggy, and wet, while winters are short, freezing, but mostly clear. Moreover, the summer season in Seoul is very humid due to sporadic monsoon rains, so most of the days are covered by heavy clouds. Satellite imagery is very vulnerable to cloud cover, as they can cover most of the land areas. As a result, the quality of the satellite imagery should be manually monitored.

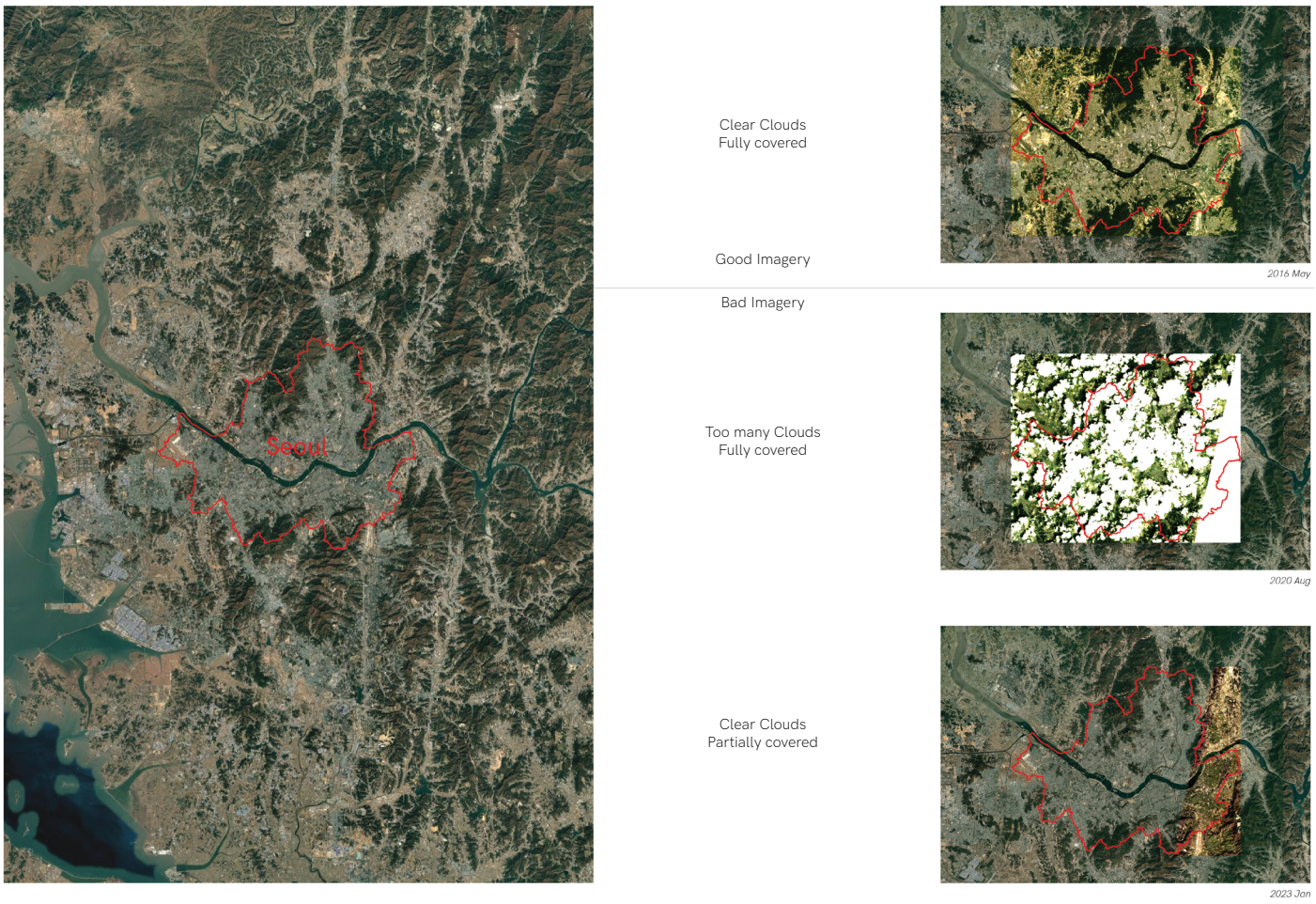

Figure 4.2 *Quality of satellite imagery (Landsat)*

The quality of the satellite imagery can be divided into good and bad imagery. Good imagery is when the satellite imagery has clear sky, so that the land of the research area is visible, and it fully covers the whole research area. On the other hand, bad imagery detects too many clouds so that the land is not clearly visible, also some of the imagery does not capture the whole research area, but only partially covers it. As a result, to proceed with calculating LST and NDVI, only good images are selected to determine a more precise and accurate correlation with urban form elements and air temperature distribution.

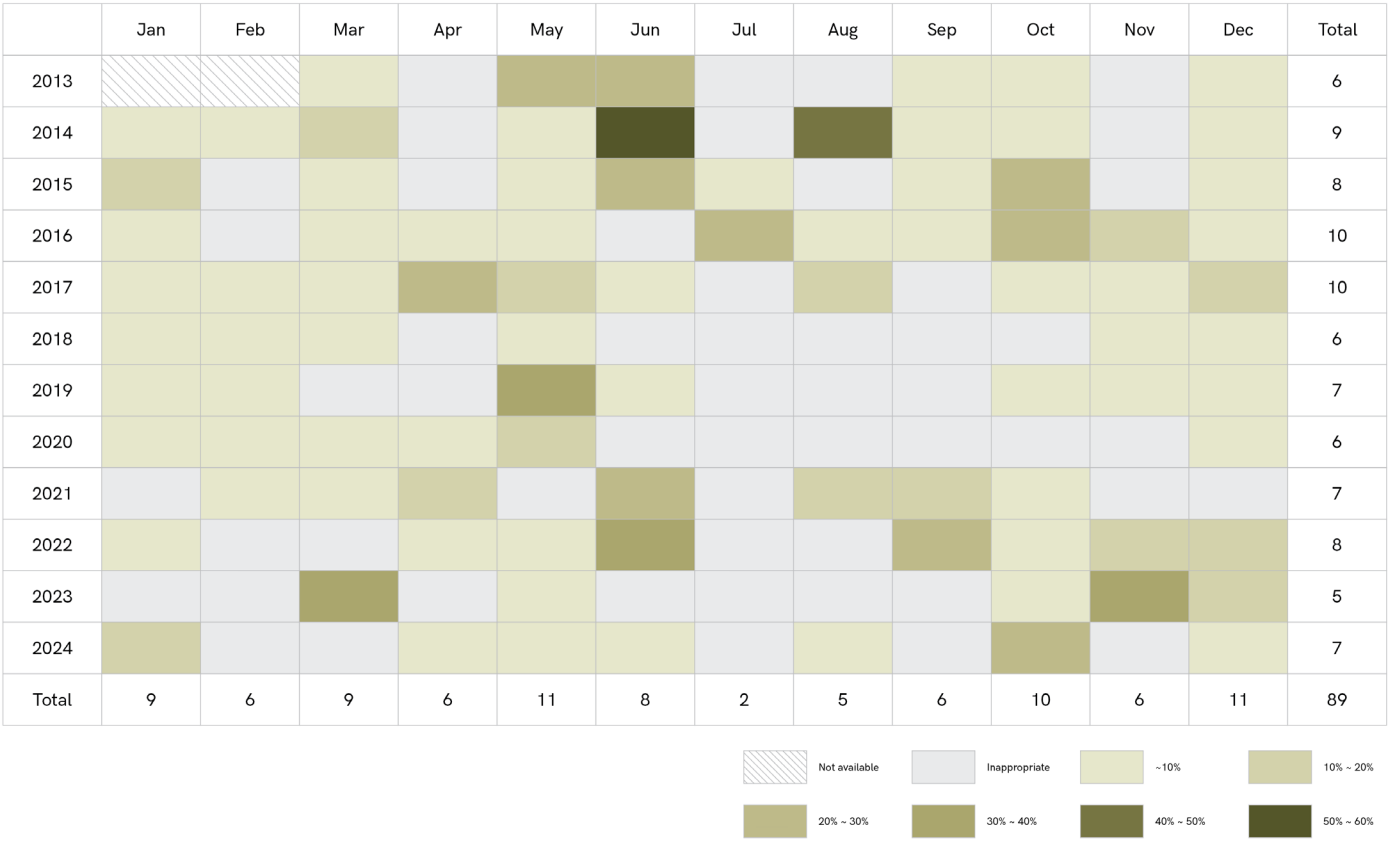

Figure 4.3 *Available Land surface temperature (LST) from 2013 with cloud covers*

LST and NDVI are derived from Landsat imagery for Seoul. The selection of satellite images involved a quality control process based on cloud coverage thresholds. Initially, a maximum cloud coverage of 30% was set as the selection criterion to ensure high-quality imagery. However, when no suitable images were available within this threshold for specific time periods, the cloud coverage limit was incrementally increased until acceptable quality images could be obtained. This adaptive approach ensured continuous temporal coverage while maintaining the best possible image quality for each month. The resulting dataset is summarized in a table showing the number of images acquired for each month and year, with cell colors indicating the cloud coverage percentage of the selected images, providing a visual representation of data quality across the temporal range.

Satellite imagries from the Landsat8 are available from March 2013. Although the research is looking at the temporal analysis of 10 years from 2015 to 2024, some satellite images in the years 2013 and 2014 are obtained as well to increase the number of samples to find the correlation with the automatic weather station later. It is possible to modify the cloud coverage of the satellite imagery, and **Figure 4.3** shows what percentage of cloud coverage was used to get images from the Landsat. Ideally, the number of images from the Landsat should be 118 from the year 2013 to 2024 (excluding January and February in 2013), but not every single month is available. Especially satellite images in summer seasons are not obtained as many as in other seasons due to cloud coverage. This is due to the unique climate conditions in Seoul in the summer season, as mentioned earlier.

Moreover, Landsat 8 orbits the Earth every 16 days, which means that the satellite only captures the area 1 or 2 times in a month (USGS, 2025). According to the Metadata from the Landsat, the research area is captured at around 11:12 in the morning, which is normally considered as the peak temperature in a day. Although it has a very high spatial resolution of around 30 by 30 meters (23.81 by 29.91 meters), it has a very limited temporal resolution as it only captures the LST and NDVI at 11:12 AM and on a biweekly basis . This temporal limitation means that the model outputs consist of single monthly values derived from these satellite observations at their specific capture times, rather than continuous temporal data. The AWS data, introduced in the next sub-chapter, serves a different purpose in the analysis rather than addressing the satellite's temporal resolution limitations.

4.2 Automatic Weather Station (AWS)

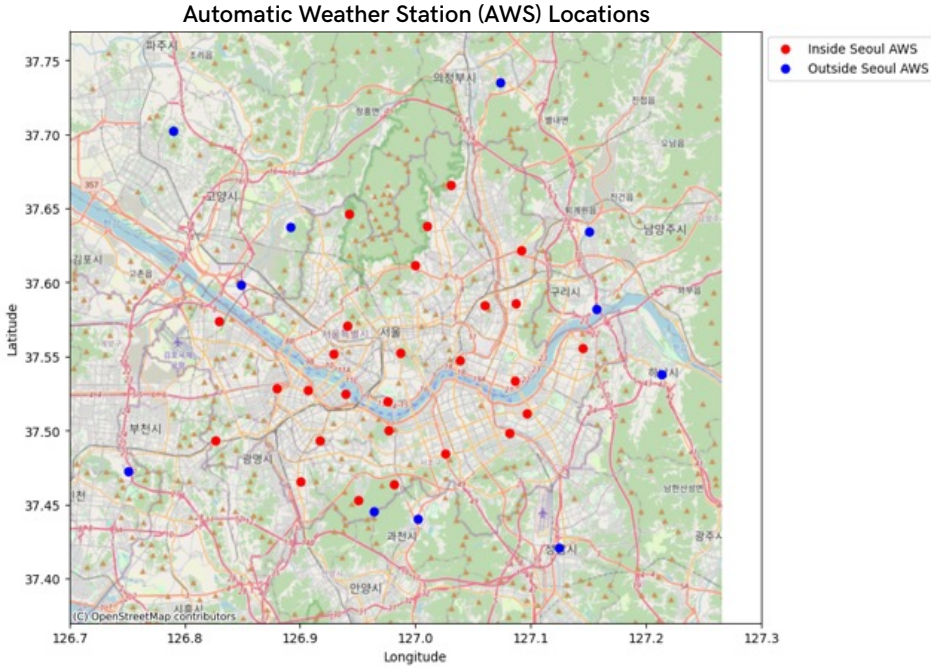

Figure 4.4 *Location of AWS in Seoul and nearby*

The Korean Meteorological Administration (KMA) first installed automatic weather stations (AWSs) throughout the country in 1997. The AWSs record air temperatures within a range of -40°C to 60°C with a ± 0.3°C accuracy using a metallic system equipped with thin film sensors, as well as wind speed, pressure, and other climatic factors, which are measured in minutes, hourly, and monthly, based on AWSs (Korea Meteorological Administration, n.d.). There are 554 AWSs in Korea, and 28 AWSs are installed in Seoul. The KMA provides detailed information on each AWS, including its exact location (longitude, latitude, and height) in the WGS84 coordinate system. However, some of the AWSs have been moved ot other locations, so some information is not available. Although the spatial resolution of the AWS is relatively low (28 AWSs in Sdoul - 605.25 km^2), it has a very high temporal resolution. Although there are 28 AWSs within the Seoul boundary, this research also considers 9 more AWSs that are located near the Seoul border to increase spatial resolution.

Figure 4.5 *Picture of AWS in Gangnam (Code 400)*

AWS Information			
Code	400	**Name**	Gangnam
Longitude	37.4892	**Latitude**	127.08162
Height (m)	12.66		
Measuring unit	Minute		
Address	Tancheon Water Recycling Center, 580 Ilwon-dong, Gangnam-gu, Seoul		
Purpose	Monitor disaster prevention		

Table 4.4 *Infomation of AWS in Gangnam (Code 400)*

4.3 S-DoT Sensors

The Korean government installed weather sensors in 2020 as part of an initiative called Seoul Data of Things (S-DoT). S-DoT is a city data sensor that collects various urban phenomena data, such as fine dust level, temperature, relative humidity, and noise, illumination level, ultraviolet, and other parameters (Park & Baek, 2023). The sensors are installed in major mountains, riversides, and downtowns to analyze how different Seoul's living environment is in each area's characteristics (Seoul City Hall, 2023). Sensors were first installed in 2020, and after the COVID-19 pandemic, more sensors were installed all around Seoul as environmental consciousness rose suddenly. The sensors are authorized by the government, and 1159 sensors are installed in 2024 (Smart Seoul Data of Things(S-DOT), 2024). Depending on the sensors, they usually provide high temporal resolution, as they mostly measure hourly. The location of the weather sensors is also provided by the Seoul municipality, which contains the exact longitude, latitude, and height of the sensors that are installed.

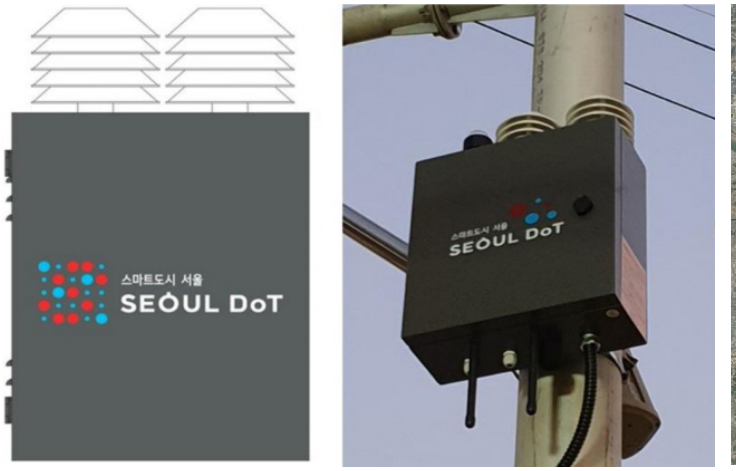

Figure 4.6 *Weather sensors installed in Seoul (Seoul City Hall, 2023)*

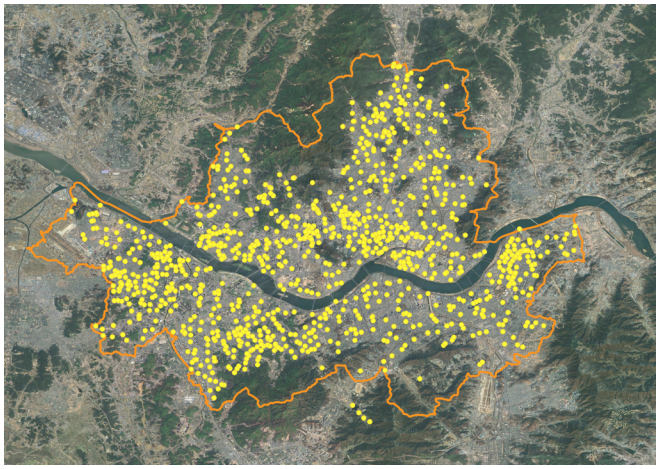

Figure 4.7 *Location of installed weather sensors in Seoul*

S-DoT sensors were already used in many published papers to explore the living environment characteristics in Seoul. Kim et al. (2023) used sensors installed in Seoul to collect living environment data such as particulate matter and noise at an hourly rate, which they then aggregated to daily, monthly, seasonal, and annual averages for analysis. Their report created detailed spatial and temporal models of environmental quality across Seoul, which could be correlated with various urban planning factors. Another research study was conducted by Park and Baek (2023), which analyzed temperature patterns during heatwaves and coldwaves throughout Seoul with sensors installed in different urban environments. The study demonstrated how sensors can provide highly granular environmental information that captures the urban heat island effect and other microclimate variations that standard weather stations miss using the newly developed QMS-SDM system.

The Seoul municipality has been distributing the results of measurement data on 10 environmental factors, including fine dust, temperature, ultraviolet rays, and noise, since 2020. According to the result they analyzed, the temperature was about 1.8°C higher than that of the AWS (Analysis of Temperature Distribution in Seoul Using Urban Data Sensors, n.d.). Even within the same city, Seoul has a rather large temperature difference between regions, and differences of up to 4°C were observed on the same day.

4.4 Urban Form Element (UFE)

There are thousands of urban form elements (UFEs) that contribute to air temperature and energy consumption of the buildings and cities, but this research considers 6 UFEs: Normalized Difference Vegetation Index (NDVI), Building ratio, Weighted height, Building volume, Floor space index (FSI), and Ground space index (GSI). These 6 UFEs are base parameters in UHI studies, which were already used in other papers (Y. Su et al., 2012; Ngarambe et al., 2021; J. Park et al., 2016). Moreover, due to the limited accessibility of the data, not every single UFE can be obtained, but only these 6 UFEs are selected, which can be calculated from the shapefiles and satellite images.

No.	Urban form element	Description	Measure
1	NDVI	Normalized difference vegetation index	Derived from the Landsat
2	Building ratio	The ratio of building in a grid cell	The ratio of total building space in a grid cell
3	Weighted height	Height of buildings account for size and footprint of buildings	Weights each building's height by its footprint area within the grid cell
4	Building volume	The volume of a building	Building height x Building footprint
5	FSI	Floor space index of a building	Gross floor area / Site area
6	GSI	Ground space index of a building	Building footprint / Site area

Table 4.5 *6 Urban form elements*

One of the first UFEs is **normalized difference vegetation index (NDVI)**, which represents how much green the area has. NDVI is a very critical UFE in the UHI study as it is considered one of the dominant drivers for temperature variation due to evapotranspiration and heat absorption (Liao et al., 2021). Another UFE, the **building ratio**, represents the compactness of the buildings, which is calculated as the ratio of the total building spaces in a grid cell from the Landsat 8. Analyzing the building ratio would provide a comprehensive analysis of how the compactness of the buildings affects the air temperature variations and building energy consumption. Instead of using the average or the sum of the building heights in each grid cell, the **weighted height** is selected as another UFE. Weighted building height shows several significant advantages over the simple average building height for analyzing UHI effects and energy consumption. By accounting for building size and footprint, this parameter better captures the actual thermal mass and shading effects within areas, which directly influence local air temperatures. **Building volume** is another UFE in this research, as D. Wang et al. (2021) mentioned the importance of the 3D morphology of the buildings when analyzing energy consumption and temperature variation due to wind flow. Building volume can be calculated by multiplying the building footprint by height. **Floor space index (FSI)**, which is also called Floor Area Ratio, shows the ratio of a building's total built-up floor area to the total area of the land plot it stands on, while **ground space index (GSI)** shows the ratio of the building's ground floor footprint area to the total site or land area. FSI and GSI show the schematic morphology and layout of the buildings in the area, which are related to temperature variations. All the urban form elements are calculated based on each grid cell. The grid is created from the LST and NDVI from the satellite, which is 23.81 meters by 29.9 meters.

To calculate these 6 UFEs, a basic building shapefile should be prepared, which is made by merging 3 shapefiles that are produced by the Seoul municipality and the Korean government.

Figure 4.8 *Shape file blue (AL_D010), green (F_FAC), red (Z_KAIS)*

These 3 shapefiles are produced for different purposes, so that the attributes and information that each shapefile contains are different. AL_D010 is GIS building integrated information, F_FAC is for building integrated floor plans, and Z_KAIS is to present buildings with new road names. AL_D010 shapefiles are used as base shapefiles and merged information from the F_FAC and AL_D010, as only AL_D010 shapefiles have at least 1 shapefile for each year from 2015 to 2024. Each shapefile extracts the buildings that are in the research area first to reduce the size of the files, and other buildings in other areas are not considered in this research.

When merging AL_D010 with other shapefiles, some requirements are made. Although each shapefile has almost the same number and shape of buildings, some of the buildings are not located in the same coordinates. To make sure each of the buildings is the same, make sure all the shapefiles are using the same CRS coordinate systems and set the minimum percentage of overlap. In addition to that, each building has a unique ID or a GIS building identification number, and these are used to identify if the buildings from different shapefiles are the same buildings or not.

However, to calculate 6 UFEs, some of the building attributes and building information are missing. To make every single building UFE attributes, especially building height, building volume, FSI, and GSI, some architectural assumptions are used.

1. If GFA (Gross floor area) is missing, it can be calculated as "Building footprint" x "Number of floors"

2. If the height of the building is missing but the number of floors is available, assume that each floor is 3 meters high

3. If the building footprint is missing, estimate using the "area" function in the Python package GeoPandas for building geometry

When all the urban form elements are ready for each year in the AL_D010 shapefiles, buildings in the research area are selected using the "clip" function in GeoPandas. When clipping shapefiles into the research area, only cells that are at least 30% within the research area are selected, and the other grid cells are excluded. In the end, the research area is covered with 3436 grid cells.

However, although AL_D010 shapefiles have one shape file for each year, they are not up to date, and some buildings and areas should have been modified. Buildings in Heukseok-dong have been continuously changed in the last 10 years due to a redevelopment project, but these are not well included in the shapefiles.

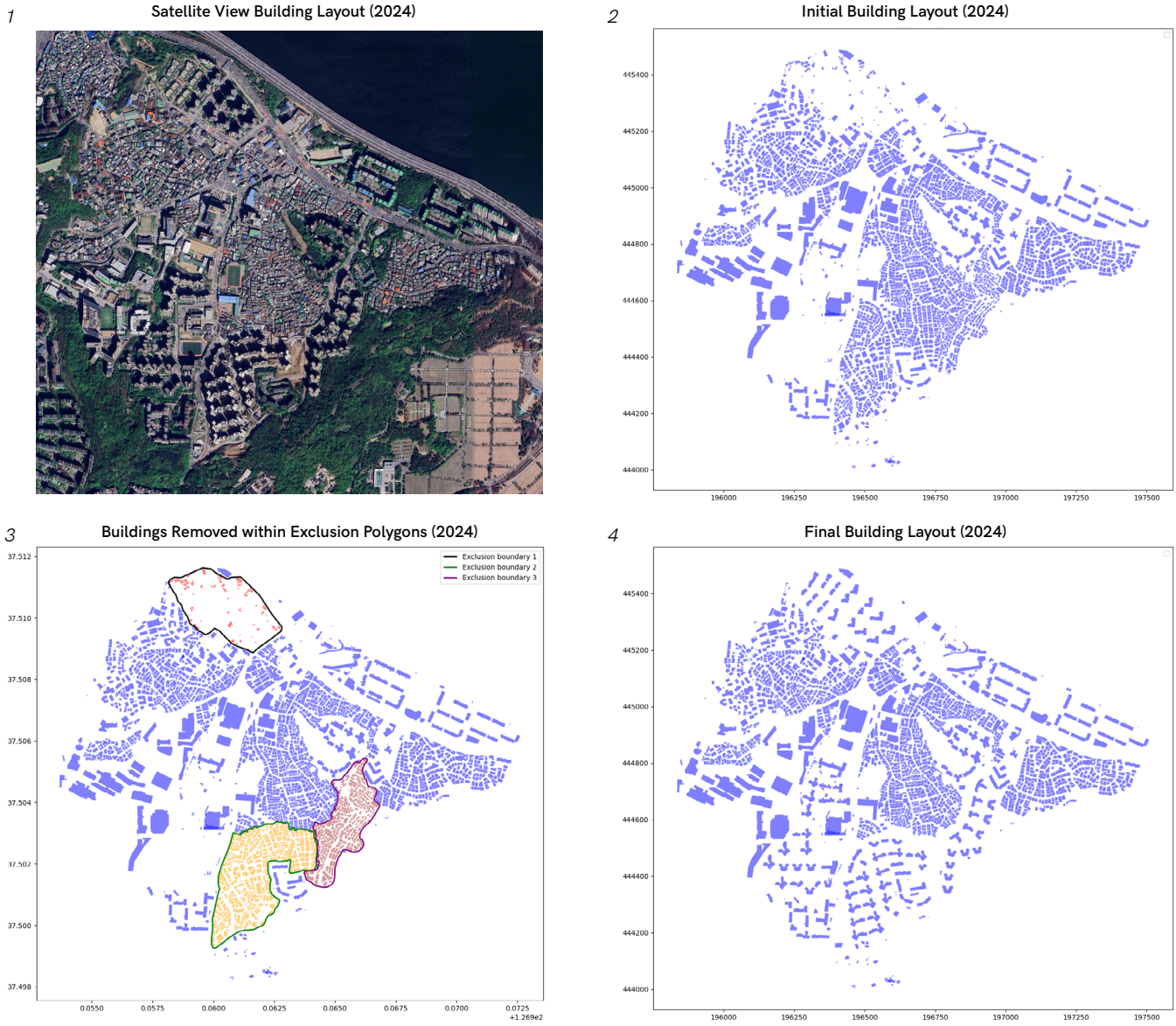

Figure 4.9 *Satellite Imagery (1st), Initial building geometry (2nd), Buildings to be removed (3rd), and the Final building geometry (4th) in 2024*

In 2017, a redevelopment project in District 7 was started in Heukseok-dong, which demolished old residential buildings and built new residential apartments and low-rise multifamily residential buildings. But the AL_D010 shapefiles do not include such redevelopment projects, but remain the old residential buildings. As a result, areas with new redevelopment projects are manually adjusted by removing all the buildings that are in the redevelopment project zones and adding updated new buildings. When adding updated new buildings to the AL_D010 shapefile, shapefile F_FAC is used, as it is the most updated shapefile (2023). Not only the year 2017, but also the years from the years 2017 to 2024 are checked for the redevelopment project zones, and new buildings are manually added. Information for the new buildings could be estimated using Google Street View, and building heights, building volume, FSI, and GSI are separately calculated using the building information on the internet.

Most of the added buildings are apartments, which have more than 15 floors. To ensure the final shapefiles of each year, the height distribution is checked, which can be easily detected and compared with the Google Street View. In the final step, buildings with less than 1m^2 are considered errors and removed.

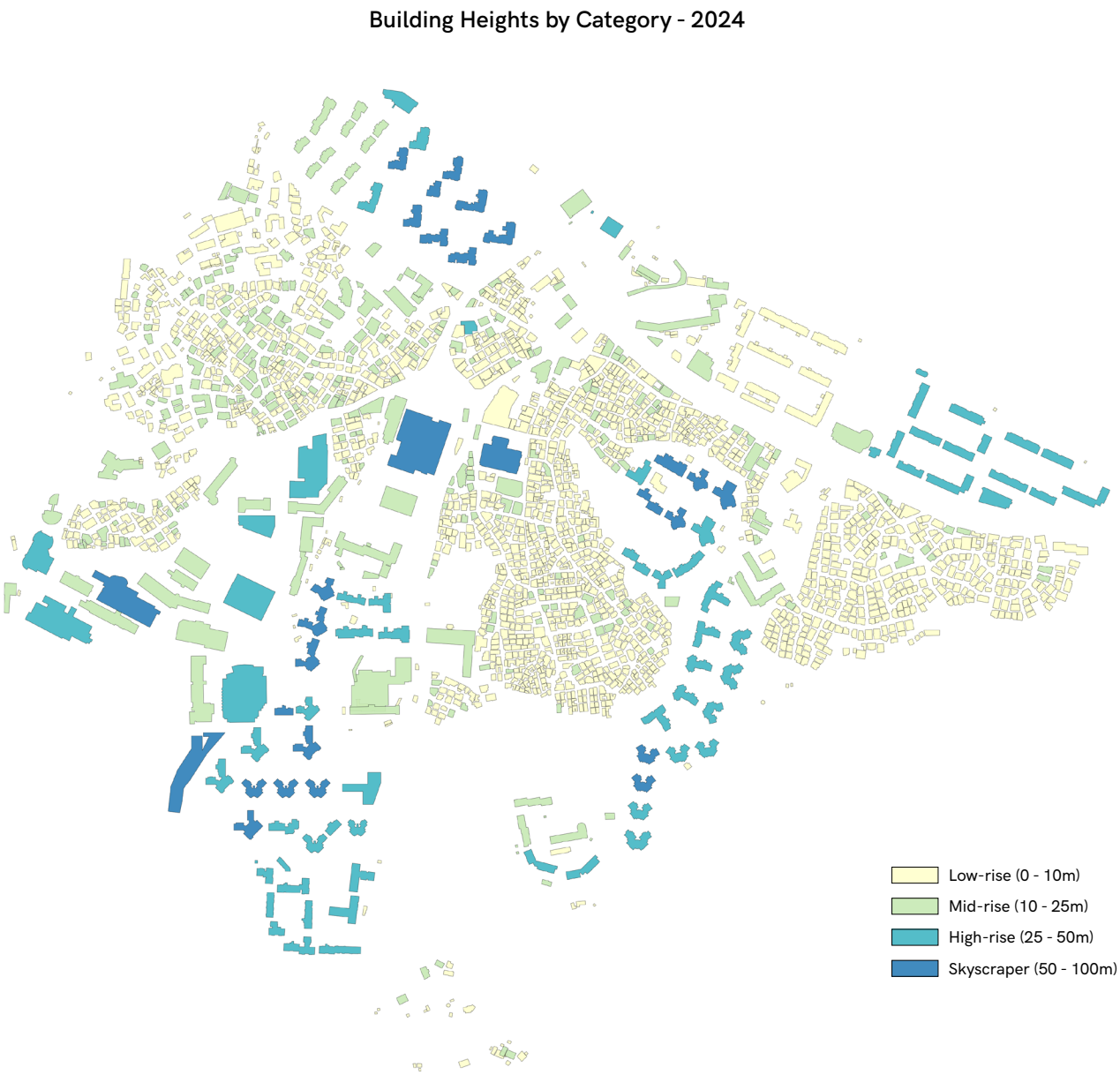

Figure 4.10 *Building heights by category in 2024*

Year	Before	After	Change
2015	3400	3399	- 1
2016	3400	3399	- 1
2017	2945	2862	- 83
2018	2947	2865	- 82
2019	2948	2387	- 561
2020	2933	2372	- 561
2021	2915	2356	- 559
2022	2820	2370	- 450
2023	2821	2371	- 450
2024	3398	2433	- 965

Table 4.6 *Number of buildings before and after processing the shapefile*

4.5 Energy Consumption

Energy consumption data of the buildings is provided by the Korean Architecture HUB (Korean Architecture Hub - Building Energy, 2025). It provides the electricity and gas consumption of the buildings per month, along with the building addresses. Electricity and gas consumption of the buildings that are in the research area are manually downloaded.

No.	Site location	District code	Neighborhood code	Y/M of use		New address road code	Amount used (kWh)
1	서울특별시 동작구 흑석동 1-3	11590	10500	202008		115903119009	765
2	서울특별시 동작구 흑석동 4	11590	10500	202008		115903119009	9225
3	서울특별시 동작구 흑석동 6-5	11590	10500	202008	...	115903119009	18643
4	서울특별시 동작구 흑석동 6-21	11590	10500	202008		115904157413	4379
5	서울특별시 동작구 흑석동 7-1	11590	10500	202008		115903119009	1876
6	서울특별시 동작구 흑석동 8-30	11590	10500	202008		115903119009	5424

Table 4.7 *2020-August electricity consumption in Heukseok-dong (Korean Architecture Hub, 2025)*

Energy demand data should be merged with the buildings in the final shapefiles of each year. To match energy data with buildings, site location from the energy demand data, and building address from the shapefiles are used. The format of the site location and building address are different, but they used the same numbering, and considers the site location and building address are matched when they shared the same numbering.

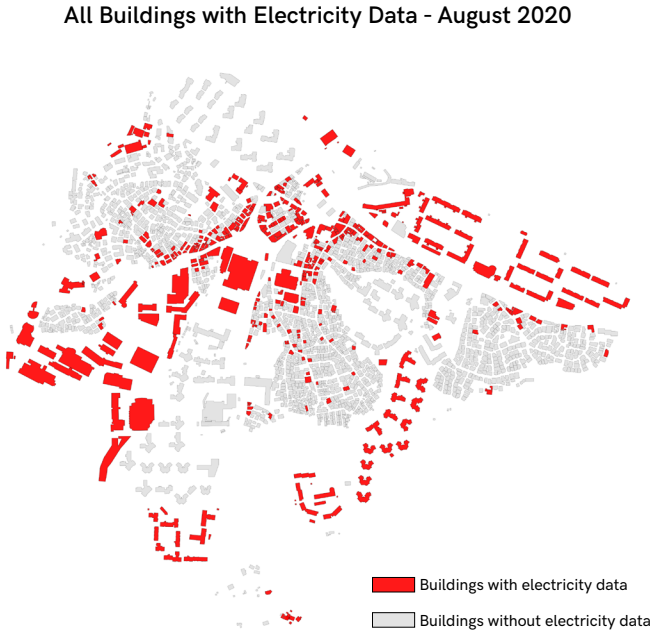

Figure 4.11 *Buildings with electricity data in August 2020*

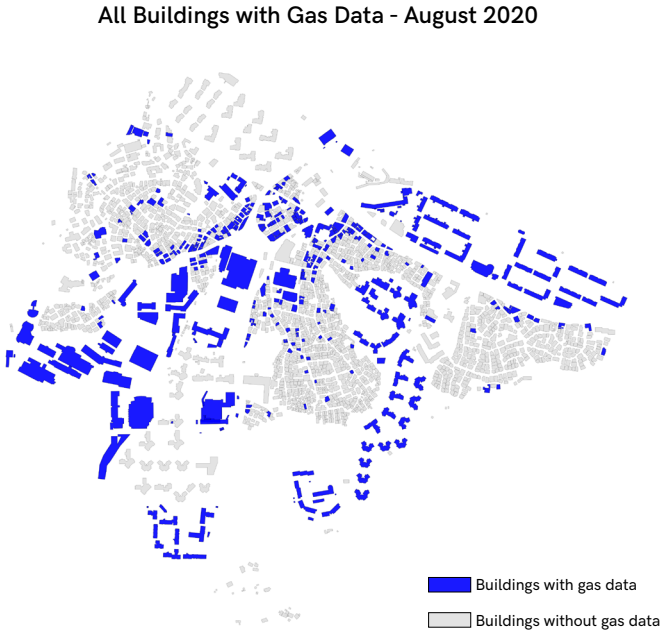

Figure 4.12 *Buildings with electricity data in August 2020*

Figure 4.11 and **Figure 4.12** show the buildings that are matched with electricity and gas consumption data in August 2020. Not all buildings have energy consumption data, however, a significant data limitation arose from the address-level aggregation of energy consumption data. In the study area, 254 addresses correspond to multiple buildings, including the 23 buildings on Chung-Ang University campus and various apartment complexes. Since the energy consumption data is reported at the address level rather than for individual buildings, it is impossible to determine the actual energy demand of each building when multiple structures share the same address.

While Energy Use Intensity (EUI) could be calculated by dividing total energy consumption by Gross Floor Area (GFA) at each address, which is a straightforward but powerful measure of how efficiently building uses energy. This would unrealistically assume that all buildings at the same address, regardless of their size, function, or occupancy patterns have identical EUI for the buildings that share the addresses. Given this limitation and the need for building-specific energy analysis, this research excluded all addresses corresponding to multiple buildings and focused only on addresses that match single buildings, ensuring more accurate representation of individual building energy consumption patterns.

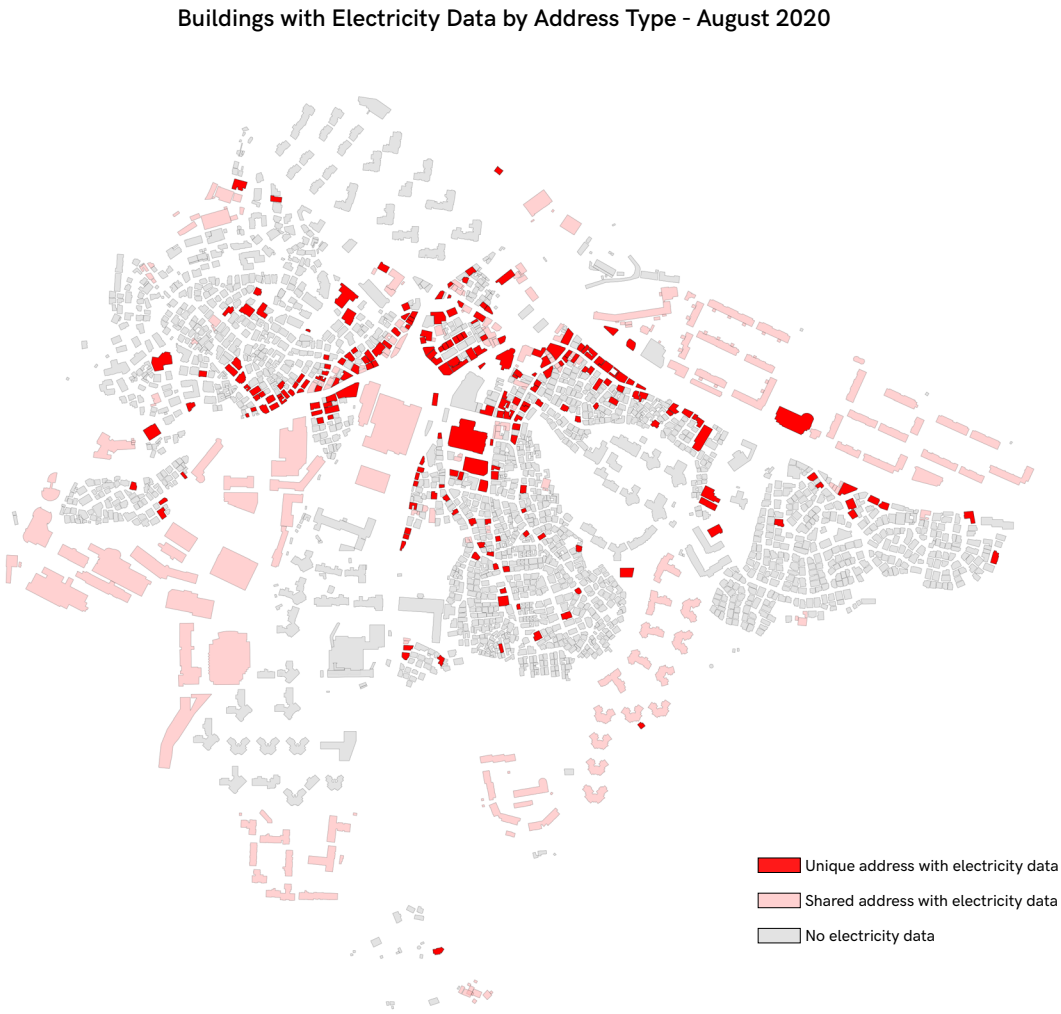

Figure 4.13 *Buildings with electricity data by address type in August 2020*

	Jan	Feb	Mar	Apr	May	Jun	Jul	Aug	Sep	Oct	Nov	Dec
2015	419	425	425	426	427	427	428	432	430	392	383	381
2016	378	375	369	364	362	359	347	351	362	359	359	358
2017	351	351	224	223	224	222	222	214	213	248	245	242
2018	242	242	244	241	236	234	234	238	241	240	239	236
2019	229	229	229	232	237	240	237	239	238	239	243	242
2020	227	227	227	228	227	225	225	224	223	223	225	225
2021	225	277	227	225	225	224	225	225	228	227	228	228
2022	229	228	228	228	228	228	231	232	232	232	225	232
2023	218	212	208	206	204	0	0	0	0	0	0	0
2024	187	188	187	188	188	189	190	191	191	192	190	190

Table 4.8 *Buildings with unique address with electricity data in August 2020*

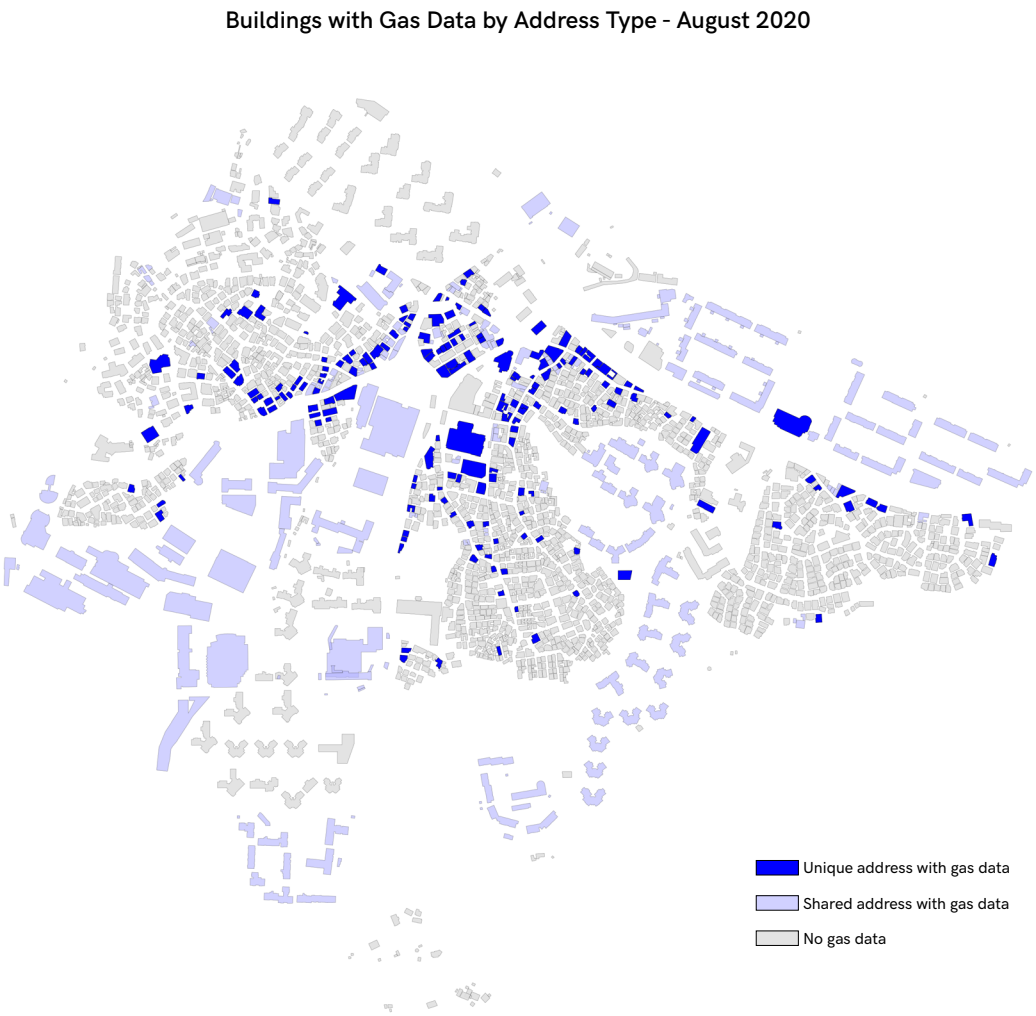

Figure 4.14 *Buildings with gas data by address type in August 2020*

	Jan	Feb	Mar	Apr	May	Jun	Jul	Aug	Sep	Oct	Nov	Dec
2015	419	425	425	426	427	427	428	432	430	307	308	309
2016	306	305	303	297	292	290	244	242	241	244	252	253
2017	258	259	197	196	209	189	186	202	205	206	211	210
2018	209	209	207	203	198	196	193	190	192	197	200	200
2019	199	198	200	198	205	202	202	200	200	201	210	91
2020	199	200	197	195	193	186	183	185	178	185	195	195
2021	197	194	193	193	193	185	184	185	183	191	196	198
2022	200	199	199	199	199	195	188	189	188	190	187	183
2023	173	170	166	165	160	0	0	0	0	0	0	0
2024	150	150	150	147	146	142	142	142	142	141	145	147

Table 4.9 *Buildings with unique address with electricity data in August 2020*

Note that energy consumption data for June through December 2023 was not available from the Korean Architecture Hub database, resulting in zero values for these months in **Table 4.8** and **Table 4.9**. Ultimately, electricity EUI data was obtained for 29,501 building-month records, and gas EUI data for 24,737 building-month records. These represent cumulative counts across all months from 2015 to 2024, not the number of unique buildings. The actual number of unique buildings with energy data varies by month, ranging from approximately 180 to 430 for electricity and 140 to 310 for gas consumption.

05

Methodology

05 Methodology

Although there are various methodologies to convert LST to air temperature, this research employs Multi Layer Perceptron (MLP). The relationship between LST and air temperature is non-linear and complex, which are affected by various factors like solar radiation, greening elements and elevation. MLP's advanced capability to model these relationships makes it more suitable than other conventional methodologies like linear regression or regression kriging. As demonstrated in **Chapter 2.3.3**, comparative studies confirmed that MLP performed the best in LST to air temperature conversion.

5.1 Multi Layer Perceptron (MLP)

The Multi Layer Perceptron (MLP) is a basic type of neural network commonly used in industrial settings and data analysis applications (Kotsiopoulos et al., 2021). An MLP consists of at least three layers: an input layer where data enters the system, one or more hidden layers that process this information, and an output layer that delivers the final results. Each layer contains computing units called neurons that are connected to neurons in the neighboring layers, with each connection having a numerical value called a weight (Gardner & Dorling, 1998).

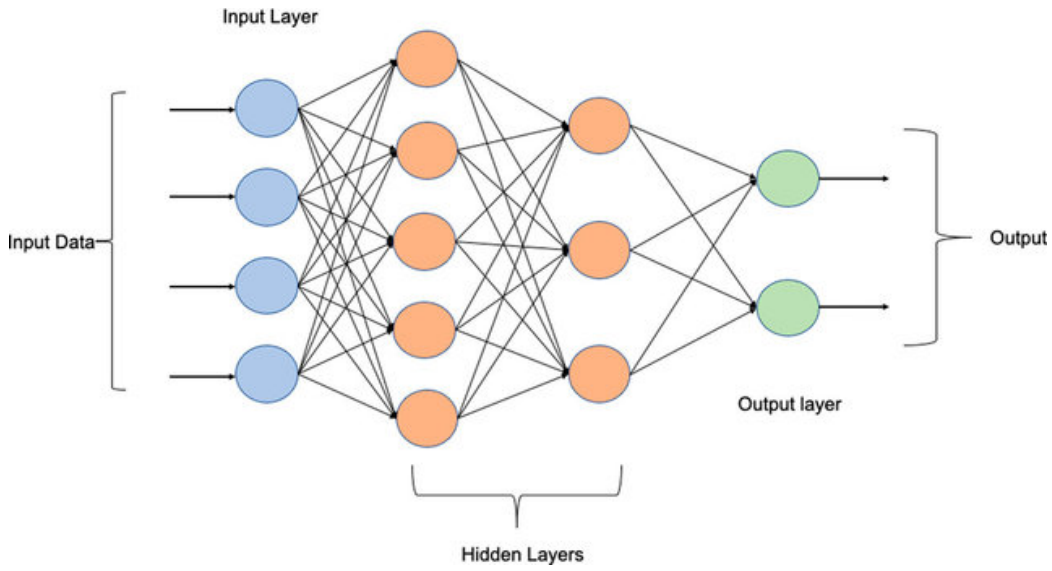

Figure 5.1 *Architecture of Multi layer perceptron*

In an MLP, data moves forward through the network in one direction only. Each neuron receives values from all neurons in the previous layer, multiplies each incoming value by its connection weight, adds these products together, and then applies a mathematical function to produce its output value (Chan et al., 2023). This function, called an activation function, is important because it allows the network to learn complex relationships in the data.

MLPs improve their performance through a learning process called backpropagation. During training, the network compares its predicted output with the correct answer and calculates the difference. This error measurement is then used to adjust the connection weights throughout the network to improve future predictions (Gardner & Dorling, 1998). The network repeats this process many times with different examples until it performs well (Kotsiopoulos et al., 2021).

These networks are effective for both classification tasks (sorting data into categories) and regression tasks (predicting numerical values), making them useful for industrial applications such as predicting equipment failures or identifying product defects (Gardner & Dorling, 1998; Chan et al., 2023). While training an MLP requires significant computing resources and careful selection of settings, their ability to discover patterns in data makes them valuable analytical tools. Unlike more specialized neural networks, MLPs work well with standard table-formatted data and do not need special data structures to perform effectively (Kotsiopoulos et al., 2021).

5.2 Methodology Overview

The methodology employs a two-stage approach to ensure both model accuracy and generalizability. Figure 5.2 shows the complete workflow, demonstrating how satellite-derived inputs and AWS data are processed through the MLP architecture to generate spatially continuous air temperature maps at 30 by 30 meter resolution.

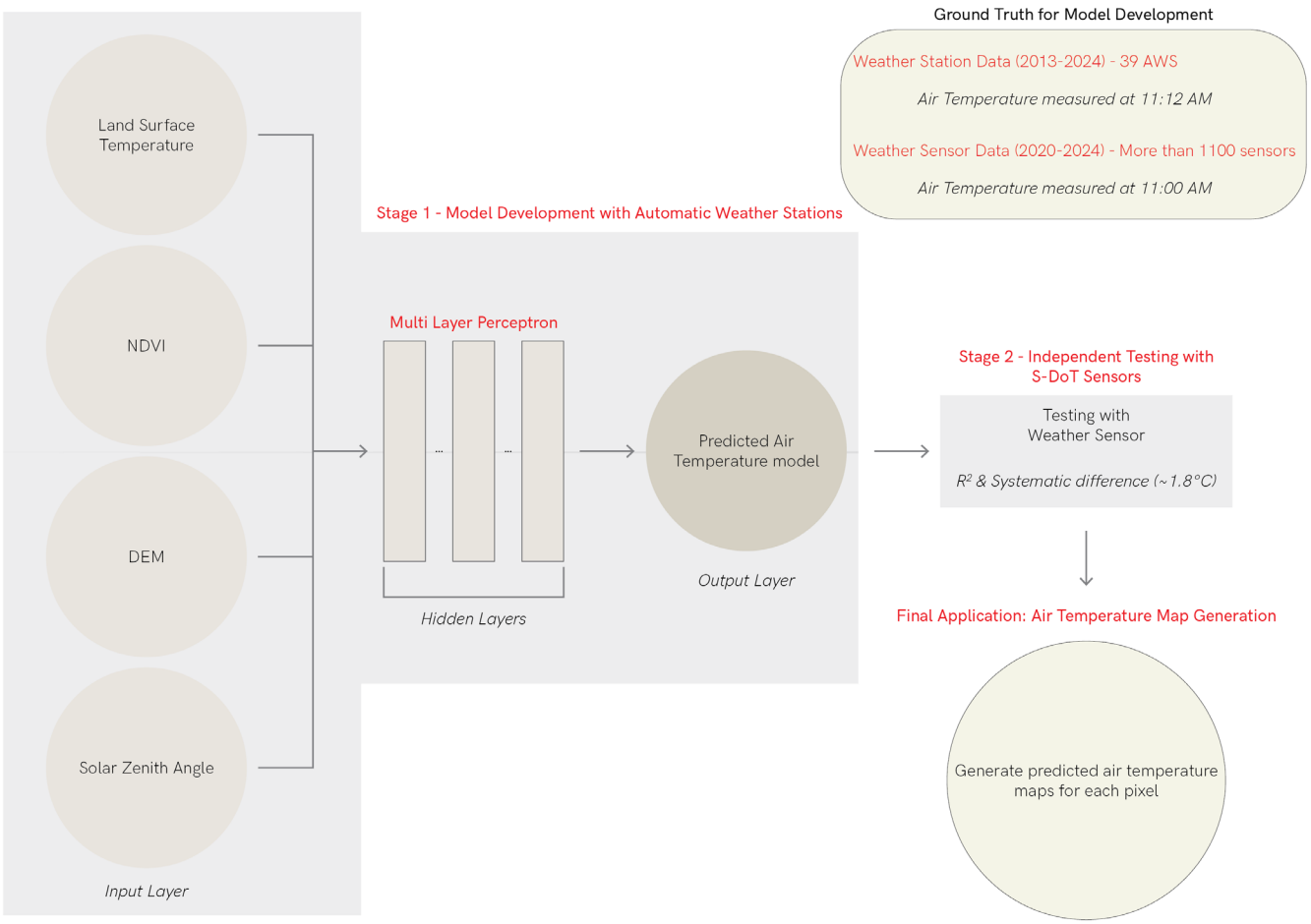

Figure 5.2 *Methodology of MLP*

Stage 1: Model Development with Automatic Weather Stations (AWSs)

Stage 1 focuses on training the MLP using 39 AWSs data as ground truth. AWSs provide accurate air temperature measurements at 11:12 AM from 2013 to 2024, which are precisely matched with the Landsat 8 overpass time. The MLP model learns the complex non-linear relationships between 4 input variables: Land Surface Temperature (LST), Normalized Difference Vegetation Index (NDVI), Digital Elevation Model (DEM), and Solar Zenith Angle (SZA), and the measured air temperature from AWSs. This stage employs a 70-15-15 split for training, validation and testing.

Stage 2: Independent Testing with S-DoT sensors

Stage 2 tests the trained model using independent data from over 1,100 S-DoT sensors across Seoul since 2021. This independent testing confirms the model's performance on a spatially dense network not used during training. According to a report published by the Seoul municipality, S-DoT sensors measure temperatures that are on average 1.8°C higher than AWS measurements during May-August 2020. This systematic difference likely reflects the urban heat island effect, as S-DoT sensors are placed within the urban environment while AWS stations are typically located in more open areas.

5.3 Stage 1: Model Development with Automatic Weather Stations

5.3.1 Input Features

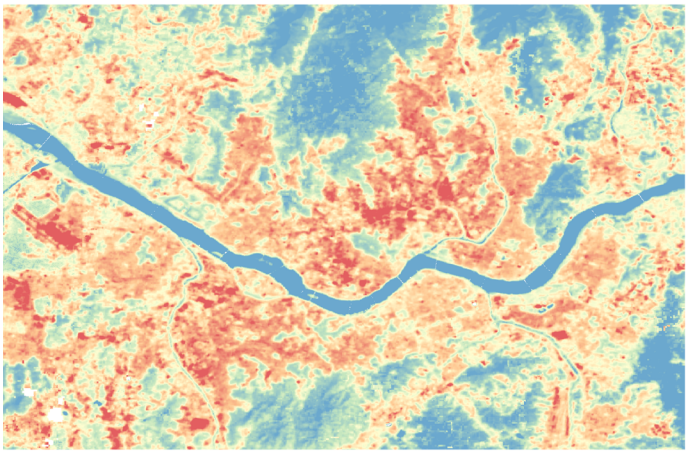

Land Surface Temperature (LST)

LST serves as the primary input, providing thermal information measured by Landsat 8 bands at 11:12 AM. Its relationship with air temperature is complex and nonlinear, influenced by atmospheric conditions. The LST values extracted at each AWS location creates the basis for learning this relationship.

Normalized Difference Vegetation Index (NDVI)

NDVI represents vegetation greenness, which significantly affects the LST and air temperature relationship through the evapotranspiration process. Areas with dense vegetation typically show smaller differences between LST and air temperature due to cooling effects, while built-up areas show larger temperature differences. NDVI values range from -1 to 1, with higher values indicating denser vegetation.

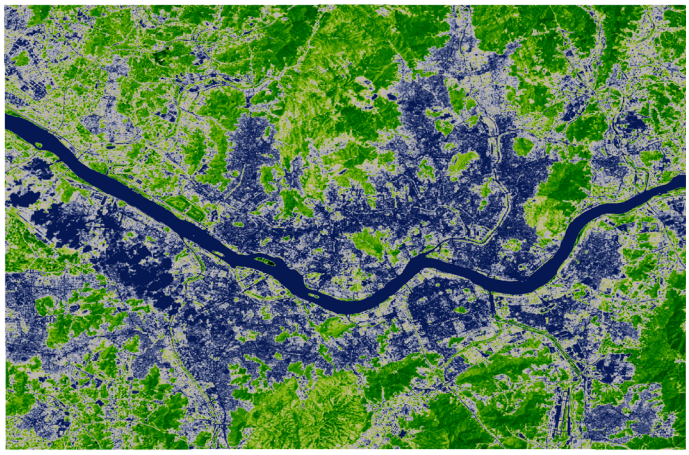

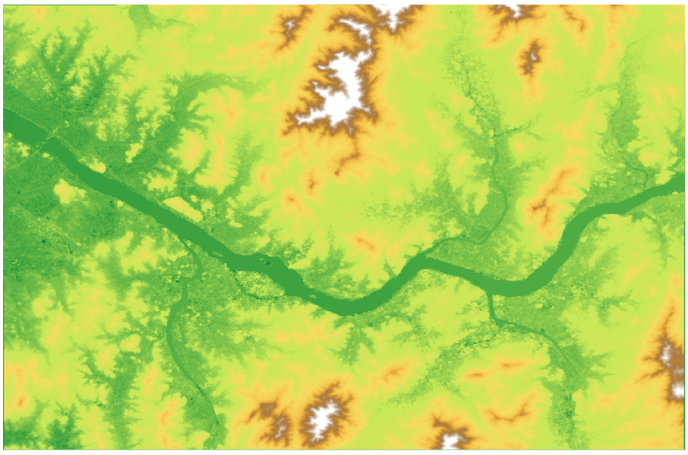

Digital Eleveation Model (DEM)

DEM represents terrain elevation, affecting air temperature through the environmental lapse rate where temperature decreases approximately 6.5°C per 1000m elevation gain. In Seoul's urban context, elevation influences wind exposure and cold air pooling, making it an essential predictor for temperature estimation.

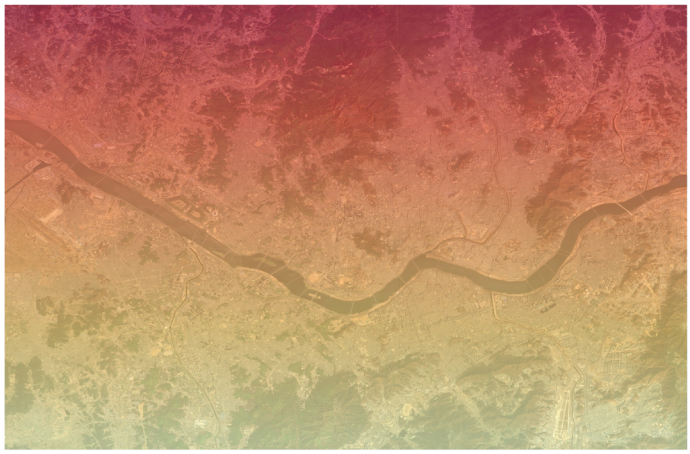

Solar Zenith Angle (SZA)

SZA represents the angle between the sun and the vertical direction, which determines the intensity of solar radiation. It influences the amount of solar radiation reaching the surface, affecting both LST and air temperature. The SZA is obtained based on the Landsat acquisition time and geographic coordinates.

5.3.2 MLP Architecture

The MLP employs a four hidden layer architecture with an input layer of 4 features and an output layer that progressively reduces the number of neurons from input features to air temperature prediction. This funnel-shaped design enables hierarchical feature learning while maintaining computational efficiency.

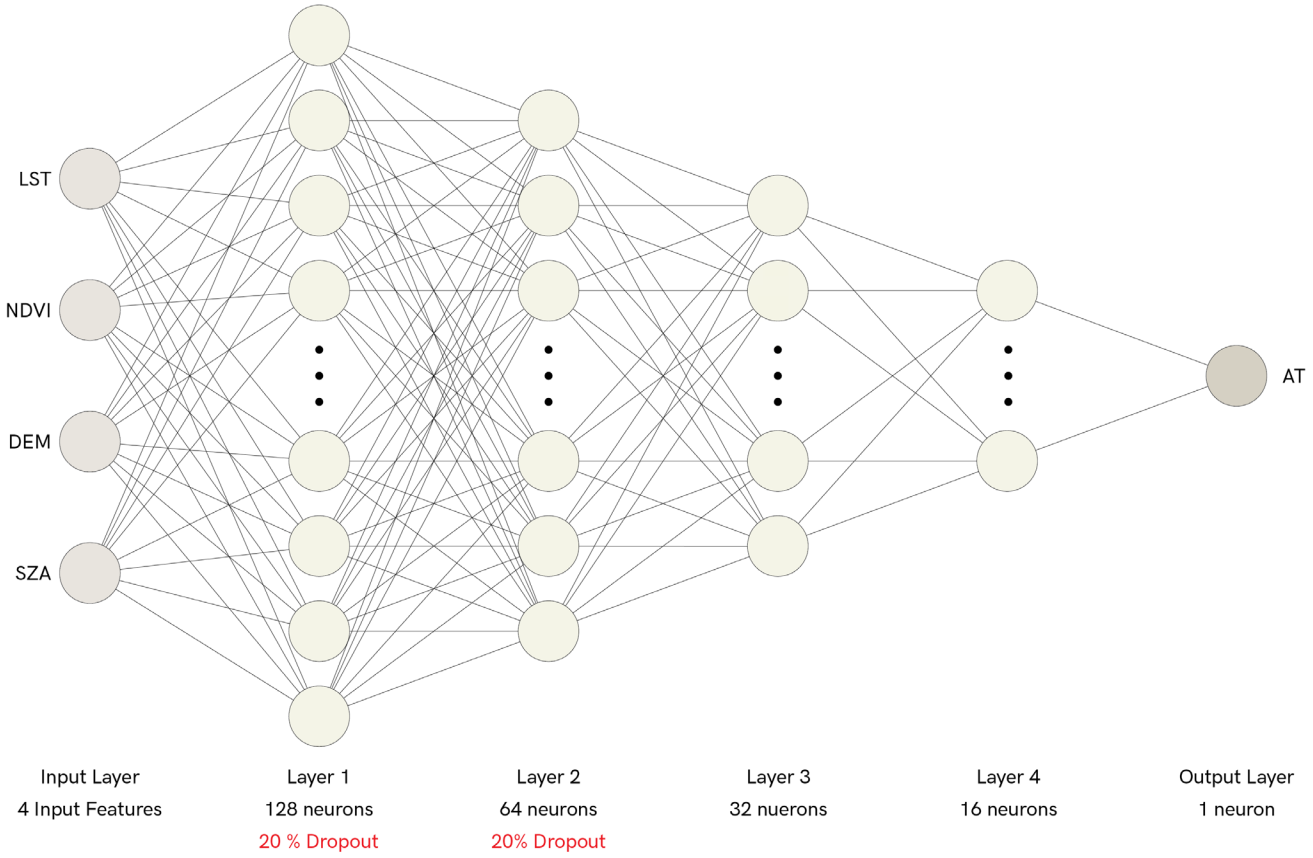

Figure 5.3 *MLP of five-layer dense architecture with dropouts*

Input Layer	4 Input features (LST, NDVI, DEM, SZA)
Layer 1	128 neurons with ReLU activation & 20% dropout
Layer 2	64 neurons with ReLU activation & 20% dropout
Layer 3	32 neurons with ReLU activation
Layer 4	16 neurons with ReLU activation
Output Layer	1 neuron for air temperature prediction

The choice of 128 neurons in the first hidden layer follows established practices in neural network design for regression tasks with limited input features. With only 4 input features (LST, NDVI, DEM, SZA), starting with 128 neurons provides sufficient capacity to capture non-linear interactions without excessive parameterization. This follows the common heuristic of having the first hidden layer size as a power of 2 between 2-5 times the number of inputs (Heaton, 2008). The 32:1 ratio (128 neurons to 4 inputs) allows the network to learn complex feature combinations while the subsequent layers progressively compress these representations. This architecture size has proven effective in similar atmospheric and environmental prediction tasks where the relationship between inputs and outputs involves multiple non-linear interactions (Rasp et al., 2018).

20% dropout is applied to the first 2 hidden layers. Dropout is one of the most popular regularization methods for preventing neural network models from overfitting in the training phase (Salehin & Kang, 2023). The dropout technique deactivates 20% of neurons during training, which allows the model to learn redundant representations and prevent overlapping features.

The Rectified Linear Unit (ReLU) activation function is used throughout the hidden layers. ReLU provides computational efficiency and addresses the vanishing gradient problem that affects traditional activation functions in deep networks (Glorot et al., 2011). ReLU enables the model to learn non-linear mappings while maintaining gradient flow during backpropagation. The output layer employs linear activation, appropriate for continuous temperature prediction.

5.3.3 Training Process

The MLP model follows a 70-15-15 split for training, validation, and testing sets respectively. The 70-15-15 split represents an optimal balance for air temperature prediction. Hastie et al. (2009) mentioned that having at least 50% of data for training in nonlinear models is recommended to ensure learning capacity, with 70% providing additional robustness for capturing complex nonlinear relationships. The 15% validation provides stable estimates for early stopping and hyperparameter selection in neural networks. The 15% for testing set aligns with best atmospheric science applications. Rasp et al. (2018) used the same proportions in their neural network of atmospheric research and mentioned that climate prediction models require substantial test sets to evaluate performance across diverse conditions. The 15% test ensures statistical reliability or performance, while maximizing available training data.

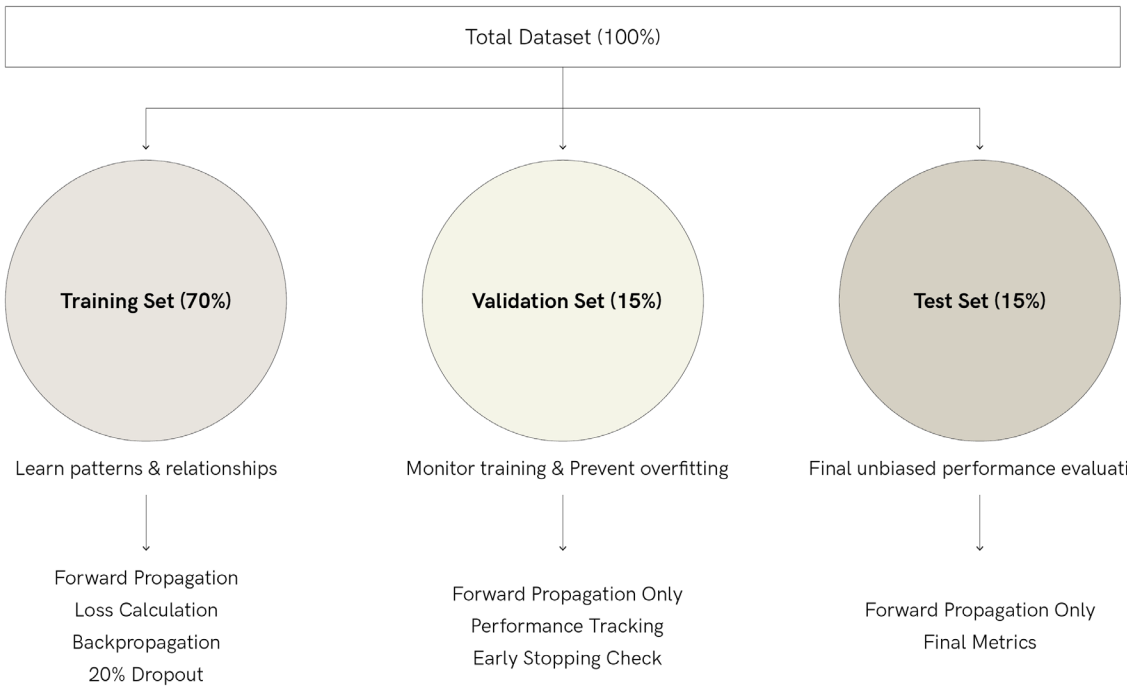

Figure 5.4 *Training set, validation set, and test set in MLP*

Training Set (70%)

The training serves as the primary source for model training. During the training phase, it undergoes complete forward and backward propagation cycles. In forward propagation, input features go through all hidden layers, with each neuron computing weighted sums and applying activation functions to generate predictions. The Mean Squared Error (MSE) loss is calculated by comparing predicted temperatures with AWS measurements. Backpropagation computes gradients, propagating error signals backwards through the neurons to update weights. The 70% ensures sufficient data diversity to capture temperature variations and patterns while maintaining adequate data for validation and testing.

Validation Set (15%)

Validation is important in the model, which does not participate in the learning process. After each training epoch, the validation data undergoes forward propagation only, without weight updates or backpropagation. It provides an unbiased estimation of model performance during training. The validation loss serves as the primary metric for early stopping, with training ending if no improvement is made for 20 consecutive epochs. This mechanism prevents overfitting by halting training at the point of optimal generalization rather than continuing until the model memorizes training data (Prechelt, 2012).

Test Set (15%)

The 15% test set remains isolated throughout the training and validation process, which only provides a final assessment of the model's performance. There is only forward propagation after all training is complete. The test set evaluation indicates the final performance metrics, including R^2, root mean squared error (RMSE), mean absolute error (MAE), and coefficient of variation of the root mean squared error (CVRMSE).

Implementation Details

The model employs several key parameters that control how the learning process unfolds. Each parameter serves a specific purpose in ensuring efficient and stable training.

The Adam optimizer guides how the model updates its weights during training. It adapts the learning rate for each weight individually, which keeps track of the average gradients and their squared values over time. This approach helps the model learn more efficiently, and parameters with consistent gradients receive larger updates, while those with fluctuating gradients receive smaller ones. Adam also incorporates momentum, which helps the optimization process continue moving in productive directions and avoid getting stuck in local minima (Kingma & Ba, 2014).

The learning rate 0.001 is used in weight updates. When the learning rate is too large, it might cause the model to overshoot optimal values, while one that is too small would make training extremely slow. The value of 0.001 is a widely tested starting point that provides stable convergence for neural networks across various applications (Bengio, 2012).

The model uses a batch size of 32, which processes 32 training examples before updating its weights. Instead of updating after every single batch or waiting until all batches are processed, training with 32 batches makes a balance. Processing 32 batches provides a more stable estimate of gradient direction while keeping computational requirements. 32 batch size provides a sufficient gradient averaging to smooth out the randomness inherent in individual samples (Masters & Luschi, 2018).

The model trains for a maximum of 200 epochs, where each epoch represents one complete pass through the entire training dataset. However, due to early stopping, training rarely continues for all 200 epochs. Early stopping patience with 20 epochs is used in this model, which monitors the validation loss after each epoch. If the validation loss does not improve for 20 consecutive epochs, training is automatically stopped. It prevents the model from overfitting, which prevents the model from memorizing training data. The patience of 20 epochs allows for natural variations in the learning process, as validation loss might slightly increase before improving again.

5.4 Stage 2: Independent Testing with S-DoT Sensors

Stage 2 of the methodology tests the trained MLP model using an independent dataset from over 1,100 S-DoT sensors throughout Seoul. This stage serves a distinct purpose from the validation set used during training, as it tests the model's performance on a completely different measurement system with known systematic temperature differences.

5.4.1 Independent Testing Methodology

The independent testing begins after the MLP model has completed training using the AWS data. The trained model generates air temperature predictions at each S-DoT sensor location by extracting the corresponding LST, NDVI, DEM, and SZA. These predictions are then directly compared with the actual air temperature measurements from the S-DoT sensors at 11:00 AM, which is the closest available time to the 11:12 AM Landsat overpass time.

This independent testing differs from the validation set in the training process. While the training validation set consisted of AWS data, the S-DoT sensor testing uses data from an entirely different sensor network. The S-DoT sensors are more densely distributed across Seoul, which provides a spatial testing that the sparse AWS can not provide. The dense network captures microclimate variations within the urban environment, testing the model's ability to predict air temperatures at locations far from any training stations.

5.4.2 Systematic Temperature Difference Approach

The S-DoT sensors show a known systematic temperature difference compared to AWS measurements. According to the Seoul Research Data Service documentation, S-DoT measurements were found to be approximately 1.8°C higher than AWS measurements during May-August 2020. This temperature difference reflects the distinct environments where these sensors are placed. S-DoT sensors are installed within the urban canopy among buildings and streets where heat accumulates, while AWS are positioned in relatively open areas following meteorological standards. This placement difference captures the urban heat island effect, with S-DoT sensors experiencing the elevated temperatures created by surrounding buildings, reduced ventilation, and heat-absorbing surfaces.

The testing process examines whether the MLP model, trained on AWS data, maintains predictions closer to AWS temperatures when applied to S-DoT sensor locations. While the 1.8°C difference was specifically measured during summer 2020, it provides a reference point for understanding the systematic temperature difference between the two sensor networks. The average difference between model predictions and S-DoT measurements helps evaluate the model's consistency and its ability to predict air temperatures rather than sensor-specific readings, acknowledging that this systematic difference may vary seasonally and annually.

5.4.3 Spatial and Temporal Considerations

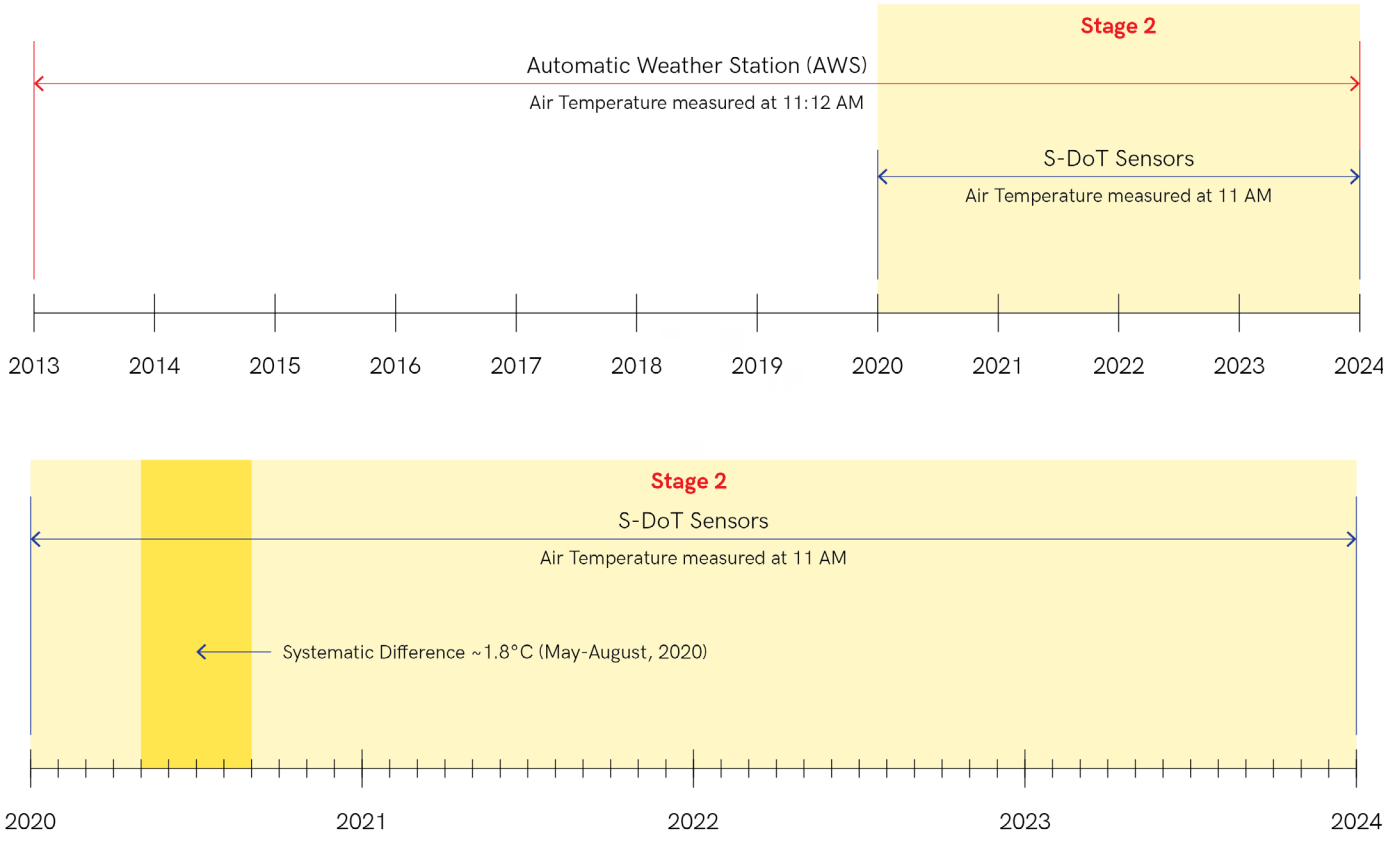

Figure 5.5 *Temporal differences between AWS and S-DoT sensors*

Stage 2 independent testing incorporates both spatial and temporal dimensions to evaluate the model performance. It examines how prediction accuracy varies across Seoul, and the high density of S-DoT sensors allows assessment of the model's spatial interpolation, especially in areas distant from AWS stations. The testing utilizes S-DoT data from 2020 to 2024, overlapping with AWS data throughout this period.

The analysis examines the mean difference between predicted air temperature from the MLP model and S-DoT sensor measurements. While the systematic temperature difference of 1.8°C between S-DoT and AWS was specifically documented for May-August 2020, this value provides a reference point for understanding the expected difference between the two sensor networks. The testing evaluates whether model predictions maintain consistency with AWS temperature patterns when applied across the entire S-DoT network from 2020-2024, acknowledging that the systematic temperature difference may vary seasonally and annually. Unlike the MLP training phase, this reflects the model's performance on a truly independent dataset with different measurement characteristics. The successful testing against S-DoT sensors, despite the systematic temperature difference between sensor types, demonstrates the model's robustness and applicability for generating air temperature maps across Seoul.

5.5 Final Application: Air Temperature Map Generation

After the 2-stage development and testing stages, the trained MLP model is applied to generate the final predicted air temperature maps for all Landsat 8 images. The final application deploys insights from both stages to create reliable air temperature predictions across Seoul.

In Stage 1, the model developed using AWS as a ground truth data provides the fundamental air temperature prediction capability, which learns the complex nonlinear relationship between LST, NDVI, DEM, SZA, and air temperature. The Stage 2 independent testing with S-DoT sensors confirms the model's spatial generalization ability, which demonstrates consistent performance even in areas without AWSs. These 2-stage approaches ensure reliability in applying the model across all pixels. During operational application, each 30 by 30 meters (23.81 by 29.91 meters) pixel in the Landsat pictures undergoes forward propagation through the trained model. The absence of dropout during inference ensures that decision outputs will involve all neurons contributing to the final prediction. This process generates continuous temperature surfaces that capture microclimate-scale temperature variations.

The Stage 2 independent testing results inform the interpretation and application of these predictions. The dense S-DoT network confirms the model's ability to interpolate between sparse training locations, supporting its application to all pixels regardless of AWS vicinity. While S-DoT sensors show systematic temperature differences compared to AWS data, the model maintains alignment with AWS temperature patterns, ensuring scientific consistency of the output air temperature maps.

The final predicted air temperature maps at 30-meter resolution between 2013 and 2024 provide high-resolution spatial thermal data that are important and necessary for analyzing relationships between urban form elements and building energy consumption. However, these maps are not sufficient for comprehensive energy analysis due to their temporal limitations. With only 1-2 snapshots per month at 11:12 AM, the data cannot capture diurnal temperature variations that drive daily energy consumption cycles, nor can they represent peak cooling or heating conditions that typically occur at different times of day. This research therefore focuses on spatial relationships at the specific satellite overpass time, acknowledging that the correlations found represent only a partial view of the complex temporal dynamics between temperature and energy consumption. The analysis examines how urban form relates to both temperature and monthly energy consumption at this specific time, rather than attempting to model full diurnal or sub-daily energy patterns.

5.6 Urban Form Elements Importance

Figure 5.6 *Methodology of urban form elements importance*

Analyzing the relative importance and directional relationships between UFEs, air temperature, and building energy consumption provides a comprehensive outline for urban planners and policymakers to design urban layouts to make cities more sustainable. The analysis employs 2 complementary statistical methods to address the challenge of highly correlated urban form elements in dense urban environments.

The analysis examines 6 UFEs: NDVI, building ratio, weighted height, FSI, GSI, and building volume. These elements often show strong intercorrelations in urban areas, where areas with high vegetation typically have a lower building ratio, while building height is highly correlated with FSI. Traditional statistical methods struggle with such multicollinearity, which would produce unreliable and misleading results. Therefore, this research uses the Genizi method to quantify relative importance and Partial correlation to determine directional relationships.

The analysis consists of 2 parts: Temperature analysis and Energy analysis, with multiple spatial scales to capture both immediate and neighborhood effects. Temperature analysis examines pixel-level and averages within 100m and 300m buffers from the centroids of each pixel, while energy analysis focuses on 100m and 300m buffers around building centroids. This multi-scale approach determines thermal and energy consumption patterns differently for urban form at various spatial extents.

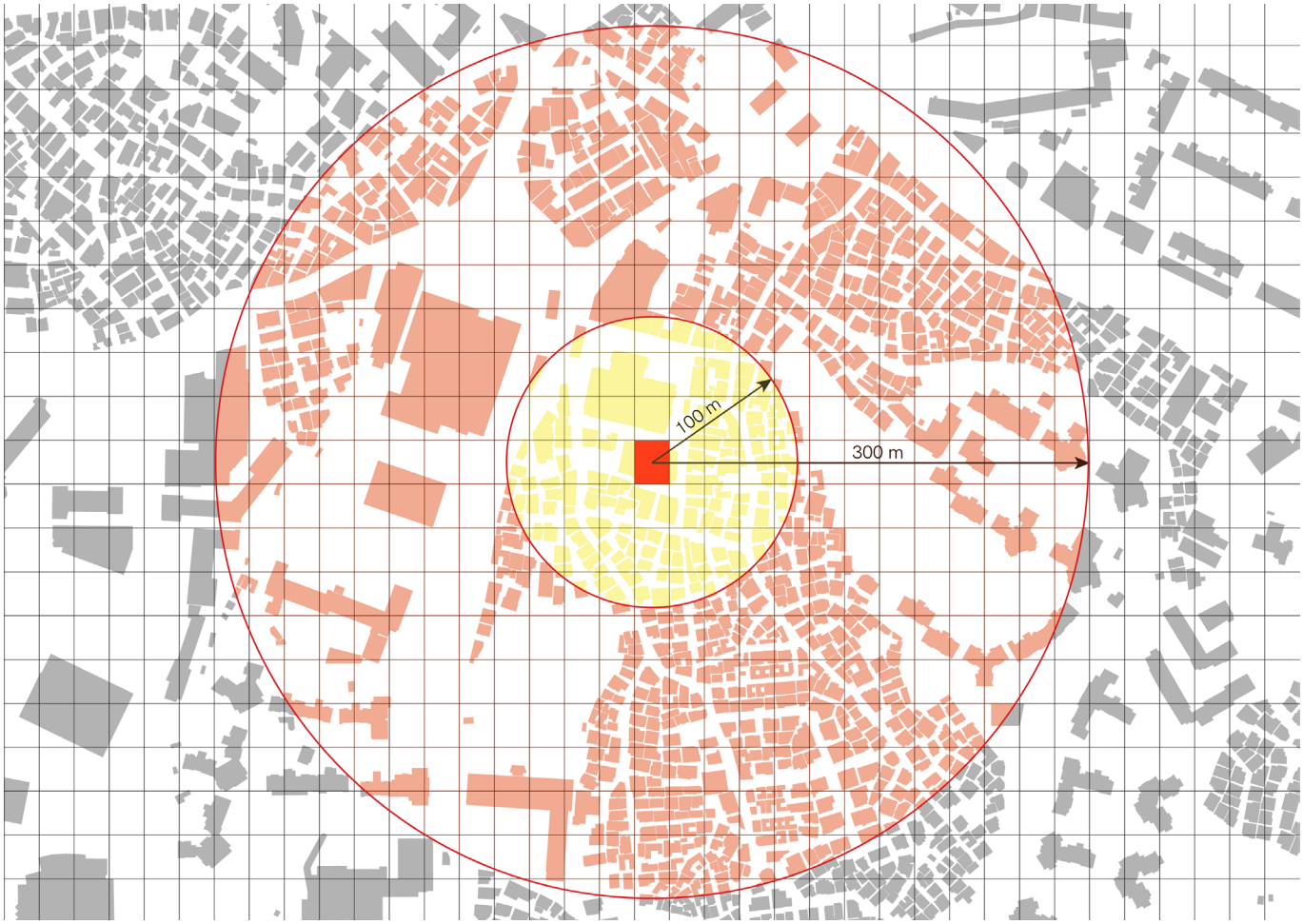

Figure 5.7 *Sptial scales in temperature analysis*

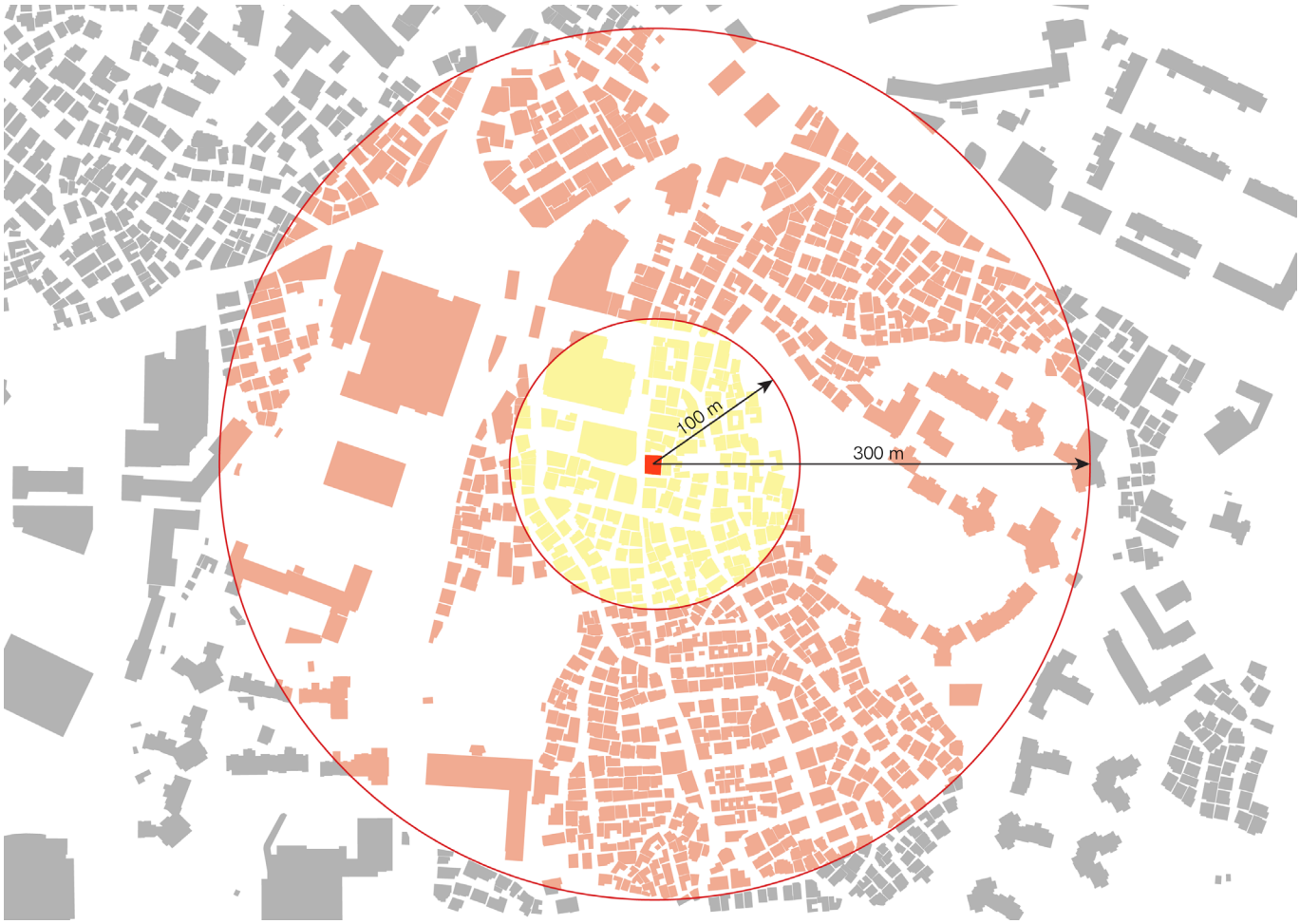

Figure 5.8 *Spatial scales in energy consumption analysis*

5.6.1 Genizi Method

Genizi Method Principle

The Genizi method works by decomposing the total R^2 from a multiple regression model to determine how much each predictor contributes to the explained variance. The method takes as inputs the correlation matrix between all predictor variables and the dependent variable, along with the regression coefficients from the full model.

The calculation process involves several steps. First, it computes the direct contribution of each variable. Second, it calculates the shared contributions between pairs and groups of variables that arise from their correlations. Third, and most importantly, it allocates these shared contributions back to individual variables based on their relative strengths in the model. For example, if NDVI and building ratio are negatively correlated and the combination explains 30% of temperature variance, the Genizi method determines how much of that 30% should be attributed to each variable based on their regression coefficients and individual correlations with temperature.

The outputs are percentage contributions for each predictor that sum to the total R^2 of the model. Unlike other standardized regression coefficients, which can be misleading when predictors are correlated, the Genizi method represents the true relative importance of each variable after accounting for multicollinearity. A variable showing 25% importance genuinely contributes one-quarter of the model's explanatory power, regardless of its correlations with other predictors. This makes the Genizi method particularly valuable for urban studies where factors like vegetation and building density are highly correlated, it allows researchers to understand which urban form elements truly drive temperature and energy patterns.

Temperature Analysis

The temperature analysis uses the Genizi method at three spatial scales: At the pixel level, each 30 by 30 meters (23.81 by 29.91 meters) cell's air temperature, derived from MLP, serves as the dependent variable, with the 6 UFEs at the exact location as predictors. This fine-scale analysis captures immediate temperature variations in relation to local urban form. UFE values are averaged within 100m and 300m buffers centered on each pixel. The 100m buffer represents the immediate thermal environment, which captures nearby effects, while the 300m buffer extends to the neighborhood scale, incorporating broader urban morphology patterns that influence local climate.

The implementation enables seasonal variation. The method uses 4 seasons: Spring (March, April, May), Summer (June, July, August), Fall (September, October, November), and Winter (December, January, February). NDVI in summer is typically higher than in winter, and if the approach does not consider seasonal effects, the results would not be reliable and trustworthy. The Genizi method quantifies these seasonal shifts in relative importance, providing percentage contributions for each UFE that vary by season and 3 different spatial scales.

Energy Consumption (EUI) Analysis

The Genizi method is also used to analyze energy consumption in EUI at the building level, with electricity and gas consumption as separate dependent variables. The predictor variables combine 2 types of measurements: environmental context and building-specific variables.

NDVI and building ratio are considered as environmental context variables, which are averaged within 100m and 300m buffers around each building's centroid that have energy consumption data. These buffers capture the surrounding urban environment that influences building energy consumption, and using average values ensures these environmental variables represent neighborhood conditions rather than point measurements.

Other UFEs (Building height, FSI, GSI, and building volume) are regarded as building-specific variables, which are used with the actual values for each individual building. This approach recognizes that a building's own physical characteristics directly determine its energy consumption through several factors. Using actual values rather than averaged values for building-specific variables maintains the direct physical relationship between building form and energy consumption pattern.

5.6.2 Partial Correlation

While the Genizi method shows the relative importance of each UFE, it does not show the directional relationships. A key distinction is that partial correlation produces signed coefficients (-1 to +1) indicating whether each UFE increases or decreases temperature and energy consumption, while the Genizi method only provides unsigned importance values. Partial correlation analysis can be used with the Genizi method by indicating whether each UFE has a positive or negative effect on air temperature and energy consumption, while controlling for the influence of other variables, which are often represented as heatmaps.

Partial Correlation Principle

Partial correlation measures the linear relationship between two variables while controlling for the effects of other variables in the system. The method takes as inputs the complete correlation matrix of all variables (both predictors and dependent variables) and calculates the correlation between any two variables after removing the linear effects of all other variables.

The calculation process involves matrix operations on the correlation or covariance matrix. For example, to find the partial correlation between NDVI and air temperature while controlling for building ratio, height, FSI, GSI, and volume, the method first removes the variance in both NDVI and temperature that can be explained by these other variables. It then calculates the correlation between the residual variations. Mathematically, this is computed using the inverse of the correlation matrix, where the partial correlation between variables i and j is calculated as -P(i,j)/sqrt(P(i,i)*P(j,j)), where P is the inverse correlation matrix.

The outputs are correlation coefficients ranging from -1 to +1 for each predictor-outcome pair. A value of -0.4 for NDVI means that, holding all other urban form elements constant, areas with higher NDVI tend to have lower temperatures. Unlike zero-order correlations which can be misleading when variables are intercorrelated, partial correlations reveal the unique relationship between each predictor and outcome. These values indicate both the strength (absolute value) and direction (positive or negative) of relationships. In this research, these coefficients are visualized as heatmaps where blue represents cooling effects (negative correlations) and red represents warming effects (positive correlations), providing an intuitive understanding of how each urban form element influences temperature and energy consumption when other factors are held constant.

Temperature Analysis

For temperature analysis at the pixel level, partial correlations reveal the direct relationship between each UFE and air temperature at 3 spatial scales. Partial correlation examines the direction and strength of linear relationships, unlike the Genizi method, which decomposes total variance to show how much each UFE contributes. The analysis examines correlations while controlling for the other 5 UFEs, which is to answer like "What is the relationship between NDVI and air temperature if all buildings had the same height, FSI, GSI, building ratio, and volume?".

At each spatial scale, the partial correlation produces a matrix of partial correlations accompanied by significance tests. These statistical measures provide information that the Genizi method cannot produce, which is the reliability and precision of each UFE relationship. This method can help urban planners to clarify how to increase or decrease each UFE to achieve the desired air temperature.

Energy Consumption (EUI) Analysis

The energy consumption analysis implements partial correlation to determine directional relationships between UFEs and building energy consumption in EUI. Partial correlation provides signed coefficients that explicitly show whether each UFE contributes to an increase or decrease in energy consumption of the building.

The analysis uses the same structure as the Genizi method. The environmental variables averaged within buffers and building-specific variables using actual values. For each UFE, the partial correlation generates correlation coefficients that indicate both direction and magnitude of association with energy consumption after removing the confounding effects of other urban form elements.
Moreover, partial correlation enables direct comparison between electricity and gas consumption patterns. While the Genizi method's importance percentages must be interpreted separately for each energy type, partial correlation coefficients can reveal opposing relationships, such as vegetation showing negative correlation with electricity (cooling effect) but positive correlation with gas (increased heating in green areas). This directional information, combined with the Genizi method results, provides a complete picture of how UFEs influence energy consumption, which can guide urban planners on which elements to prioritize and in which direction to modify them.

5.7 Changes over a Decade

Examining changes over a decade offers important insights into the relationship between urban form evolution and air temperature variations. This analysis examines the transformation of UFEs and air temperature in Heukseok-dong between 2015 and 2024, with additional focus on a specific district as a detailed case study. This temporal monitoring captures both area-wide development trends and localized changes, demonstrating how urban morphology and thermal conditions have evolved together over the decade.

5.7.1 Changes in Heukseok-dong

The methodology follows changes by calculating yearly average values across the Heukseok-dong from 2015 to 2024. The analysis follows:

- Seasonal average values for air temperature and NDVI, calculated separately for spring, summer, fall, and winter each year.

- Annual average values for building ratio, building height, FSI, GSI, and building volume.

For air temperature and NDVI, seasonal averages capture the varying impacts throughout the year. These seasonal analysis aligns with Heukseok-dong's climate patterns and vegetation cycles. The other 4 UFEs use annual averages, as they are stable urban characteristics that do not change seasonally.

5.7.2 District 3 Case Study

Figure 5.9 *Location of District 3 in Heukseok-dong (red)*

As **Chapter 3.3.1** mentioned that there were several districts in Heukseok-dong undergoing redevelopment, which are valuable opportunities to examine substantial UFE and air temperature changes over the past decade. This research specifically focuses on District 3 in southern Heukseok-dong, which underwent a major transformation from 2018 to 2022. The temporal monitoring methodology is applied specifically to this district to document its distinct evolution patterns. The same methodology is applied exclusively to District 3.

- Seasonal values for air temperature and NDVI within District 3 boundaries
- Annual average values for building ratio, building height, FSI, GSI, and building volume within District 3.

This case study analysis captures how the transformation from low-rise residential to high-rise apartments affected both UFE and environmental conditions. The seasonal air temperature and NDVI data are particularly valuable for understanding how the redevelopment affected the local microclimate across different times of year.

06

Results

06 Results

6.1 MLP Model Performance

The MLP model was developed for converting LST to air temperature using AWS data as ground truth and further tested with an independent S-DoT sensor. The results show the model's effectiveness through both internal evaluation and external testing.

6.1.1 Model Training and Performance Metrics

The MLP model training process converged efficiently, which achieved optimal performance at the 71st epoch out of a maximum of 200 epochs. The earthly stopping monitored validation loss with a patience of 20 epochs, which successfully prevented the model from overfitting while ensuring learning the complex non-linear relationships between LST and air temperature.

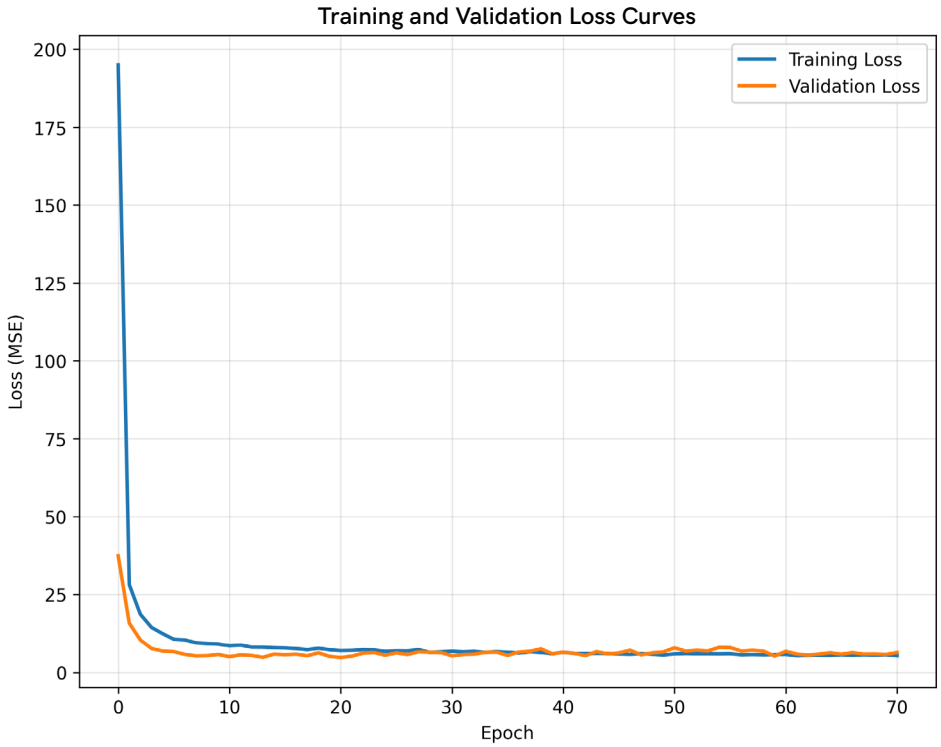

Figure 6.1 *Training and validation loss curves*

The blue line represents training loss, showing how well the model fits the training data with each epoch, while the orange line represents validation loss. Validation loss measures the model's performance on the held-out validation set. Both curves show successful learning behavior, as they decrease rapidly in early epochs as the model learns patterns, then they gradually stabilize from around the 25th epoch. The convergence of both training and validation curves at similar loss values around 30-60 epochs indicates successful training without overfitting. If overfitting had occurred, the validation loss would increase, while the training loss continued to decrease, which creates a divergence. The early stopping activated at epoch 71 when validation loss showed no improvement for 20 consecutive epochs, which prevents unnecessary computation while ensuring learning.

R^2	RMSE	MAE	CVRMSE
0.9684	2.095 °C	1.616 °C	15.50 %

Table 6.1 *Performance metrics of MLP*

The R^2 (coefficient of determination) value of 0.9684 indicates that the model explains approximately 96.8% of the variance in air temperature, demonstrating a strong predictive capability. The performance of this MLP aligns with recent studies in urban temperature estimation, where Salih et al. (2025)'s MLP model using TEMLI obtained an R^2 of 0.91. A high R^2 value can represent a well-captured nonlinear relationship between LST and air temperature.

The RMSE (Root Mean Square Error) of 2.095 °C represents the average magnitude of prediction errors. The RMSE value shows that the model's air temperature predictions are off from the actual measurements from AWS by around ±2.1°C. 2.095 °C RMSE is in a similar range compared to other papers, where Choi et al. (2021) got RMSE of 2.19 °C using an artificial neural network (ANN).

The MAE (Mean Absolute Error) of 1.616 °C provides the average absolute difference between predicted and actual air temperatures, while the CVRMSE (Coefficient of Variation of RMSE) of 15.50% represents the normalized error relative to the mean air temperature, which suggests that the typical error is about 15.50% of the average air temperature.

6.1.2 Independent S-DoT Testing Results

The trained MLP model is further tested with independent S-DoT sensors. The independent testing using S-DoT sensors provides crucial evidence of the model's real-world applicability beyond the trained model.

The analysis was conducted in two phases: first examining the specific period (May-August 2020) for which the systematic temperature difference between S-DoT and AWS was documented, then extending to the full available period (2020-2024) to assess long-term model consistency.

May-August 2020 Independent Testing

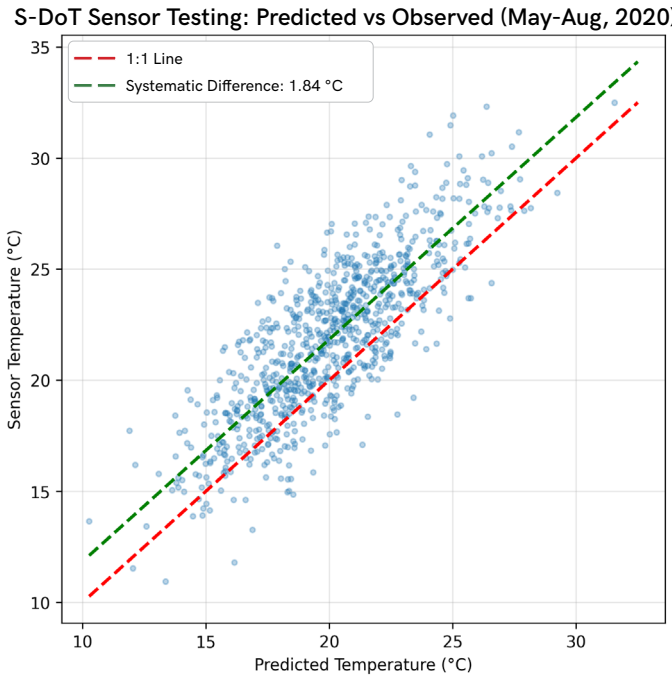

Figure 6.2 *Predicted air temperature testing with S-DoT sensors (May-August, 2020)*

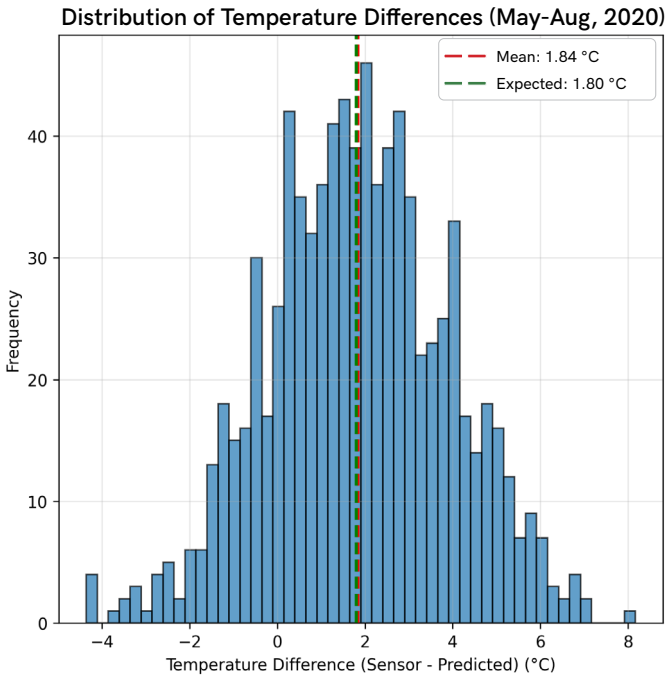

Figure 6.3 *Temperature difference between predicted and measured (May-August, 2020)*

Metric (May-August, 2020)	Value
Mean Temperature Difference (Sensor - Predicted)	1.84 °C
Standard Deviation	2.06 °C
RMSE	2.76 °C
MAE	2.25 °C
R^2	0.653
CVRMSE	12.63 %
Number of Testing Points	1,391

Table 6.2 *Independent testing metrics with S-DoT sensors (May-August, 2020)*

Figure 6.2 shows the predicted versus observed air temperatures at S-DoT sensor locations during May-August 2020. The mean difference between S-DoT measurements and MLP predictions is 1.84°C, which is remarkably close to the expected 1.8°C known systematic temperature difference documented by Seoul municipality for this period. This alignment confirms that the MLP model, trained on AWS data, successfully maintains AWS temperature characteristics when applied to urban locations.

The distribution of temperature differences for this period, showing a narrow distribution centered at 1.84°C with a standard deviation of 2.06°C. **Figure 6.3** indicates the consistent model performance across different urban environments during the summer months.

Table 6.2 summarizes the performance metrics for May-August 2020. The R^2 of 0.653 and CVRMSE of 12.63% demonstrate reasonable predictive capability, while the RMSE of 2.76°C and MAE of 2.25°C reflect the combined effects of the systematic temperature difference and prediction uncertainty. The close match between the observed difference (1.84°C) and expected difference (1.8°C) confirms the model's validity.

Full Period (2020-2024) Independent Testing

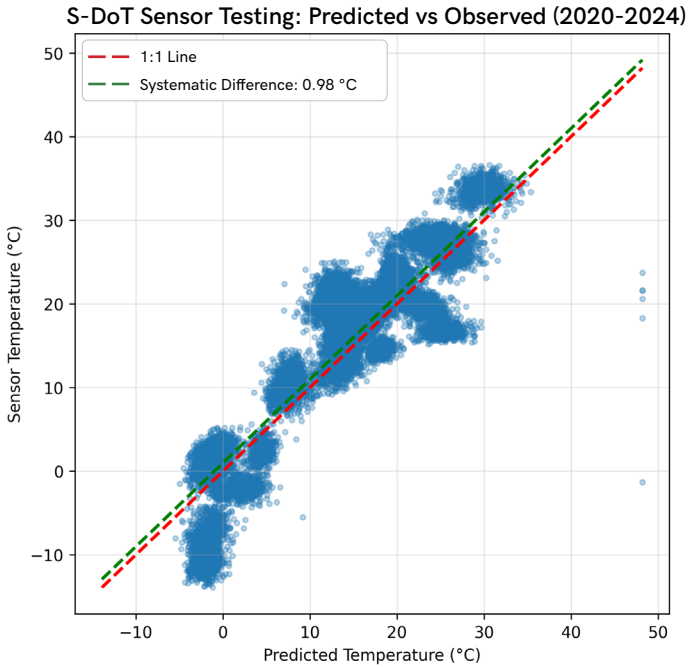

Figure 6.4 *Predicted air temperature testing with S-DoT sensors (2020-2024)*

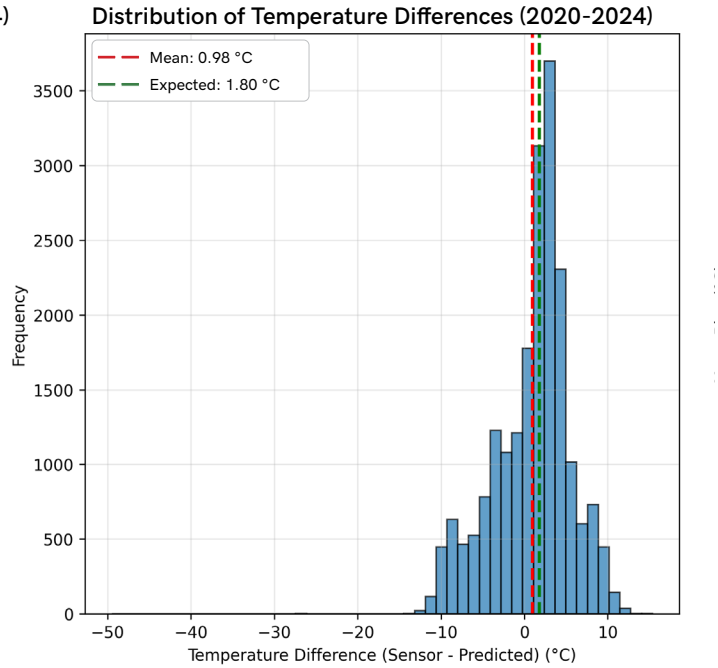

Figure 6.5 *Temperature difference between predicted and measured (2020-2024)*

Metric (2020-2024)	Value
Mean Temperature Difference (Sensor - Predicted)	0.98 °C
Standard Deviation	4.63 °C
RMSE	4.73 °C
MAE	3.87 °C
R^2	0.807
CVRMSE	31.17 %
Number of Testing Points	23,465

Table 6.3 *Independent testing metrics with S-DoT sensors (2020-2024)*

To assess the model's long-term consistency, the analysis was extended to all available S-DoT data from 2020-2024. **Figure 6.4** shows the scatter plot for this extended period, with points clustering along the 1:1 line. The mean difference of 0.98°C is lower than the summer 2020 value, suggesting that the systematic temperature difference between S-DoT and AWS varies seasonally, with smaller differences during non-summer months.

Figure 6.5 demonstrates the distribution of temperature differences across all seasons and years. The distribution remains approximately normal but with a larger standard deviation of 4.63°C, reflecting greater variability across different seasons and weather conditions. **Table 6.3** shows the full period metrics, with an improved R^2 of 0.807 indicating strong overall predictive capability.

The analysis demonstrates that the MLP model successfully converts LST to air temperature across different temporal periods and seasonal conditions. The summer 2020 independent testing confirms the model maintains AWS temperature patterns even when applied to systematically warmer urban locations, while the full period analysis shows robust performance across diverse conditions. The variation in systematic temperature differences (1.84°C in summer 2020 vs 0.98°C overall) likely reflects seasonal variations in urban heat island intensity, with stronger effects during summer months.

6.1.3 Final Predicted Air Temperature Maps

Following the successful independent testing, the MLP model converted LST from satellite to final predicted air temperature maps. **Figure 6.6** and **Table 6.4** show the temperature difference between LST and predicted air temperatures.

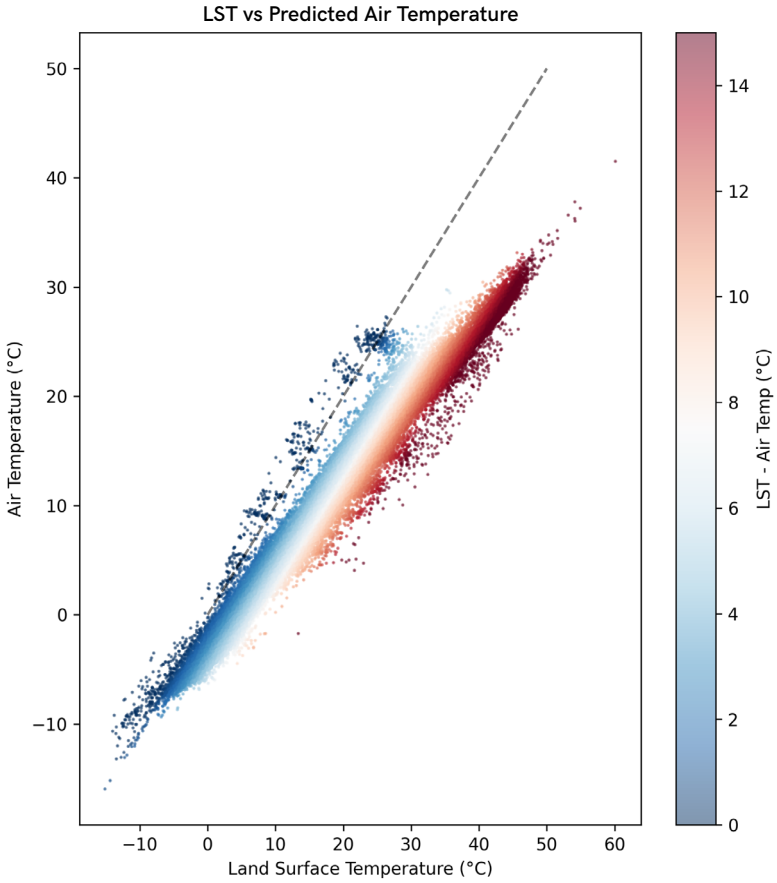

Figure 6.6 *Scatter plot of land surface temperature and final predicted air temperature*

LST to Final Predicted Air Temperature	
Metric	**Value**
Mean Temperature Difference	7.78 °C
Median Temperature Difference	7.58 °C
Standard Deviation	3.88 °C
Mean Spring Temperature Difference	9.40 °C
Mean Summer Temperature Difference	12.24 °C
Mean Fall Temperature Difference	7.51 °C
Mean Winter Temperature Difference	3.94 °C
Data Points	13,049,546

Table 6.4 *Difference between land surface temperature and final predicted air temperature*

The difference between LST and predicted air temperature is crucial for understanding the model's physical validity and its implications for urban planning. These differences directly relate to how urban surfaces store and release heat, which affects both the urban heat island effect and building energy consumption patterns. Understanding these temperature differentials helps explain why certain urban form elements have stronger impacts during specific seasons.

Table 6.4 reveals clear seasonal patterns in LST and air temperature differences, with mean differences ranging from 3.94°C in winter to 12.24°C in summer. This seasonal variation following the order summer (12.24°C) > spring (9.40°C) > fall (7.51°C) > winter (3.94°C), which aligns with Naserikia et al. (2023)'s findings, which observed greater temperature differences between LST and air temperature in built environments compared to natural Local Climate Zones (LCZ), especially during warm days.

The 12.24°C summer difference at 11:12 AM satellite overpass time reflects intense solar heating of urban surfaces during peak radiation hours, while winter's lower sun angle and reduced radiation result in smaller differences of 3.94°C. This consistent seasonal pattern validates the model's physical realism and demonstrates that the MLP successfully captures the varying thermal relationships throughout the year.

These temperature differentials are crucial for understanding the physical processes underlying urban heat island formation. The magnitude of difference indicates how much urban surfaces contribute to local heating above ambient air temperature conditions, with implications for both microclimate formation and building energy demand. The larger summer differentials suggest that surface heating plays a more significant role during cooling-demand periods, while smaller winter differences indicate reduced surface heating contribution during heating-demand periods.

The comprehensive analysis confirms that the MLP model successfully captured the complex non-linear relationship between satellite-based LST and AWS-based air temperatures. The patterns across seasons validate the model's physical realism, while the magnitude of temperature differences aligns with published studies on LST and air temperature relationships.

LST vs Predicted Air Temperature on 25th May 2022 at 11:10:19

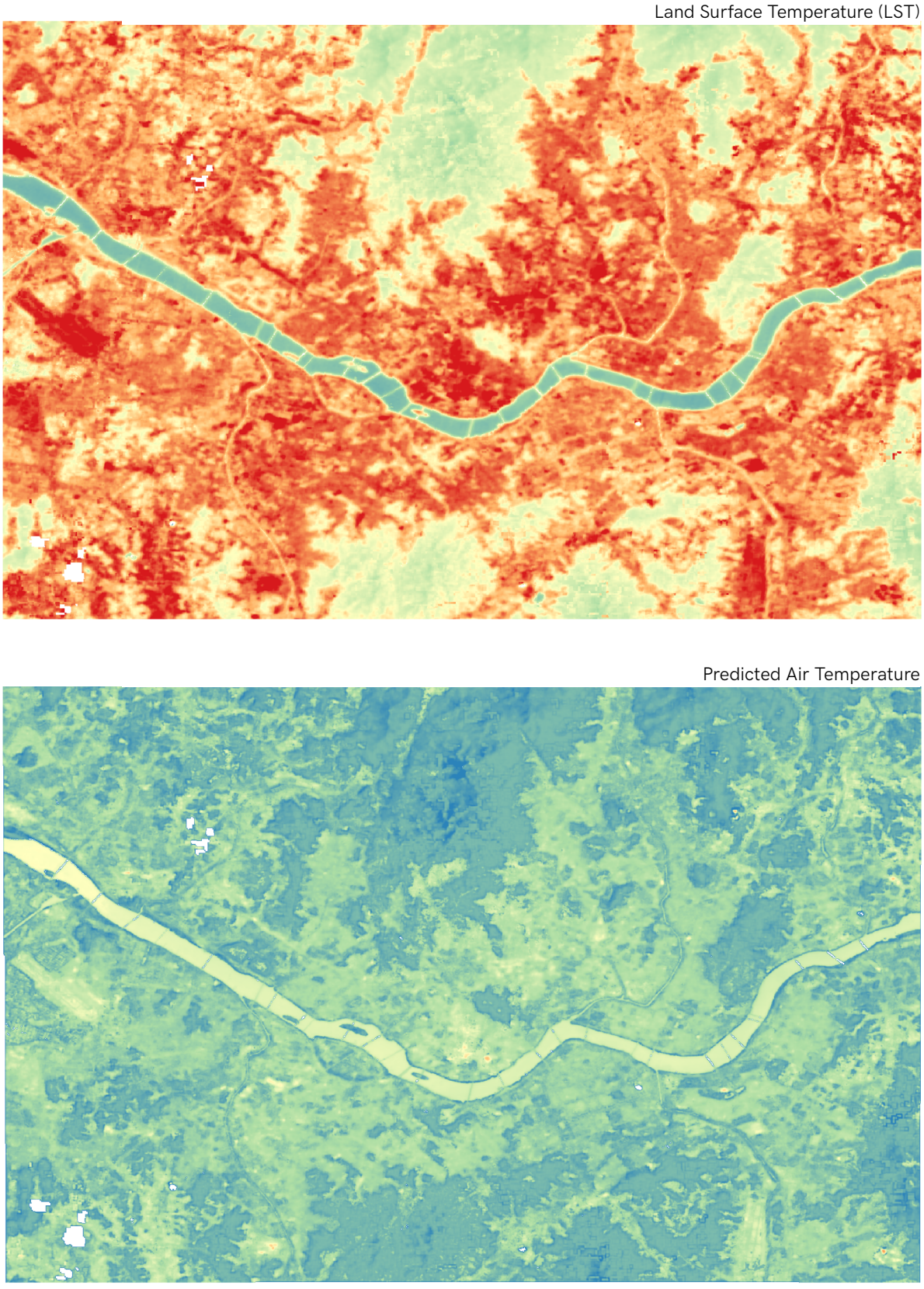

Figure 6.7 *Land surface temperature and predicted air temperature on 25th May 2022 11:10:19*

The final predicted air temperature and NDVI maps focus only on Heukseok-dong using the GeoPandas clip tool, and other grids are removed. In the end, the research area is covered with 3436 grid cells of 30 by 30 meters (23.81 by 29.91 meters). These grid cells are overlapped with building shapefiles and calculate 6 UFE of each grid cell for relative importance analysis.

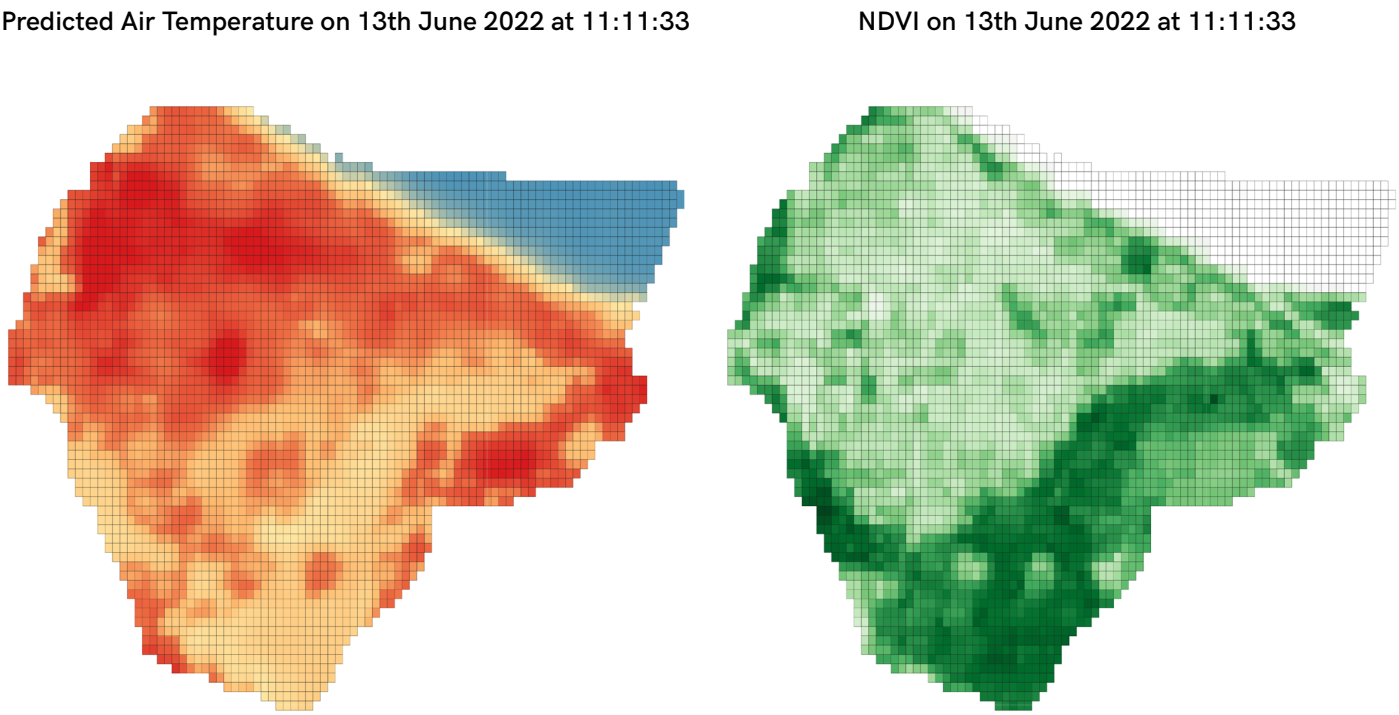

Figure 6.8 *Clipped air temperature and NDVI map with 23.81m x 29.91m pixels*

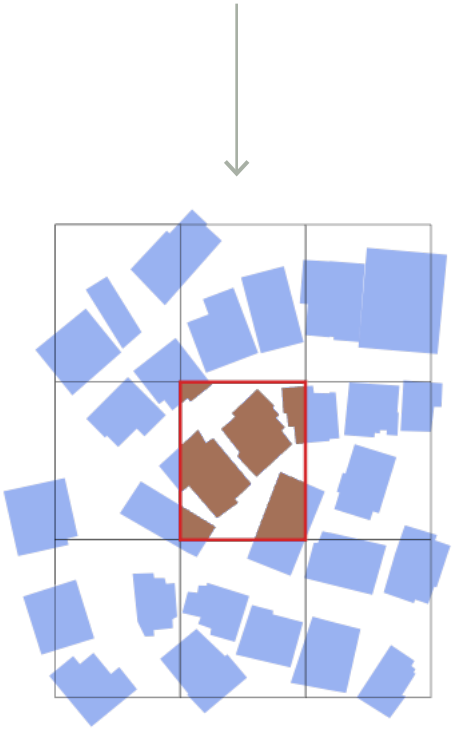

Figure 6.9 *Buildings overlap in multiple pixels*

6.2 Energy Consumption

Energy consumption data for both electricity and gas obtained from the Korean Architecture Hub were used to calculate the EUI of each building in Heukseok-dong. Calculated electricity and gas EUI show distinctive seasonal patterns.

6.2.1 Electricity EUI Pattern

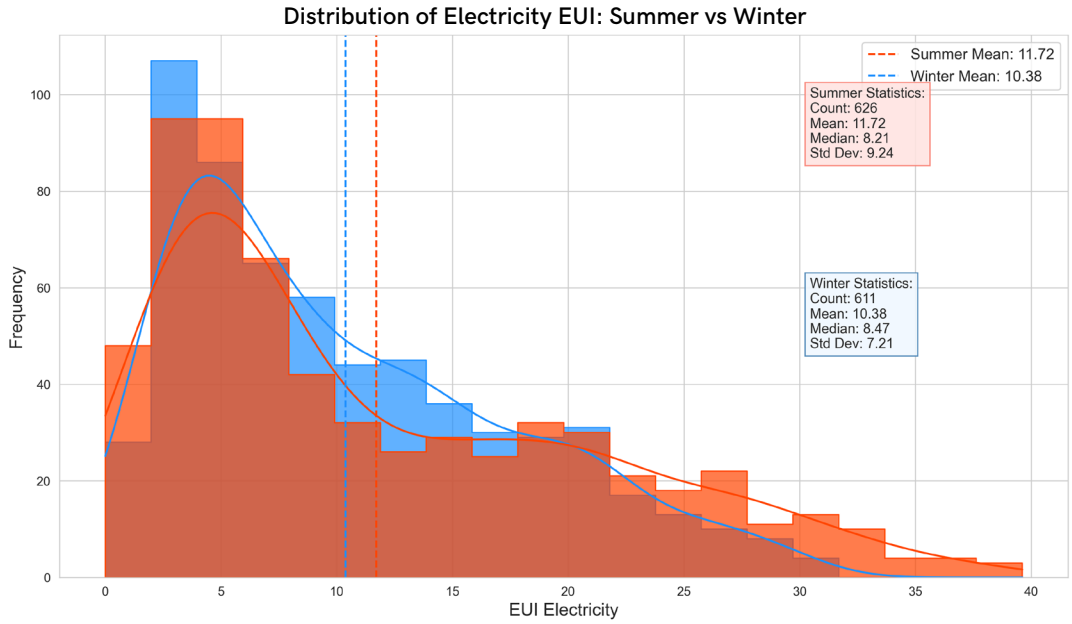

Figure 6.10 *Mean Electricity EUI by Month and Year*

The distribution of the electricity EUI shows distinct patterns between summer and winter seasons. In summer seasons, buildings have a slightly higher mean electricity EUI of 11.72 kWh/m^2, compared to buildings in winter seasons, 10.38 kWh/m^2. This shows that the electricity consumption is significant throughout the year, but it mostly intensifies during the summer months. **Figure 6.10** clearly shows that both summer and winter seasons have substantial electricity usage, though with different distribution patterns.

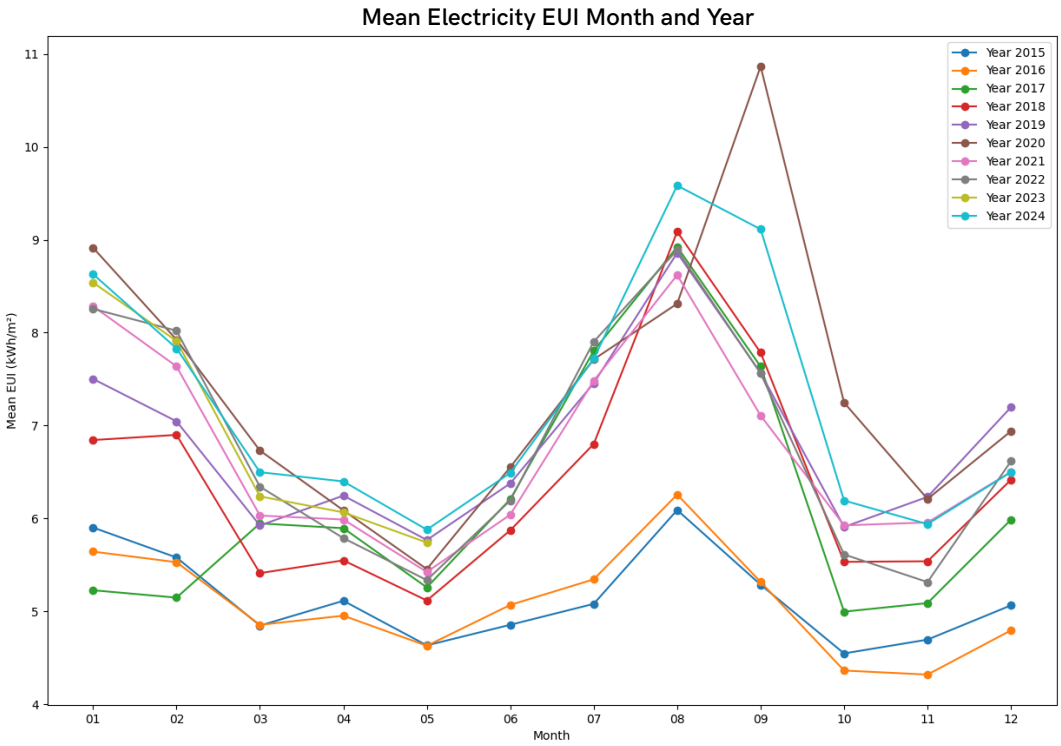

Figure 6.11 *Mean Electricity EUI by Month and Year*

When looking at the monthly trends across months and years, electricity consumption follows distinctive patterns with peaks mostly in the late summer season (August). Most years show higher electricity usage in January, a gradual decline through the spring season, and reach a minimum usage in May. Then, there is a steady increase through summer with a peak in August or September, before declining again in Autumn. This pattern explains that electricity is used year-round, not only for cooling, but also for other living appliances in all seasons, with increased electricity EUI during both winter and summer, although summer seasons appear to create higher consumption.

6.2.2 Gas EUI Pattern

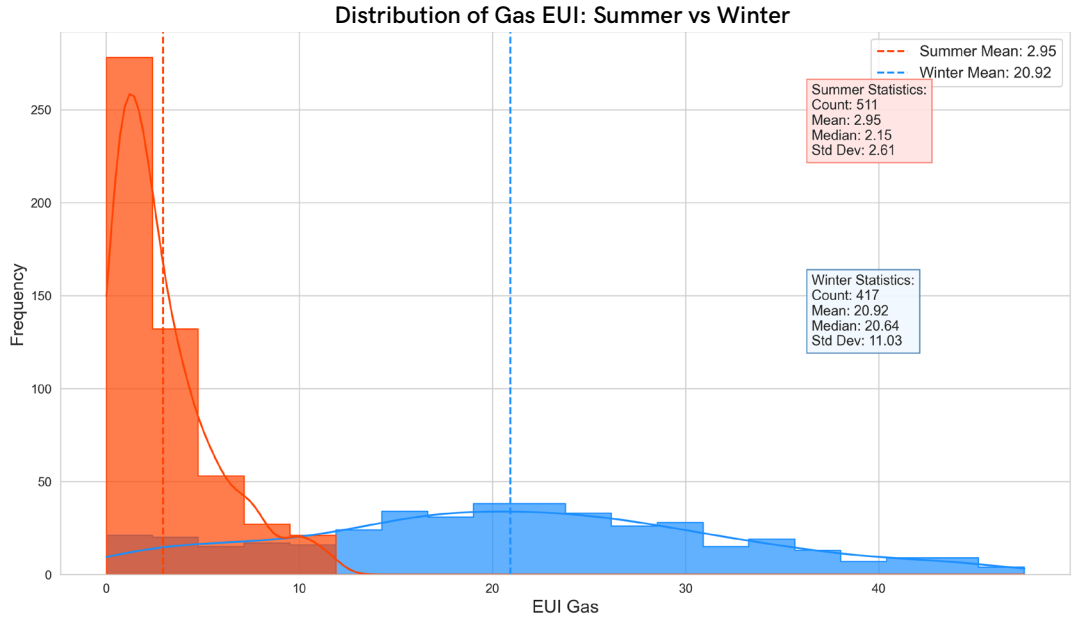

Figure 6.12 *Histogram of Gas EUI in Summer and Winter*

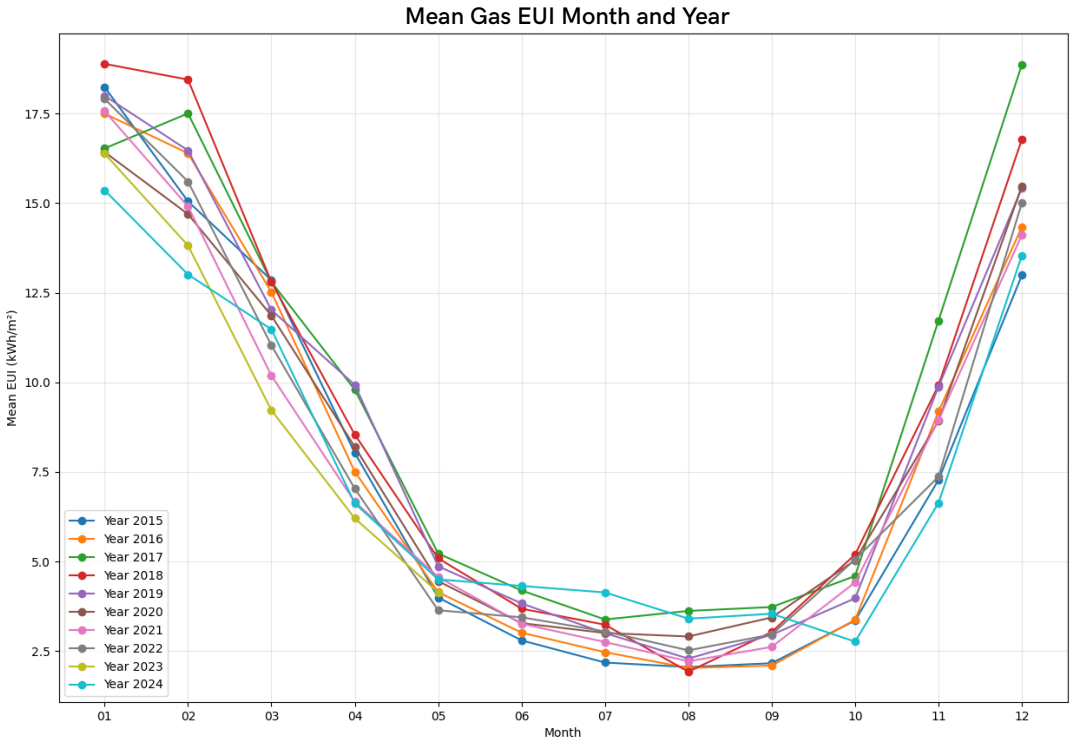

Figure 6.13 *Mean Gas EUI by Month and Year*

Unlike electricity EUI consumption, the gas EUI consumption data shows a dramatically different seasonal pattern. In the winter season, the gas EUI is an average of 20.92 kWh/m^2, which is significantly higher than the summer average of only 2.95 kWh/m^2. This huge difference demonstrates that gas is the predominant energy source for heating the buildings in Heukseok-dong.

Figure 6.13 shows a very definite relationship between the months and gas EUI. It shows a clear U-shaped pattern across all years, where the gas consumption consistently peaks in the winter season (December - February), and rapidly decreases through spring and reaches the lowest gas EUI level during the summer months (June - August) and September, then it increases rapidly again in autumn. This pattern is shown consistently across all years.

6.2.3 Building Type and Energy Use

While **Chapter 6.2.1** and **Chapter 6.2.2** examined seasonal patterns in energy consumption, to understand how building usage affects energy demand is equally important for urban energy planning. This analysis compares energy consumption patterns between low-rise residential buildings and commercial buildings in Heukseok-dong. Considering that the study area's energy data is mostly from these two building types, analyzing their seasonal consumption pattern can provide insights of how building function, operational patterns, and occupancy differences influence energy use beyond physical building characteristics alone.

Building Use	Commercial Building
Building Volume	10,361 m^3
Building Height	19.9 m
Number of Floors	5
Average Electricity EUI/month	13.10 kWh/m^2
Average gas EUI/month	12.73 kWh/ m^2

Shape ID: 6540

Shape ID: 28022

Building Use	Residential Building
Building Volume	813 m^3
Building Height	9.1 m
Number of Floors	3
Average Electricity EUI/month	8.31 kWh/m^2
Average gas EUI/month	9.04 kWh/m^2

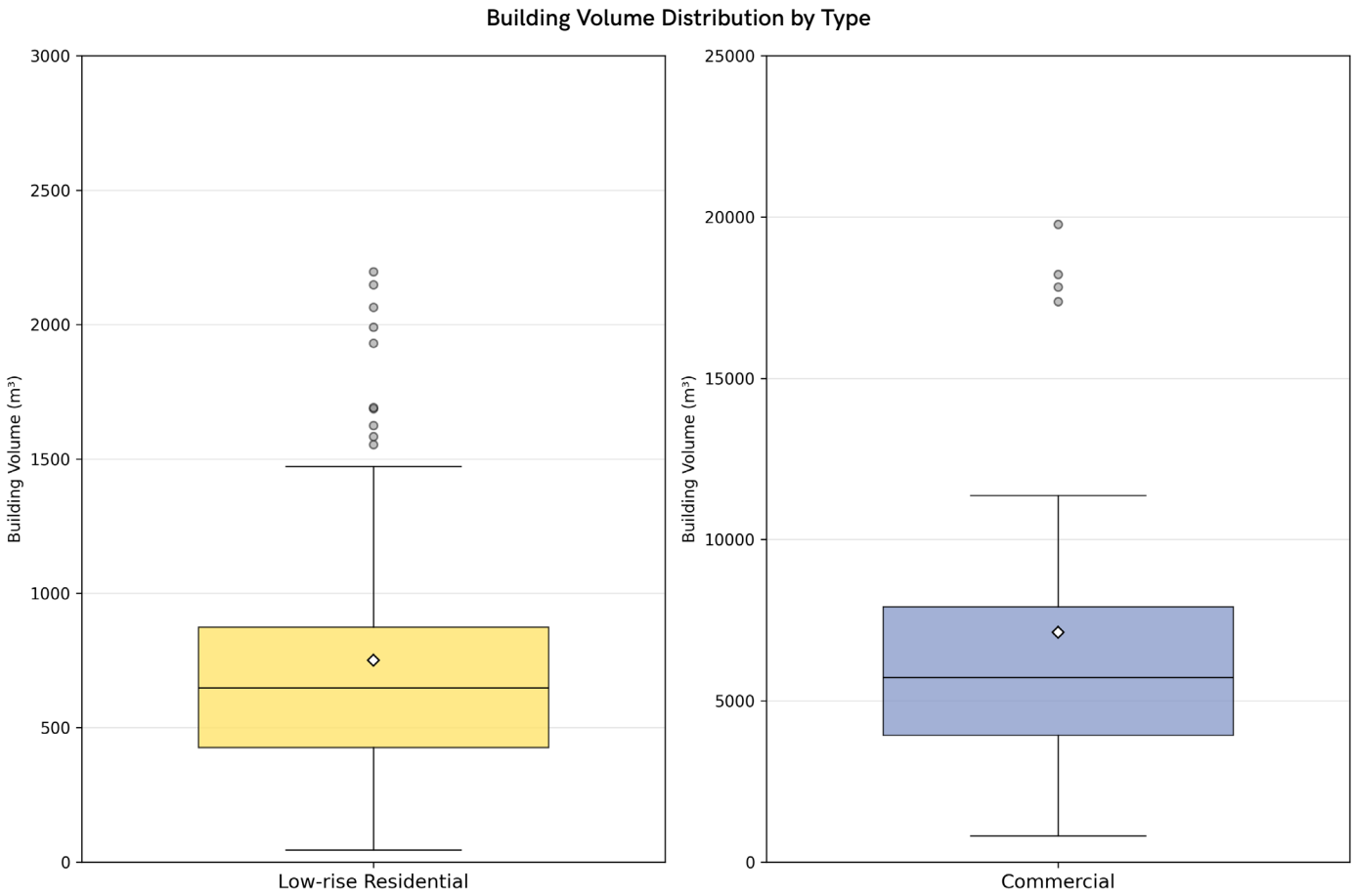

Figure 6.14 *Building Volume Distribution by Type*

Building Volume	Low-rise Residential Buildings	Commercial Buildings
Mean Volume	751.2 m^3	7,123.9 m^3
Maximum Volume	2,197.3 m^3	19,781.1 m^3
Minimum Volume	45.0 m^3	817.0 m^3

Table 6.5 *Building Volume Distribution by Type*

The analysis on the energy consumption patterns shows significant differences between building types in Heukseok-dong. **Figure 6.14** shows the distribution of building volumes for low-rise residential and commercial buildings with available EUI data. Commercial buildings have a mean volume of 7,123.9 m^3, approximately 9.5 times larger than low-rise residential buildings at 751.2 m^3. This substantial size difference provides important context for understanding energy consumption patterns.

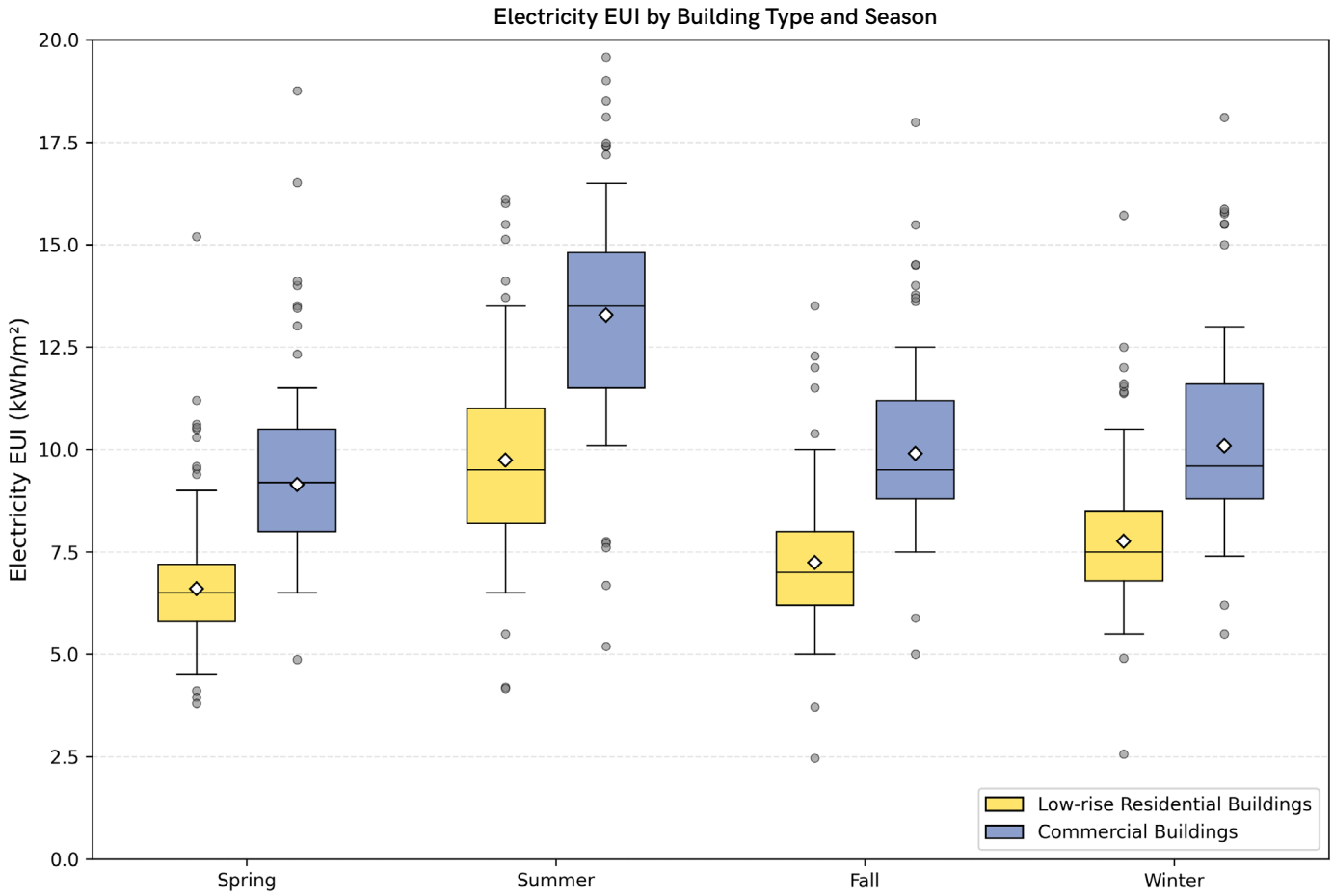

Figure 6.15 *Electricity EUI by Building Type and Season*

Mean EUI (kWh/m³)	Spring	Summer	Fall	Winter
Low-rise Residential	6.60	9.74	7.24	7.76
Commercial	9.14	13.28	9.90	10.08
Difference	2.54	3.54	2.66	2.32

Table 6.6 *Electricity EUI by Building Type and Season*

Figure 6.15 shows the electricity EUI patterns across seasons for both low-rise residential and commercial buildings. Commercial buildings consistently show higher electricity EUI throughout the year, with mean electricity consumption from 9.14 kWh/m^2 in spring to 13.28 kWh/m^2 in summer. In contrast, low-rise residential buildings consume less electricity per square meter, ranging from 6.60 kWh/m2 in spring to 9.74 kWh/m^2 in summer. The difference is the highest during summer months (3.54 kWh/m^2), which explains that the higher cooling demands in commercial buildings are due to factors such as greater occupancy density, extended operating hours, and higher internal heat gains from equipment and lighting.

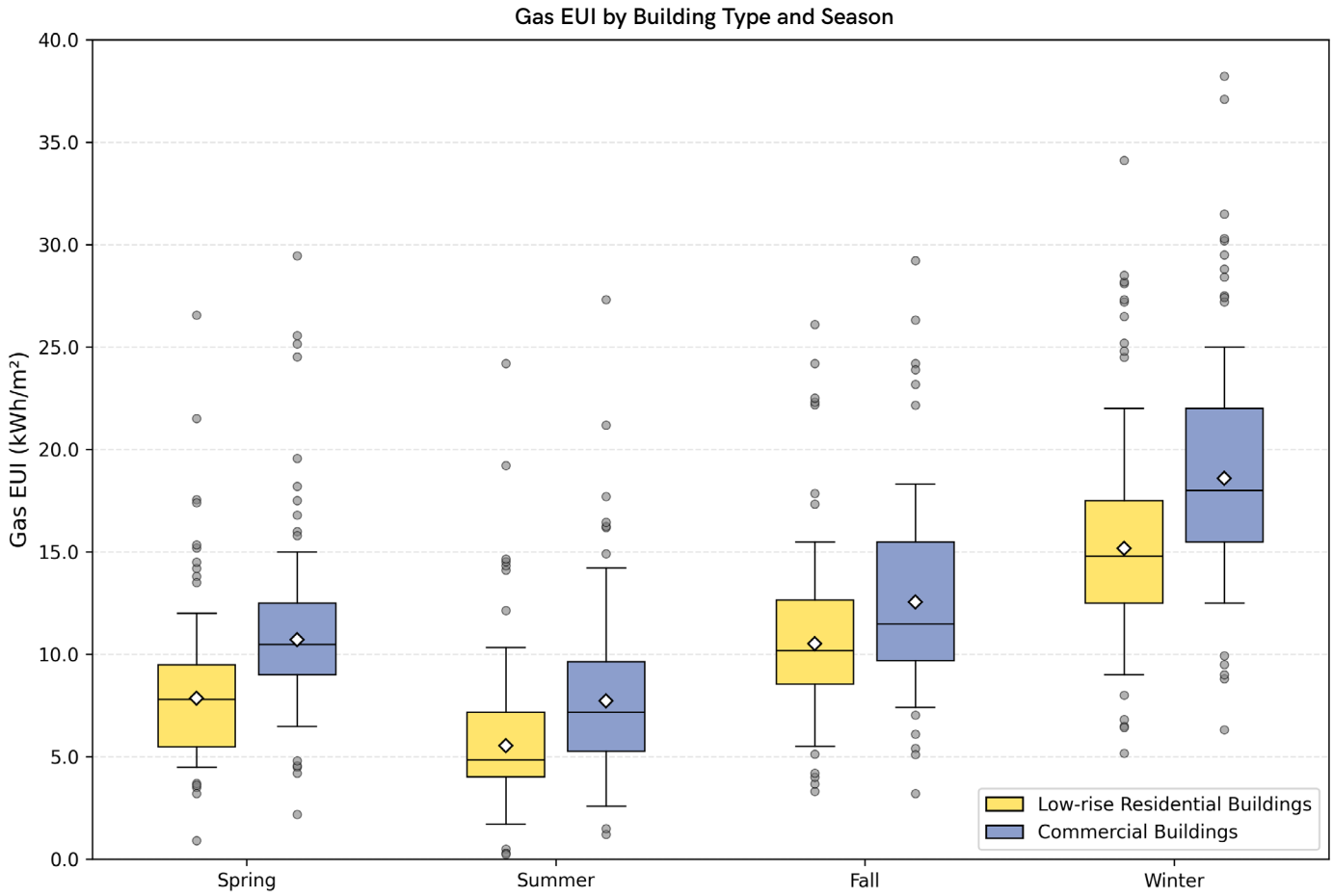

Figure 6.16 *Gas EUI by Building Type and Season*

Mean EUI (kWh/m³)	Spring	Summer	Fall	Winter
Low-rise Residential	7.86	5.54	10.52	15.16
Commercial	10.70	7.72	12.55	18.60
Difference	2.84	2.18	2.03	3.44

Table 6.7 *Gas EUI by Building Type and Season*

Gas consumption shows a similar pattern, with commercial buildings showing higher EUI across all seasons. The difference is particularly the highest in winter, where the commercial buildings use an average of 18.60 kWh/m^2 compared to 15.16 kWh/m^2 for residential buildings. Both building types use the least gas during the summer months, confirming that gas is primarily used for heating. The consistently higher consumption in commercial buildings likely reflects their larger open spaces, which require more heating, different operational schedules, and potentially less efficient heating systems in older commercial structures.

Table 6.7 indicates that building type significantly influences energy consumption patterns beyond what can be explained by size alone. Despite EUI is normalized by floor area, commercial buildings demonstrate 30-40% higher EUI, suggesting fundamental differences in building operation, occupancy patterns, and system requirements between commercial and residential uses in this old urban district.

6.3 Genizi Method

This research employed the Genizi method to determine the relative importance of each UFE to address the challenge of multicollinearity. The analysis was conducted separately for each season and at multiple spatial scales to capture both seasonal and spatial variations in UFE impacts. It is particularly valuable as it properly allocates shared variance among correlated predictors (High NDVI with low building ratios). The result shows percentage contributions that reveal which UFEs drive the most variation in air temperature and energy consumption (EUI).

6.3.1 Air Temperature Relative Importance

Air temperature analysis used 3 spatial scales (pixel scale, 100m buffer, and 300m buffer) with 4 different seasons. A comprehensive result is demonstrated in **Figure 6.17**, **Figure 6.18** and **Figure 6.19**.

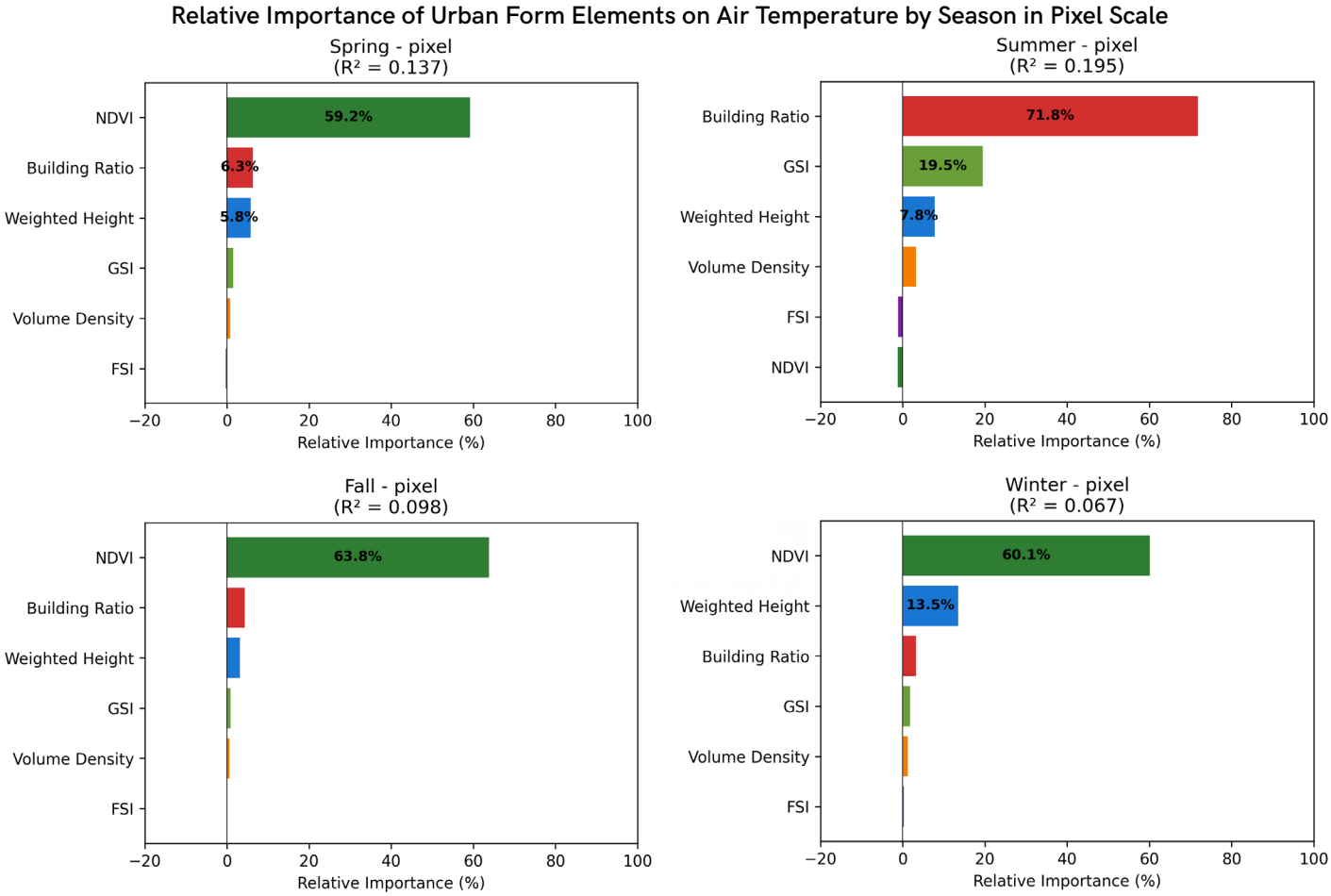

Figure 6.17 *Relative importance of urban form elements on air temperature by season and scale using Genizi method*

The air temperature analysis finds distinct seasonal patterns in how UFEs affect air temperature variations. At the pixel scale, NDVI plays as the dominant predictor for three seasons, contributing 59.2% in spring, 63.8% in fall, and 60.1% in winter. This consistent pattern highlights vegetation's role as the primary temperature changer throughout most of the year. However, summer shows a dramatic shift: building characteristics become dominant, with building ratio (71.8%) and GSI (19.5%) together explaining over 90% of temperature variance. This seasonal flip suggests that during extreme heat, the physical presence and thermal mass of buildings overtake vegetation's cooling effects.

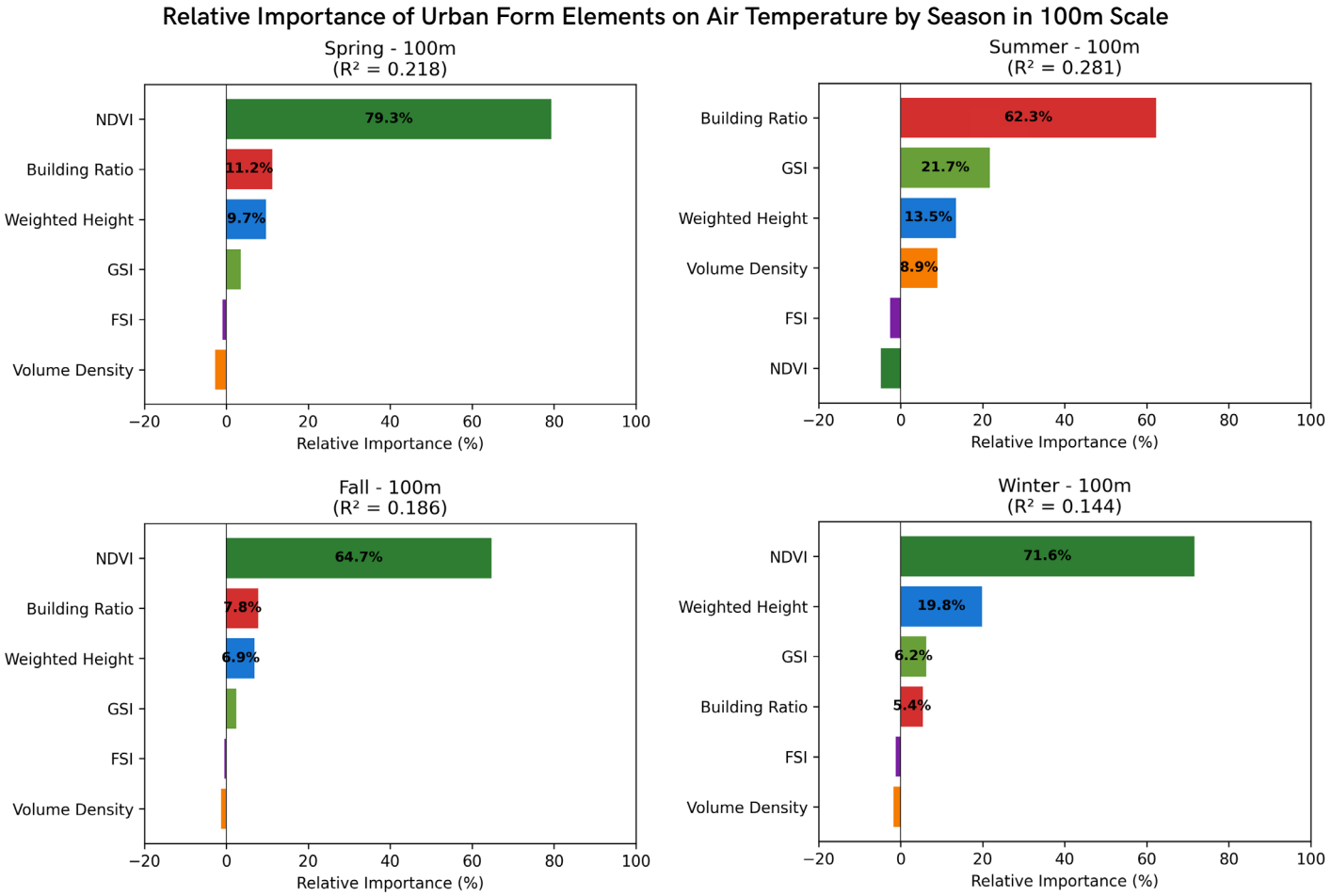

Figure 6.18 *Relative importance of urban form elements on air temperature by season and scale using Genizi method*

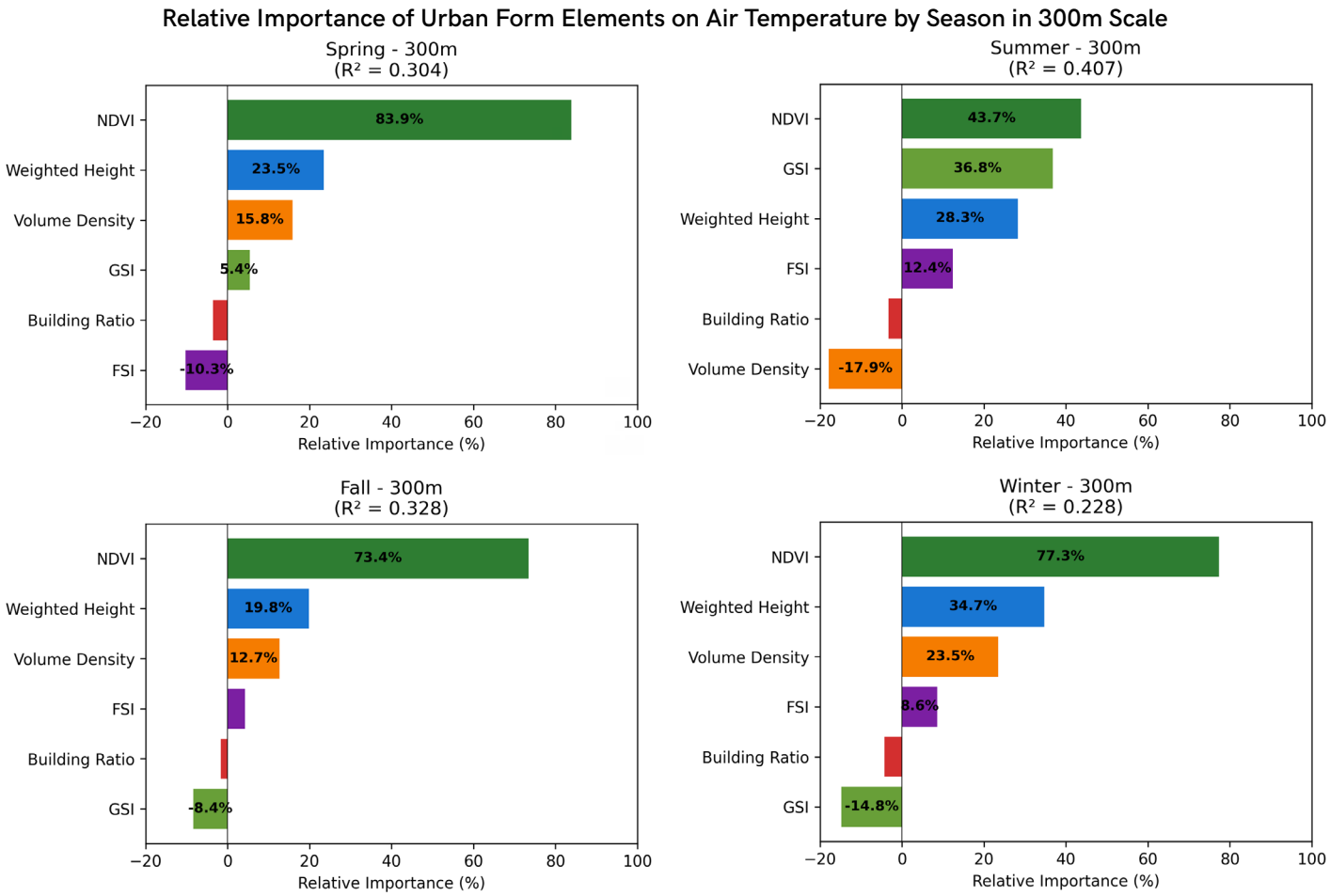

Figure 6.19 *Relative importance of urban form elements on air temperature by season and scale using Genizi method*

This dramatic summer reversal reflects the extreme thermal contrasts created by peak temperatures. At 11:12 AM in summer, building surfaces can exceed 40°C while vegetated areas maintain relatively stable temperatures around 22-26°C. This binary thermal pattern means that at pixel scale, temperature variance is overwhelmingly determined by whether a building is present rather than variations in vegetation density. The near-zero importance of NDVI (-1.2%) occurs because most vegetated pixels have similar temperatures, while building pixels create the extreme values that drive overall variance.

The 100m buffer analysis shows an intensification of patterns in the pixel scale. NDVI's importance increases to 79.3% in spring, 64.7% in fall, and 71.6% in winter, which demonstrates that vegetation's cooling effects are more powerful at the larger scale. In summer, the building ratio maintains its dominance at 62.3%, while GSI contributes 21.7%. The R^2 values show improvement from pixel to 100m scale from 0.137 to 0.218 in spring, which suggests that immediate neighborhood characteristics provide better explanatory power for temperature variations.

At the 300m neighborhood scale, the patterns become more complex with the highest R^2 values across all seasons. NDVI continues to dominate with 82.9% in spring, 73.4% in fall, and 77.3% in winter. Summer shows a more balanced distribution at this scale, with NDVI increases to 43.7% while GSI reaches 36.8%.

The dramatic reduction in building ratio importance from 71.8% at pixel scale to 7% at 300m scale occurs because neighborhood buffers equalize building coverage, where most areas contain similar 20-30% building ratios, eliminating its discriminating power. Instead, the quantity and distribution of neighborhood green infrastructure becomes the primary temperature determinant, explaining why NDVI rebounds to 43.7%. This scale-dependent behavior demonstrates that extreme summer heat fundamentally alters temperature controls: building presence dominates at fine scales, while neighborhood vegetation patterns determine area-wide thermal conditions.

Interestingly, some variables show negative importance values at this scale, such as FSI at -10.3% in spring and volume density at -17.9% in summer, which indicate suppressor effects where these variables enhance other predictors' explanatory power through their correlations.

6.3.2 Electricity Consumption Relative Importance

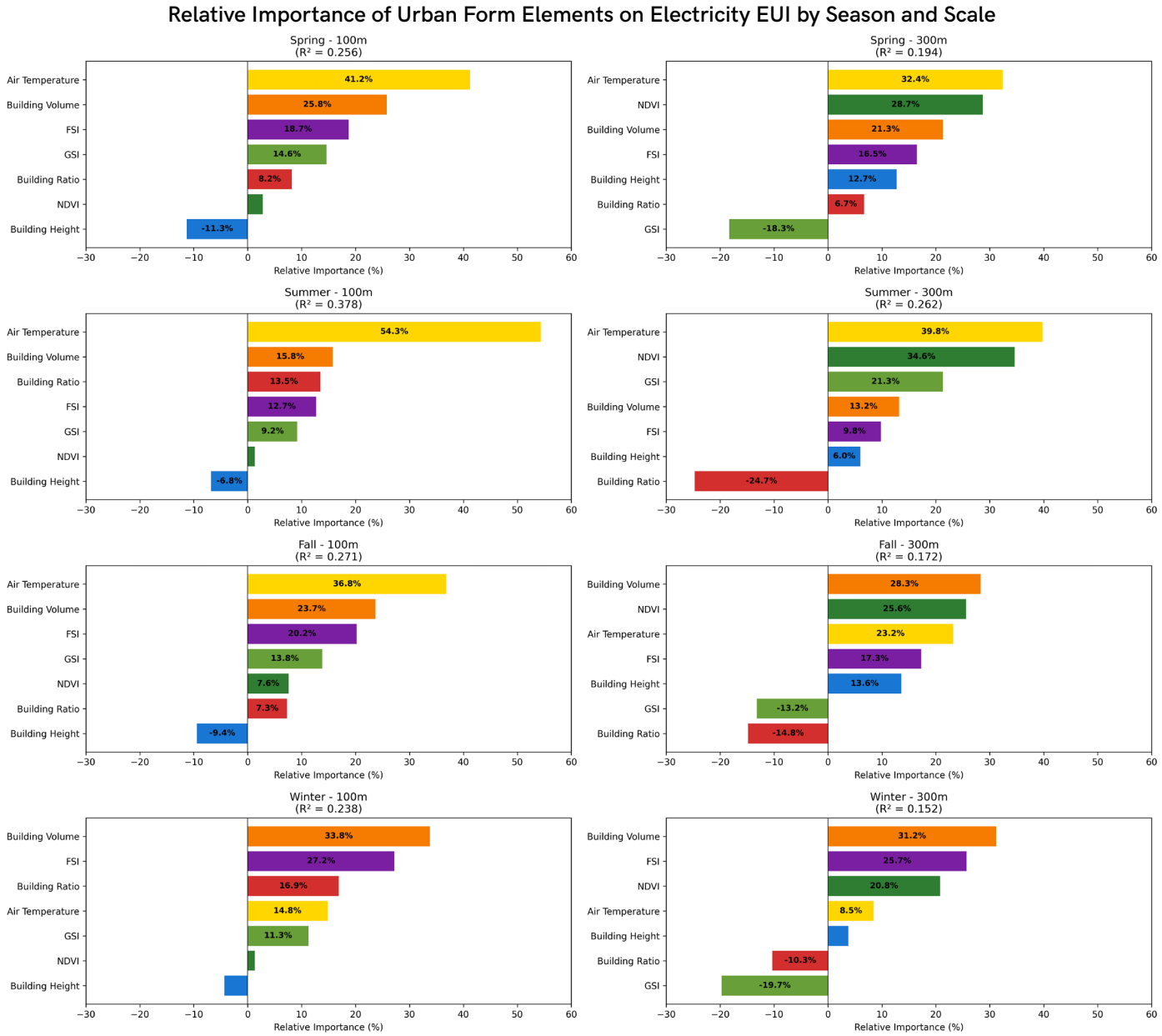

Figure 6.20 *Relative importance of urban form elements on electricity EUI by season and scale using Genizi method*

The Genizi method for electricity consumption in EUI reveals that air temperature emerges as the important driver across all seasons and scales, but its dominance varies seasonally. At the 100m scale, air temperature contributes 41.2% in spring, the highest at 54.3% in summer, and decreases to 36.8% in fall and 14.8% in winter. This seasonal pattern aligns with cooling demands as the stronger influence of temperature in summer reflects the heavy reliance on air conditioning during hot months, while its reduced importance in winter, which indicates that electricity use becomes less temperature-dependent when cooling is not needed.

Building volume shows the second most important predictor at the 100m scale except for winter, with contributions ranging from 15.8% to 33.8%. Its importance is comparably higher in winter (33.8%) when it becomes the dominant factor, suggesting that larger buildings require more electricity for lighting, ventilation, and general operations regardless of temperature. FSI follows as the third predictor, showing relatively stable importance across seasons (12.7% to 27.2%), with its highest contribution in winter, indicating that floor space intensity drives baseline electricity consumption.

At the 300m scale, a similar pattern is shown, but with some notable variations. Air temperature maintains its dominance in spring and summer, but shows suppressor effects in winter, with building ratio displaying large negative importance values (-24.7% in summer, -14.8% in fall, and -10.3% in winter). These negative values indicate that building ratio, while not directly explaining electricity consumption variance, enhances the predictive power of other variables through its correlations. Areas with high building ratios tend to have low NDVI values when both are included in the model, building ratio's negative importance means it helps NDVI better explain the variance by accounting for their shared relationship. This statistical phenomenon occurs when a variable improves the model's overall explanatory power despite showing negative individual importance. NDVI shows positive importance at the 300m scale, particularly in summer (34.6%) and fall (25.6%), suggesting that vegetation's cooling effects become more apparent at neighborhood scales, indirectly reducing electricity demand.

The R^2 values range from 0.152 to 0.378, with the lowest at 300m scale in winter and the highest at 100m scale in summer. These modest R^2 values indicate that UFEs explain only 15-38% of the variance in electricity consumption, suggesting that many other factors not captured in this analysis such as building age, occupancy patterns, equipment efficiency, and behavioral differences play substantial roles. The seasonal variation shows stronger relationships between UFEs and electricity consumption in summer, though even the best model explains less than 40% of variance. The analysis indicates that electricity use in Heukseok-dong is partially influenced by temperature-related cooling needs in warm months and building characteristics in cooler months, while the majority of variation remains unexplained. The scale comparison shows that the 100m scale captures more direct relationships with higher R^2 values, while the 300m scale reveals more complex neighborhood-level interactions, including the indirect benefits of vegetation on reducing cooling demands, though these relationships remain moderate at best.

6.3.3 Gas Consumption Relative Importance

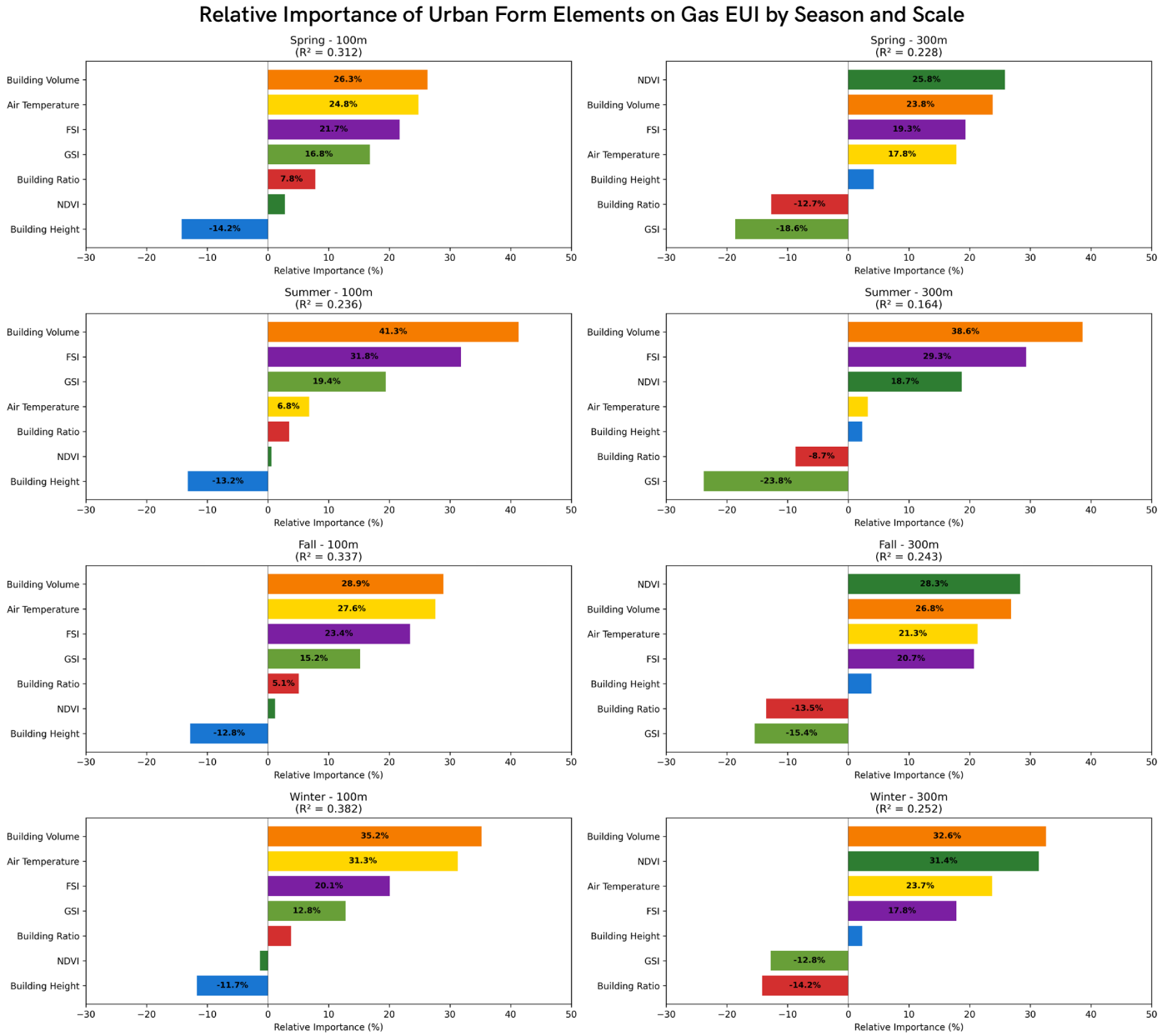

Figure 6.21 *Relative importance of urban form elements on gas EUI by season and scale using Genizi method*

The Genizi method for gas consumption shows different patterns compared to electricity consumption, which reflects the distinct role of gas as primarily a heating energy. Building volume emerges as the dominant predictor across all seasons and scales, with its importance ranging from 26.3% to 41.3% at the 100m scale. This dominance is most pronounced in winter and summer, but for different reasons. Winter reflects actual heating demands, while summer's high percentage occurs despite very low overall gas consumption, making small variations appear proportionally large.

Air temperature shows the second-highest importance, but with a clear seasonal pattern that inversely shows in electricity consumption. At the 100m scale, air temperature contributes 31.3% in winter, 27.6% in fall, 24.8% in spring, but drops to just 6.8% in summer. This pattern directly reflects heating demands. Lower temperatures drive higher gas consumption, while summer's minimal heating needs reduce temperature's explanatory power. The relationship is even more highlighted at the 300m scale.

FSI shows relatively stable importance across seasons (19.4% to 31.8% at 100m scale), which indicates that it is a reliable indicator of heating demand. On the other hand, building height shows strong negative importance values across most seasons and scales, particularly at the 100m scale (-14.2% in spring, -13.2% in summer, -12.8% in fall, -11.7% in winter). These consistent negative values suggest that taller buildings are more heating-efficient per unit volume, possibly due to reduced surface-to-volume ratios.

The R^2 values show strong seasonal and spatial variation, ranging from 0.164 in summer at a 300m scale to 0.382 in winter at a 100m scale. Low R^2 in summer explains the minimal and irregular gas use during non-heating months, while winter's higher values indicate moderate relationships between UFE and heating demands. The 300m scale shows similar patterns, but NDVI shows substantial positive importance at this scale (25.8% in spring, 28.3% in fall, 31.4% in winter), which seems counterintuitive but likely reflects the spatial distribution of building types and ages in Heukseok-dong. At the 100m scale, immediate vegetation has little direct impact on heating needs. However, at the 300m neighborhood scale, areas with high vegetation coverage often correspond to newer residential developments with modern insulation, while areas with low NDVI typically contain older buildings from the 1960s-1970s with poor heating efficiency. The Genizi method captures this spatial coincidence rather than direct causation.

To test whether building volume truly drives gas consumption or correlates with building type, the analysis in **Chapter 6.2.3** examined energy patterns by building use. Commercial buildings average 7,123.9 m^2 compared to 751.2 m^2 for low-rise residential buildings. However, when normalized as EUI, commercial buildings still consume 22% more gas per square meter in winter (18.60 vs 15.16 kWh/m^2). This confirms that building type influences consumption beyond volume effects alone. Overall, the analysis confirms that gas consumption in Heukseok-dong is driven by a combination of building size and building type characteristics, with temperature-related heating needs showing clear seasonal patterns that reflect the primary use of gas for heating.

6.4 Partial Correlation

While the Genizi method reveals the relative importance of UFEs, partial correlation provides the directional information, whether each UFE increases or decreases air temperature and energy consumption. It uses the same spatial scales and seasonal analysis as the Genizi method, which would provide a comprehensive understanding of how UFEs directly affect temperature and energy use patterns in Heukseok-dong.

6.4.1 Air Temperature Directional Importance

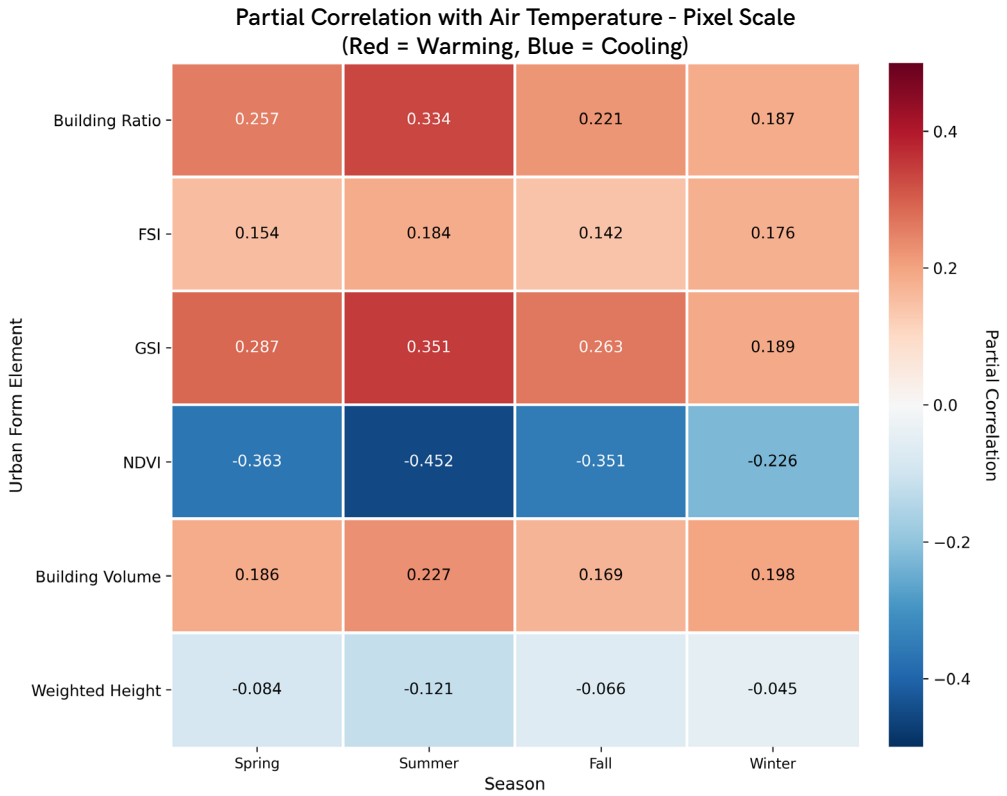

Figure 6.22 *Partial correlation of urban form elements on air temperature by season in pixel scale*

The partial correlation reveals consistent directional patterns across all scales and seasons. NDVI shows the strongest cooling effect, with a range from -0.208 to -0.452 at different scales, peaking at -0.452 in summer at the pixel scale. This confirms vegetation's role as the primary cooling mechanism, with effects intensifying during hot weather when evapotranspiration and shading are most active. The cooling effect remains substantial across all scales, though slightly decreased at the 300m neighborhood level.

In contrast, GSI consistently shows warming effects across all seasons and scales, with the strongest correlation of 0.440 in summer at the 300m scale. This indicates that higher ground coverage by buildings creates heat islands through reduced pervious surfaces and increased heat absorption. Building ratio similarly shows consistent positive correlations (0.125 to 0.334), which confirms that denser building coverage leads to higher temperatures. The warming effect of both GSI and building ratio is most pronounced in summer, aligning with the UHI effects.

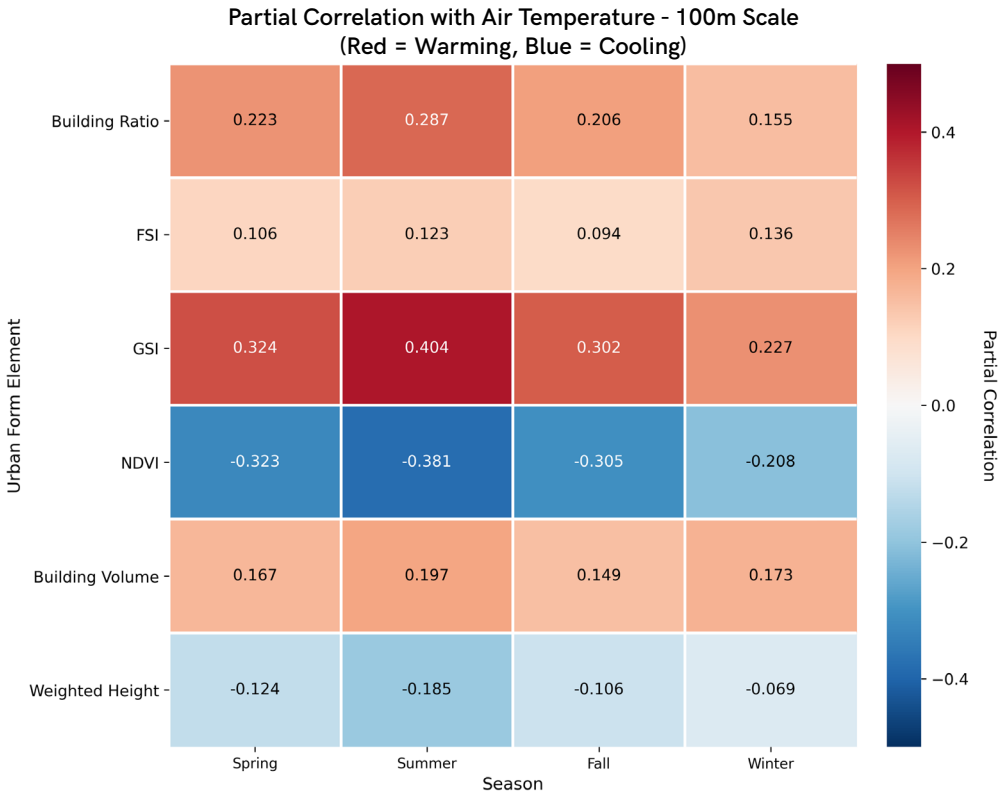

Figure 6.23 *Partial correlation of urban form elements on air temperature by season in 100m scale*

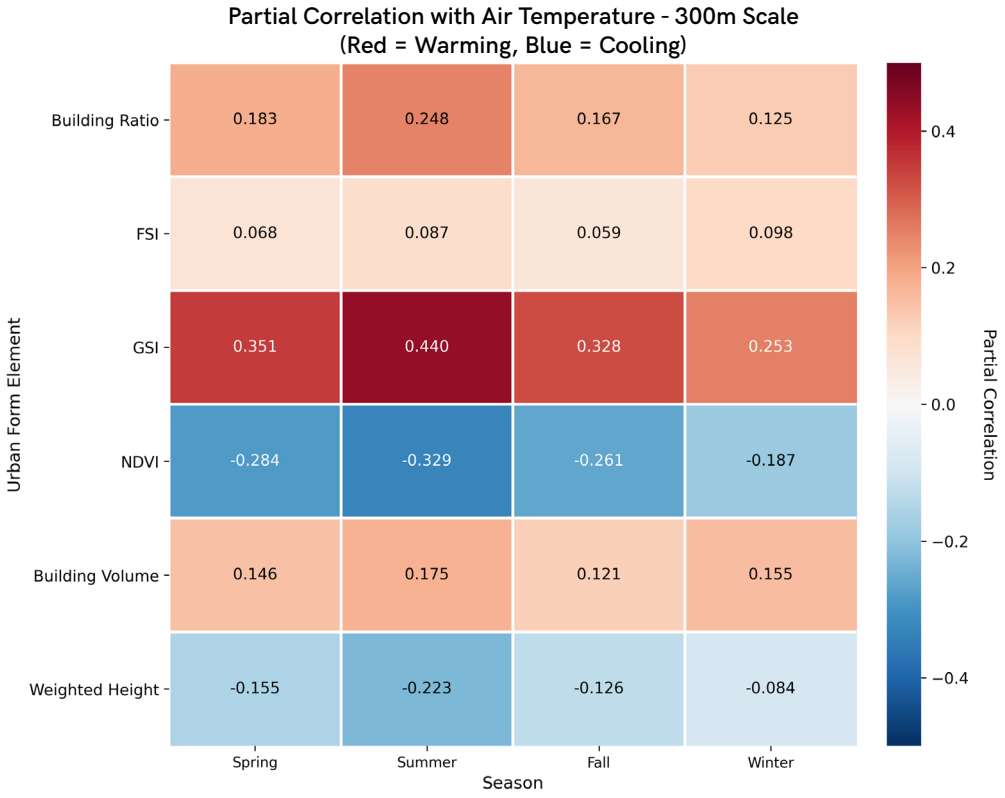

Figure 6.24 *Partial correlation of urban form elements on air temperature by season in 300m scale*

Building volume shows moderate warming effects (0.146 to 0.227), while FSI displays relatively weak positive correlations (0.059 to 0.184). Weighted height shows consistent cooling effects across most seasons and scales (-0.045 to -0.223), suggesting that taller buildings may provide more shading or better air circulation. The seasonal patterns clearly show that summer has the strongest correlations for all variables, indicating that UFE effects on temperature are highlighted during hot weather. Winter shows the weakest correlations overall, suggesting that other factors like anthropogenic heat may play larger roles during cold months.

The scale analysis explains that the pixel scale shows the strongest correlations, particularly for NDVI's cooling effect, while the 300m scale shows enhanced warming effects for GSI. This suggests that vegetation's cooling benefits are most effective at immediate scales for direct temperature reduction. These directional insights, combined with the Genizi importance rankings, provide clear guidance for urban planning. Maximizing NDVI while minimizing GSI and building ratio would be most effective for temperature reduction, particularly during summer months.

6.4.2 Electricity Consumption Directional Importance

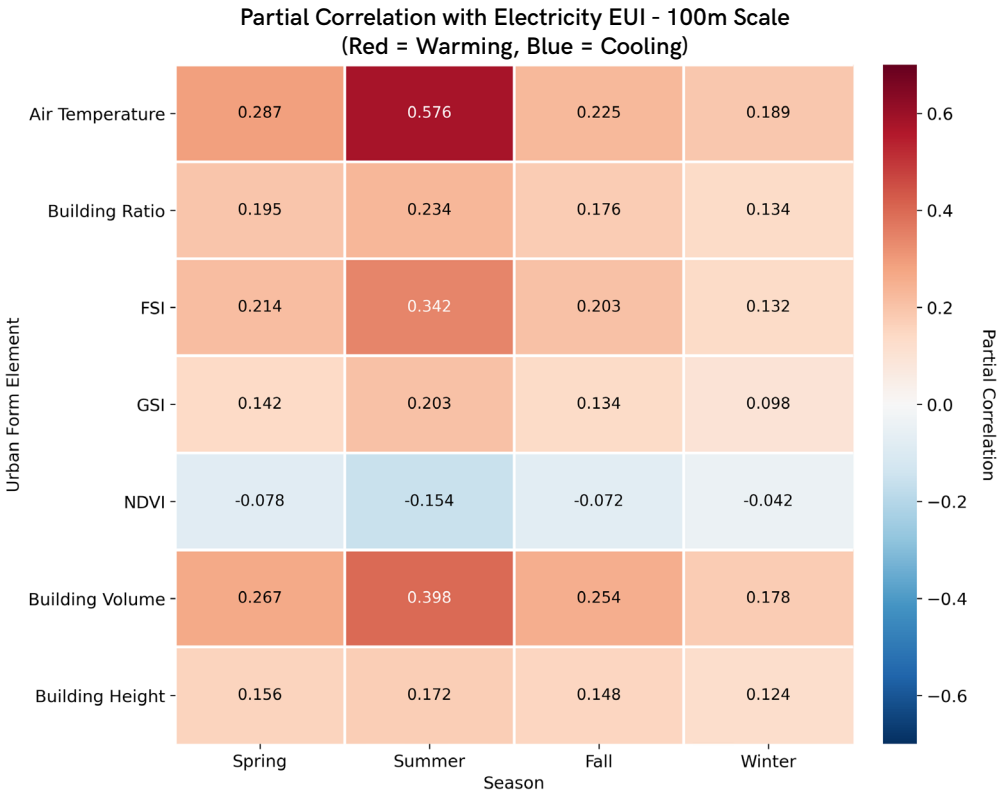

Figure 6.25 *Partial correlation of urban form elements on electricity EUI by season in 100m scale*

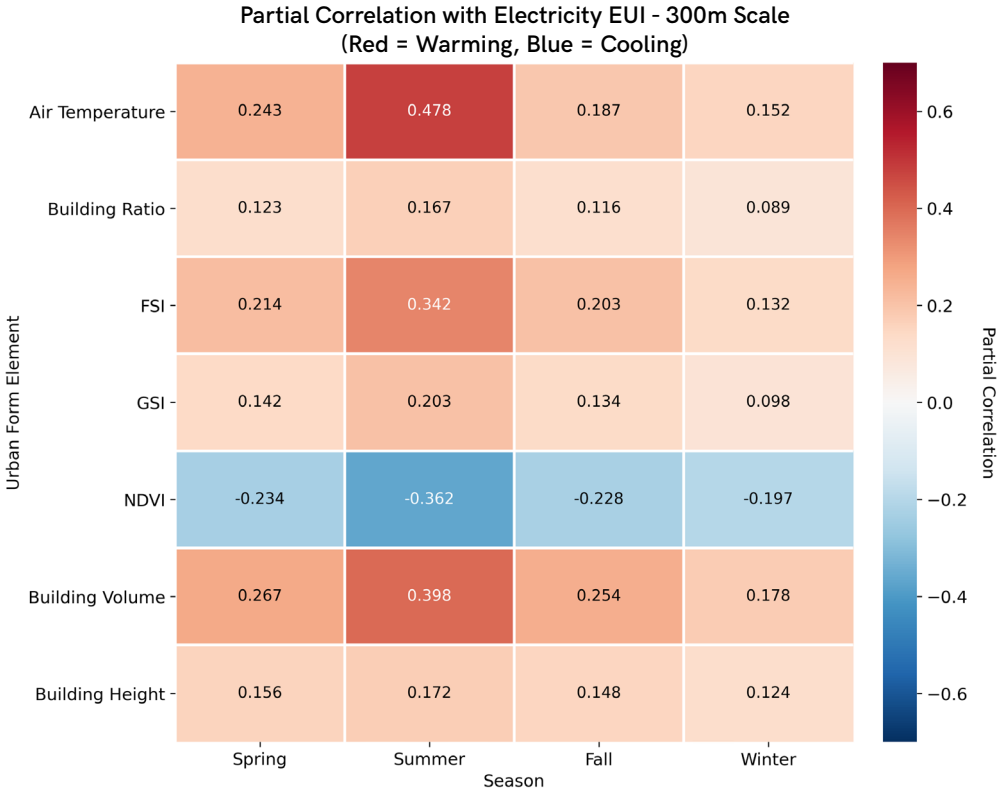

Figure 6.26 *Partial correlation of urban form elements on electricity EUI by season in 300m scale*

The partial correlation for electricity consumption (EUI) reveals that air temperature is the dominant positive driver across all seasons, with correlations ranging from 0.152 to 0.576. The relationship is most pronounced in summer, reaching 0.576 at the 100m scale, which directly reflects cooling demands during hot weather. This strong positive correlation confirms that higher temperatures lead to increased electricity consumption, due to air conditioning use. The correlation weakens progressively through fall (0.225) and winter (0.189 at 100m scale), as air conditioning needs less.

Building volume shows the second strongest positive correlation with electricity consumption, ranging from 0.178 to 0.398 across seasons and scales. The relationship remains remarkably consistent across seasons, suggesting that larger buildings require more electricity for lighting, ventilation, and equipment regardless of temperature. FSI follows a similar pattern with positive correlations (0.132 to 0.342), which indicates that larger floor space needs higher electricity demand. These building-related factors maintain relatively stable correlations across seasons, unlike the temperature-dependent variations.

NDVI demonstrates a consistent cooling effect, resulting in reduced electricity consumption, with negative correlations ranging from -0.042 to -0.362. The effect is most demonstrated at the 300m scale, where NDVI reaches -0.362 in summer, suggesting that neighborhood-level vegetation provides substantial indirect cooling benefits that reduce electricity demand.

However, as shown in the air temperature consumption analysis (**Chapter 6.4.1**), NDVI's effect on reducing air temperature is stronger at the pixel scale (-0.452) than at 100m and 300m scales (-0.381 and -0.329). This scale-dependent reversal indicates different mechanisms: vegetation directly cools air temperature locally, but its energy-saving benefits operate through neighborhood-scale cumulative cooling and microclimate creation. This cooling effect remains significant across all seasons, though weakest in winter when cooling is not needed.

Building height shows modest positive correlations (0.124 to 0.172), while GSI and building ratio show weaker positive relationships with electricity consumption. The seasonal patterns clearly show summer as the period of strongest correlations for all variables, reflecting the dominance of cooling-related electricity use. Winter shows the weakest correlations overall, indicating that baseline electricity consumption for lighting and equipment is less sensitive to urban form variations. The scale comparison reveals that while the 100m scale shows stronger correlations for air temperature, the 300m scale better captures NDVI's cooling benefits, suggesting that electricity consumption is influenced by both immediate building characteristics and broader neighborhood conditions.

6.4.3 Gas Consumption Directional Importance

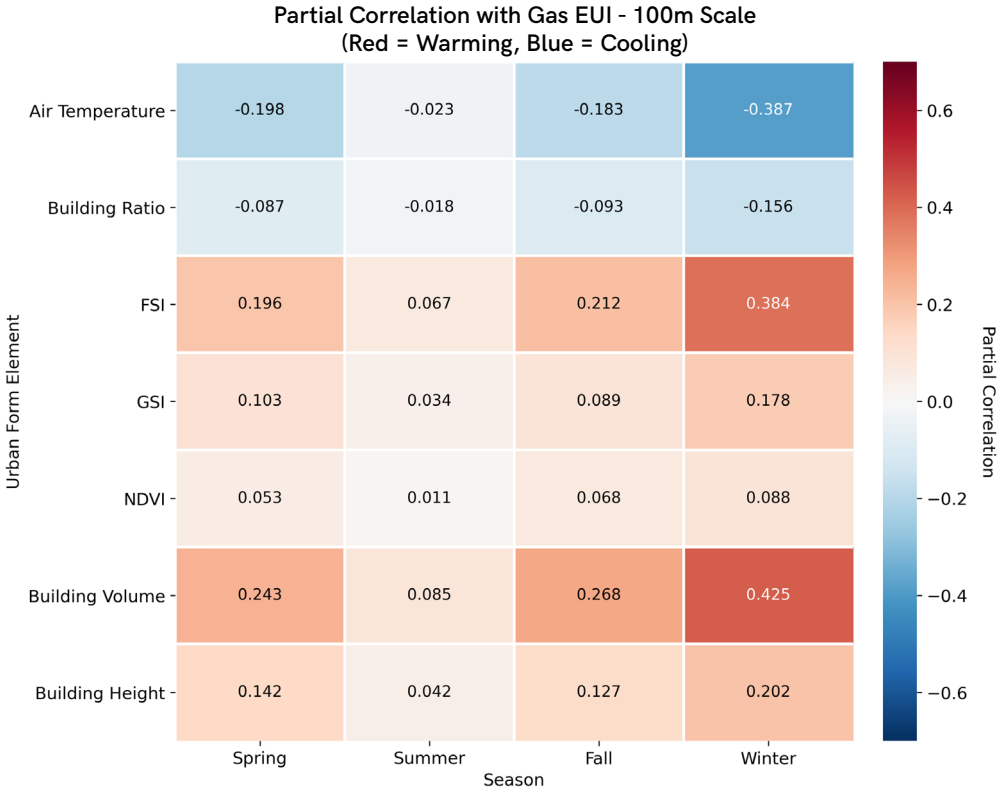

Figure 6.27 *Partial correlation of urban form elements on gas EUI by season in 100m scale*

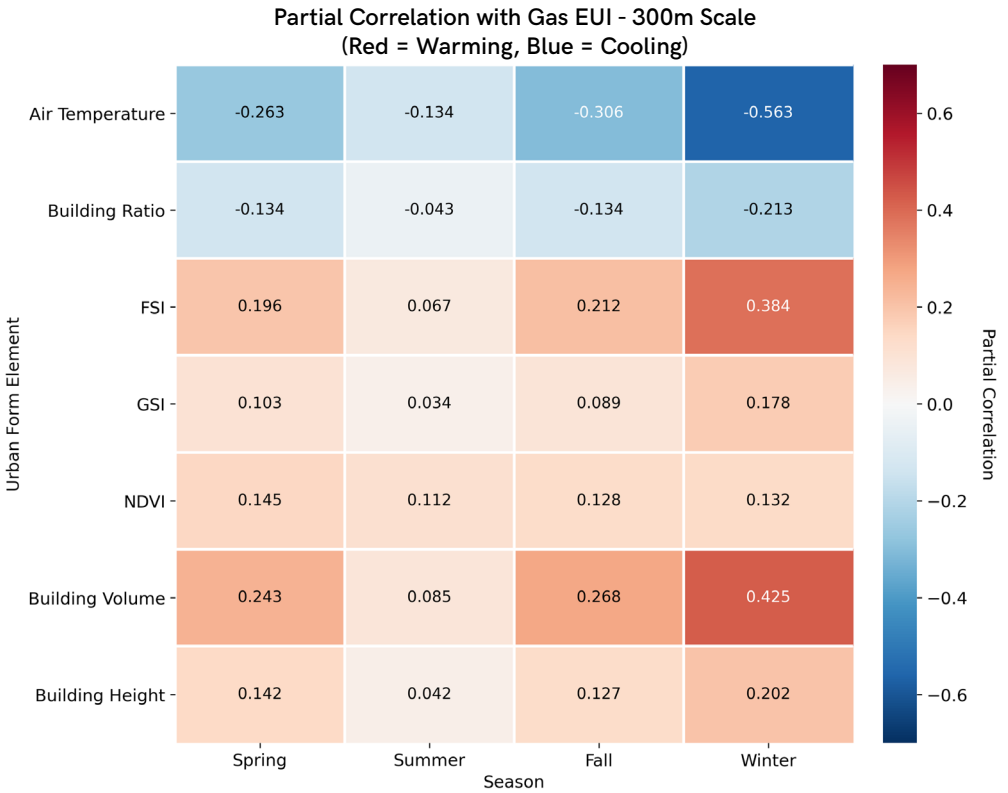

Figure 6.28 *Partial correlation of urban form elements on gas EUI by season in 100m scale*

Gas EUI shows completely different patterns from electricity, which makes sense since gas is mainly used for heating. The most distinct finding is that air temperature has a negative relationship with gas use, as when the temperature is lower, people use more gas for heating. This negative correlation is strongest in winter (-0.387 at 100m scale, -0.563 at 300m scale) and nearly disappears in summer (-0.023 to -0.134) when heating is not needed.

Building volume stands out as the biggest positive factor for gas consumption, but unlike electricity, its importance changes dramatically with seasons. In winter, the correlation increases to 0.425, while in summer it drops to 0.085. However, since this analysis uses EUI, this positive correlation indicates that larger buildings have higher gas intensity per square meter, not just higher total consumption. As shown in **Chapter 6.2.3**, commercial buildings use 22% more gas per square meter than low-rise residential buildings in winter, which confirms that building type and operational characteristics, not just volume, drive these patterns. FSI shows the same seasonal pattern, reaching 0.384 in winter but staying low in summer. Surprisingly, building ratio actually reduces gas consumption (negative correlations from -0.018 to -0.213). This might be because buildings packed closer together share walls and lose less heat. NDVI shows small positive correlations (0.011 to 0.145).

The 300m scale shows stronger relationships than the 100m scale, especially for the air temperature's effect on gas EUI. This suggests that air temperature patterns on a larger scale predict heating needs better than just looking at immediate surroundings. Building height also increases the gas EUI (0.042 to 0.202), with the strongest effect in winter. Overall, these findings confirm that gas consumption depends mainly on how cold it is and building characteristics, including both size and type. The usage patterns are basically the opposite of electricity—high in winter for heating instead of high in summer for cooling.

6.5 UFE Changes over a Decade

The decade from 2015 to 2024 showed significant urban transformation in Heukseok-dong, due to large scale redevelopment projects that changed the area's urban forms. The analysis covers the entire Heukseok-dong and focuses on District 3, which had the most dramatic transformation. These real-world changes help confirm the relationships found in earlier Genizi method and partial correlation analyses.

6.5.1 UFE Changes in Heukseok-dong

Satellite Picture of Heukseok-dong in Feburary 2015

Satellite Picture of Heukseok-dong in March 2024

Mean Air Temperature Change over a Decade in Heukseok-dong				
Year	**Spring**	**Summer**	**Fall**	**Winter**
2015	13.35 °C	23.80 °C	12.75 °C	-0.32 °C
2024	15.13 °C	26.78 °C	15.44 °C	-0.59 °C
Change	+13.1 %	+12.5 %	+21.1 %	-86.5%
Mean NDVI Change over a Decade in Heukseok-dong				
Year	**Spring**	**Summer**	**Fall**	**Winter**
2015	0.068	0.117	0.086	0.037
2024	0.089	0.131	0.108	0.042
Change	+30.3 %	+11.6 %	+25.8 %	+ 13.5 %

Table 6.8 *Mean air temperature and NDVI change over a decade in Heukseok-dong*

Urban Form Elements Change over a Decade in Heukseok-dong					
Year	**Average Building Volume**	**Average Building Height**	**Average FSI**	**Average GSI**	**Average Building Ratio**
2015	2,161 m^3	8.9 m	1.311	0.675	0.189
2024	3,116 m^3	9.3 m	1.384	0.550	0.167
Change	+44.2 %	+4.5 %	+5.6 %	-18.5 %	-15.7 %

Table 6.9 *Average urban form elements change over a decade in Heukseok-dong*

Urban Form Element	**Heukseok-dong Trend Line**
Air Temperature (°C)	
Spring	Temp = 0.3156 × Year - 624.23
Summer	Temp = 0.2192 × Year - 418.42
Fall	Temp = 0.1712 × Year - 333.63
Winter	Temp = 0.0545 × Year - 111.28
NDVI	
Spring	NDVI = 0.00298 × Year - 5.9408
Summer	NDVI = 0.00230 × Year - 4.5537
Fall	NDVI = 0.00152 × Year - 2.9993
Winter	NDVI = 0.000606 × Year - 1.1884
Building Metrics	
FSI	FSI = 0.004091 × Year - 6.892
GSI	GSI = -0.00632 × Year + 13.383
Building Volume (m^3)	Volume = 45.87 × Year - 90,278.12
Building Height (m)	Height = 0.0256 × Year - 42.84
Building Ratio	Ratio = -0.00323 × Year + 6.726
Number of Buildings	Buildings = -42.68 × Year + 89,286.72

Table 6.10 *Trend line of urban form elements change over a decade in Heukseok-dong*

The analysis of Heukseok-dong from 2015 to 2024 reveals significant changes in urban form, though these changes were not uniformly distributed across the entire area. **Table 6.9** shows that average building volume increased by 44.2% from 2,161 m^2 to 3,116 m^2, while building height increased by 4.5%. The linear trend analysis further confirms this pattern, with building volume increasing at 45.87 m^2 per year and building height at 0.0256 m per year. These transformations occurred primarily in specific districts through redevelopment projects, while other neighborhoods remained largely unchanged.

Ground coverage patterns show consistent decline across both snapshot and trend analyses. **Table 6.9** indicates GSI decreased by 18.5% (from 0.675 to 0.550) and building ratio dropped by 15.7% (from 0.189 to 0.167). The trend analysis supports this, showing GSI decreasing by 0.00632 units per year and building ratio by 0.00323 units per year. This reduction in ground coverage reflects the redevelopment in certain districts where older, low-rise residential buildings that covered more ground were replaced with high-rise apartments with smaller footprints.

Temperature patterns from satellite observations at 11:12 AM show complex changes. **Table 6.8** indicates temperature differences between 2015 and 2024 snapshots, with spring showing +1.78°C, summer +2.98°C, and fall +2.69°C, while winter showed a change from -0.32°C to -0.59°C. However, these represent individual observations on specific days. The trend analysis provides a more robust assessment, revealing increasing temperature trends of 0.3156°C per year in spring, 0.2192°C per year in summer, 0.1712°C per year in fall, and 0.0545°C per year in winter over the decade.

NDVI shows improvement across all measures. **Table 6.10** shows increases ranging from 11.6% to 30.3% between 2015 and 2024 snapshots, while trend analysis confirms positive trajectories with spring NDVI increasing by 0.00298 per year, summer by 0.00230 per year, fall by 0.00152 per year, and winter by 0.000606 per year. This indicates gradual improvement in vegetation coverage associated with mandatory green space requirements in redevelopment projects.

The combined evidence from both snapshot comparisons and trend analysis reveals a paradox: despite declining ground coverage (lower GSI and building ratio) and increasing vegetation (higher NDVI), temperature trends continue upward. While the snapshot data must be interpreted cautiously as it represents specific days that may not be representative, the consistent upward temperature trends across all seasons suggest that urban redevelopment's thermal impacts extend beyond simple relationships with green space. This demonstrates that while some districts of Heukseok-dong maintained their original UFEs, the areas that underwent redevelopment created impacts that affected the entire district's environmental conditions. It is important to note that these temperature data represent satellite observations at a single time point (11:12 AM) and may not capture the full diurnal temperature cycle or variations in weather conditions between observation days.

6.5.2 UFE Changes in District 3

Satellite Picture of District 3 in Feburary 2015

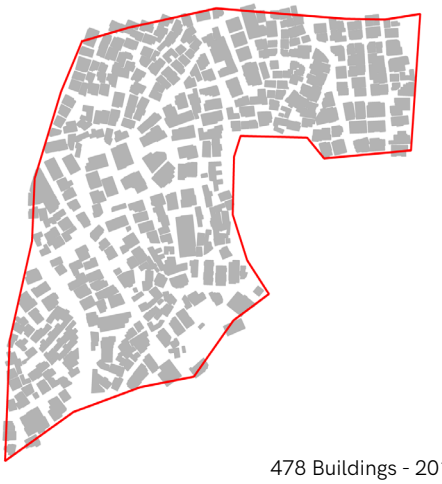

478 Buildings - 2015

Satellite Picture of District 3 in March 2019

Satellite Picture of District 3 in March 2024

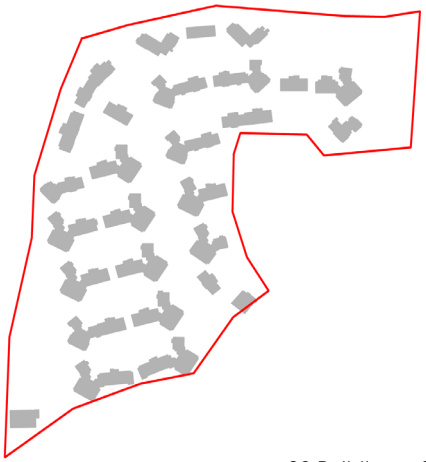

28 Buildings - 2024

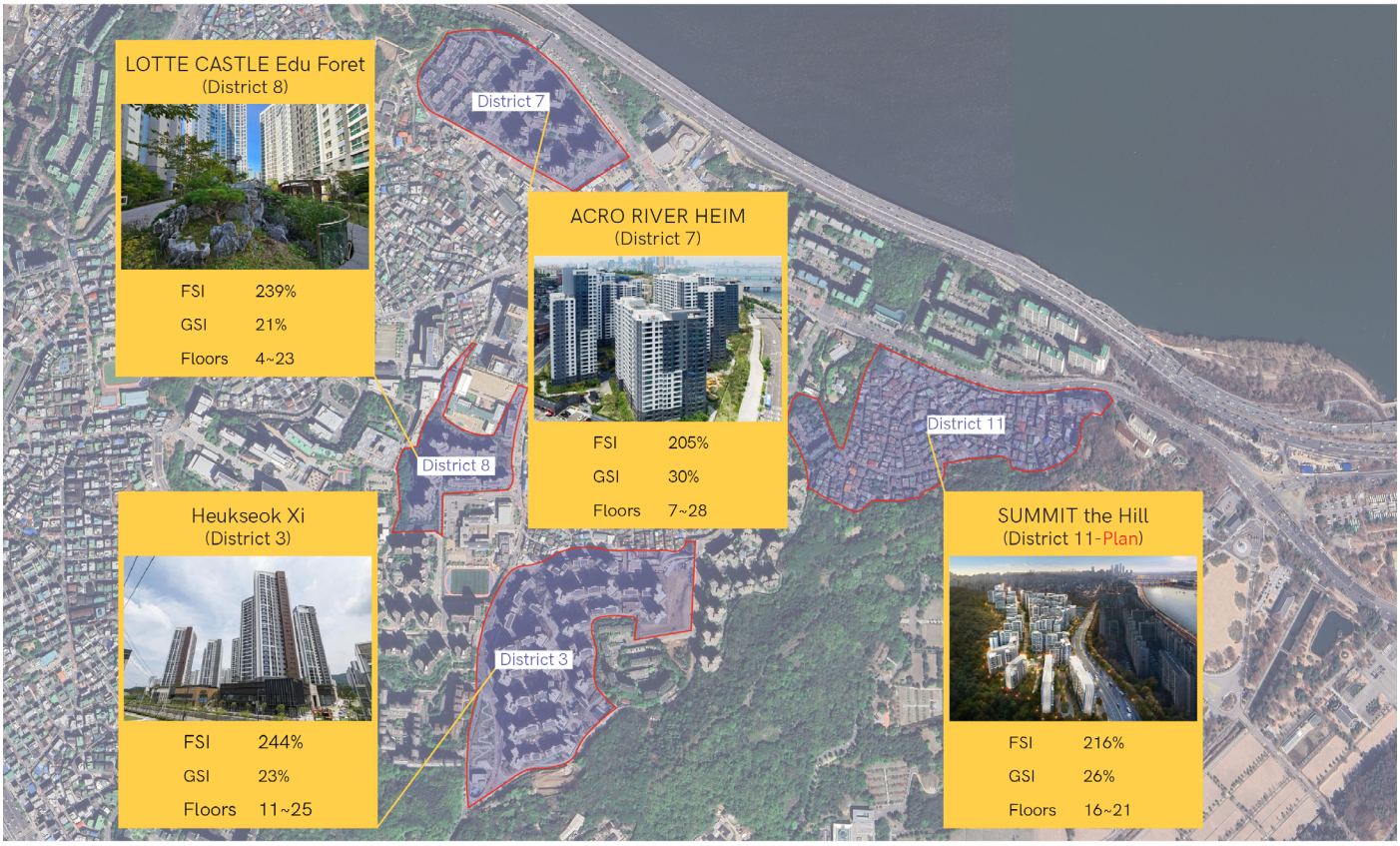

Figure 6.29 *Redvelopment plan in Heukseok-dong*

District 3 represents the most dramatic transformation within Heukseok-dong, serving as a clear example of how intensive redevelopment reshapes urban environments. It underwent one of the most significant transformations through redevelopment in Heukseok-dong. Before redevelopment, the district contained 478 buildings in 2015, consisting primarily of low-rise residential buildings. The redevelopment project began in 2017 and was completed in 2022, resulting in a fundamental change to the urban form. The transformation reduced the number of buildings to 28 high-rise apartment compound, each ranging from 11 to 25 floors, while creating substantially more open space between buildings.

This redevelopment has established District 3 as one of Heukseok-dong's most modern residential areas. The new development offers improved living conditions through increased open space and advanced building systems that were not available in the previous low-rise buildings. These improvements have enhanced residents' quality of life by providing better amenities and more efficient open spaces. However, this transformation has also produced huge impacts on the local environment, particularly affecting air temperature and NDVI throughout the district.

Mean Air Temperature Change over a Decade in District 3				
Year	**Spring**	**Summer**	**Fall**	**Winter**
2015	12.76 °C	23.15 °C	13.52 °C	-0.15 °C
2024	14.20 °C	24.31 °C	14.75 °C	-0.26 °C
Change	+11.3 %	+5.0 %	+9.1 %	-73.3 %
Mean NDVI Change over a Decade in District 3				
Year	**Spring**	**Summer**	**Fall**	**Winter**
2015	0.051	0.104	0.074	0.025
2024	0.082	0.164	0.109	0.067
Change	+60.8 %	+57.7 %	+ 47.3 %	+168.0 %

Table 6.11 *Mean air temperature and NDVI change over a decade in District 3*

Urban Form Elements Change over a Decade in District 3					
Year	**Average Building Volume**	**Average Building Height**	**Average FSI**	**Average GSI**	**Average Building Ratio**
2015	1,175 m^3	10.0 m	1.331	0.705	0.263
2024	25,998 m^3	43.2 m	2.442	0.233	0.122
Change	+2,112.6 %	+332 %	+83.5 %	- 66.9%	-53.6 %

Table 6.12 *Average urban form elements change over a decade in District 3*

Urban Form Element	District 3 Trend Line
Air Temperature (°C)	
Spring	Temp = 0.1503 × Year - 291.04
Summer	Temp = 0.1632 × Year - 21.84
Fall	Temp = 0.1027 × Year - 193.73
Winter	Temp = 0.0353 × Year - 72.43
NDVI	
Spring	NDVI = 0.00353 × Year - 7.0720
Summer	NDVI = 0.00450 × Year - 8.9742
Fall	NDVI = 0.00219 × Year - 4.3412
Winter	NDVI = 0.00253 × Year - 5.0666
Building Metrics	
FSI	FSI = 0.3055 × Year - 617.70
GSI	GSI = -0.1088 × Year + 220.87
Building Volume (m^3)	Volume = 2,456.63 × Year - 4,968,062.56
Building Height (m)	Height = 2.81 × Year - 5,667.86
Building Ratio	Ratio = -0.0514 × Year + 104.43
Number of Buildings	Buildings = -99.32 × Year + 201,593.03

Table 6.13 *Trend line of urban form elements change over a decade in District 3*

The changes in District 3 show more dramatic transformations than Heukseok-dong's overall averages. **Table 6.12** shows building volume increasing by 2,112.6% from 1,175 m^2 in 2015 to 25,998 m^2 in 2024. This represents a complete transformation from a low-rise residential area to a high-rise development zone, confirmed by the trend analysis in **Table 6.13** showing building volume increasing at 2,456.63 m^2 per year. The vertical transformation is also greatly increased, with average building height from 10.0 m to 43.2 m, a 332% increase, with a trend of 2.81 m per year. FSI nearly doubled from 1.331 to 2.442 (83.5% increase), showing a trend of 0.3055 per year, yet GSI dropped dramatically by 66.9% (from 0.705 to 0.233), with a declining trend of -0.1088 per year, and building ratio fell by 53.6% (from 0.263 to 0.122). This means that while buildings became much taller and contained more floor space, they covered far less ground area.

Despite this dramatic reduction in GSI and building ratio, which should theoretically improve ventilation and reduce heat accumulation, temperatures in District 3 still increased across most seasons. **Table 6.11** shows that the air temperatures in spring increased by 11.3%, summer by 5.0%, and fall by 9.1% between 2015 and 2024 snapshots. Moreover, the trend analysis confirms that air temperatures have increased by 0.1503°C per year in spring, 0.1632°C per year in summer, and 0.1027°C per year in fall. However, when it is compared to the entire Heukseok-dong, the temperature increases in District 3 were much lower. On the other hand, Heukseok-dong's trends show 0.3156°C, 0.2192°C, and 0.1712°C per year for spring, summer, and fall, respectively, District 3's trends are approximately half these rates. This suggests that despite a huge increase in building volume, the reduced GSI and increased NDVI provided mitigation of temperature increases.

The average NDVI after redevelopment shows substantial increases across all seasons. Winter NDVI showed the most dramatic improvement at 168.0%, while summer increased by 57.7%. These improvements significantly exceeded the entire Heukseok-dong averages, which ranged from 11.6% to 30.3%, reflecting the mandatory green space requirements and modern landscaping in the new development. The trend analysis shows positive NDVI increases of 0.00353 per year in spring and 0.00450 per year in summer. However, these trends may not account the actual construction period, as they include the period of complete vegetation removal during construction (2018-2022).

While the air temperatures still increased in District 3, the smaller rate of increase compared to Heukseok-dong as a whole suggests that thoughtful redevelopment design can partially offset warming effects. The temperature increases cannot be attributed solely to local urban form changes, as unpredictable factors like global warming might affect the entire region. The fact that District 3's temperature increased less than Heukseok-dong's average, despite its dramatic increase in building volume, indicates that the combination of reduced ground coverage, increased open space, and enhanced vegetation provided meaningful benefits. This real-world example demonstrates that while complete temperature neutrality may be difficult to achieve in high-density redevelopment, careful design incorporating substantial green infrastructure and open space can minimize warming impacts.

6.6 Overall Analysis

The analysis of UFEs in Heukseok-dong reveals complex non-linear relationships between building characteristics, NDVI, air temperature, and energy consumption. By combining the Genizi method results with partial correlations and real-world changes over a decade, several important patterns emerge that show both the power and limitations of urban form in shaping environmental conditions. The most important finding is the gap between the individual correlation strength from the partial correlation and the overall explanatory power from the Genizi method. While NDVI shows strong cooling effects with correlations reaching -0.381 in summer at the 100m scale, the R2 values from the Genizi method range only from 0.067 to 0.328. This means that the model explains less than 33% of air temperature variance, leaving the majority influenced by factors not captured in this analysis. This finding becomes even more meaningful when examining District 3's transformation, where NDVI improvements ranging from 47.3% to 168.0% across seasons with temperature increases of 5.0% to 11.3% between the 2015 and 2024 observations. However, these snapshot comparisons must be interpreted cautiously, as they represent specific days that may have different weather conditions. The trend analysis provides more robust evidence, showing that District 3's temperature increase rates were approximately half of Heukseok-dong's temperature increase rates. This suggests that the urban form changes may have provided partial mitigation despite the warming trends.

Scale effects play a crucial role in understanding these relationships. The 100m buffer scale better captures energy consumption patterns, with the highest R^2 of 0.378 for electricity in summer. This makes sense because energy use depends on individual building characteristics and immediate surroundings. In contrast, the 300m buffer scale better explains air temperature variations, reaching R^2 values up to 0.328, as temperature is influenced by broader neighborhood conditions and heat movement across areas. The scale effect is already confirmed by H. Chen et al. (2019) and Godoy-Shimizu et al. (2021), where building-level analysis at finer spatial resolutions (such as the 100m scale) was necessary for accurate energy flux estimation, while neighborhood-level analysis at broader scales (such as the 300m scale) better captured area-wide temperature variations. However, these larger scales also introduce complexity, shown by negative importance values like FSI at -10.3% in spring, which indicate suppressor effects where variables enhance other predictors' explanatory power through their correlations.

Seasonal patterns dramatically shift the importance of different urban form elements. NDVI dominates air temperature variance in three seasons, contributing 79.3% importance in spring, 64.7% in fall, and 71.6% in winter at the 100m scale. This vegetation dominance is supported by Liao et al. (2021), who applied the Genizi method in Seoul and identified green space ratio as one of the dominant variables affecting surface temperatures. However, while Liao et al.'s methodological approach was comprehensive, their analysis was limited to only four days of data (two summer and two winter days) and focused solely on LST rather than air temperature. This research builds upon Liao et al.'s framework by examining multiple satellite images across a full decade from 2015 to 2024, converting LST to air temperature for more direct relevance to building energy consumption, and extending the analysis to examine the complete cascade relationship from urban form through temperature to actual building energy consumption data.

Additionally, Raj and Yun (2024) found strong negative correlations between NDVI change and surface urban heat island intensity ($R = -0.81$) over 20 years in Seoul. While their study provided valuable long-term trends across Seoul, it focused on city-wide patterns rather than district-level analysis and did not examine energy consumption relationships. This research complements their findings by providing fine-scale analysis at the district level with multiple spatial scales and directly linking temperature changes to building energy consumption patterns.

However, summer shows a complete pattern, with the building ratio taking over at 71.8% importance at the pixel scale, while NDVI drops to -1.2%. This result contradicts Wu et al. (2022)'s finding, which found that NDVI's importance is the highest in summer. This contradiction is likely due to the different temperature metrics used. Wu et al. (2022) analyzed daily average temperatures, which integrate nighttime cooling effects of vegetation throughout the 24-hour cycle. In contrast, this study examines air temperatures at 11:12 AM, when the temperature difference between building and vegetated areas is at its highest. At this specific time, the presence of buildings creates significant temperature differences that overwhelm the variations in vegetation area, making building characteristics dominate the temperature variance. This seasonal flip suggests that during extreme heat, the physical presence and thermal mass of buildings overwhelm vegetation's cooling capacity. The partial correlations support this pattern, with GSI showing its strongest warming effect in summer, with 0.440 at a 300m scale.

Air temperature drives electricity consumption with correlations up to 0.576 in summer, when cooling demands are highest. The relationship is the opposite for gas consumption, with negative correlations reaching -0.387 in winter at the 100m scale, reflecting heating needs. This pattern is confirmed by P. Wang et al. (2023), who reported strong negative correlations between air temperature and gas use. The weak correlation in summer confirms that gas consumption is non-temperature dependent, such as in cooking and water heating. Surprisingly, building volume shows positive correlations with both electricity (0.178 to 0.398) and gas EUI (0.085 to 0.425), despite EUI already being normalized. This suggests that larger buildings in Heukseok-dong have higher energy intensity per m2, possibly due to differences in building use types, age, or systems. This is confirmed by the analysis in **Chapter 6.2.3**, which shows that commercial buildings consume 30-40% more electricity and 22% more gas per square meter than residential buildings. This explains why building volume correlates with higher EUI.

Analysis of District 3 over the last decade provides real-world validation of the statistical patterns while revealing their limitations. Building volume in District 3 increased by 2,112.6% and height by 332%, while GSI decreased by 66.9% and building ratio decreased by 53.6%. These changes created a fundamentally different urban form, which is from low-rise residential buildings covering most of the ground to high-rise apartments with substantial open space. Despite these improvements and significant NDVI increases, temperatures still rose across all seasons except winter. However, district 3's air temperature increases were lower than Heukseok-dong's overall changes, suggesting that redevelopment can provide partial air temperature mitigation. The trend analysis provides more robust evidence of this mitigation effect. While Heukseok-dong's temperature trends show increases of 0.3156°C/year in spring, 0.2192°C/year in summer, and 0.1712°C/year in fall, District 3's trends are 0.1503°C/year, 0.1632°C/year, and 0.1027°C/year respectively, even though the building volume increases of 2,456.63 m2/year. This suggests that the combination of reduced GSI, increased NDVI, and improved spatial configuration provided measurable temperature mitigation.

Building ratio shows an interesting negative correlation with gas consumption (-0.018 to -0.213), suggesting that compact development patterns improve heating efficiency through shared walls and reduced heat loss. This finding, combined with the negative importance values at larger scales, demonstrates how UFEs interact in complex ways that simple correlations might miss.

The overall analysis reveals that while UFEs significantly influence air temperature and energy consumption, they operate within a complex system where unmeasured factors play major roles. The scale-dependent nature of these relationships suggests that interventions must consider both immediate building characteristics and broader neighborhood patterns. Most importantly, the gap between strong individual correlations and modest overall explanatory power, validated by District 3's real-world experience, shows that urban form modifications alone cannot fully address environmental challenges, though they can provide meaningful improvements when thoughtfully implemented.

07

Conclusion

07 Conclusion

This research investigated the complex non-linear relationships between urban form elements (UFEs), air temperature, and energy consumption of buildings in Heukseok-dong, Seoul, through an integrated analysis spanning a decade from 2015 to 2024. The study aimed to understand how physical characteristics of the urban environment influence local climate conditions and building energy use patterns, providing empirical evidence for sustainable urban development strategies in dense residential districts.

The research successfully developed a Multi-Layer Perceptron model to convert satellite-based Land Surface Temperature (LST) to air temperature using Normalized Difference Vegetation Index (NDVI), Digital Elevation Model (DEM), and Solar Zenith Angle (SZA) using air temperature data from Automatic Weather Stations (AWSs) as ground truth data. The MLP model achieved an R^2 of 0.9684 and tested with independent S-DoT sensor data.

The independent testing was conducted in two phases: examining May-August 2020, where the mean temperature difference was 1.84°C, remarkably close to the known systematic temperature difference of 1.8°C between S-DoT sensors and AWS during this period. When extended to the full available period, the mean difference was 0.98°C. The independent testing demonstrated an R^2 of 0.807, confirming that satellite imagery provides a reliable method for urban temperature monitoring when ground-based stations are limited. The study analyzed six urban form elements: NDVI, building ratio, building height, Ground Space Index (GSI), Floor Space Index (FSI), and building volume, examining their impacts across multiple spatial scales and seasons.

Through the application of the Genizi method to address multicollinearity and partial correlation to determine directional relationships, the research found several key findings. NDVI emerged as the dominant cooling factor in most seasons, explaining up to 79.3% of temperature variance in spring, but surprisingly showed reduced importance in summer when building characteristics took dominance. The analysis also revealed scale-dependent relationships, with energy consumption patterns best captured at the 100m scale while temperature variations emerged more clearly at the 300m scale.

The examination of energy consumption patterns showed distinct seasonal dependencies. Air temperature strongly correlated with electricity consumption in summer ($r = 0.576$), reflecting cooling demands, while showing a negative correlation with gas consumption in winter ($r = -0.387$), indicating heating needs. Building volume consistently showed positive correlations with both electricity and gas EUI, which is confirmed in **Chapter 6.2.3** where the commercial buildings consuming 22-40% more energy per m^2 than the residential buildings. However, the low R^2 values (0.067-0.378) across all analyses indicated that UFEs explain only a portion of variance, with factors such as building age, occupancy behaviors, and other system characteristics likely accounting for much of the unexplained variation, which were clearly mentioned by Yoshino et al. (2017) and Bäcklund et al. (2023).

The decade-long transformation of District 3 provided important real-world validation of the statistical findings. Despite huge increases in building volume (2,112.6%) and height (332%), combined with substantial NDVI improvements (up to 168%), temperature trend analysis showed increases of 0.10-0.16°C per year, which are approximately half of Heukseok-dong's overall rates of 0.17-0.32°C per year. This demonstrates that thoughtful urban design can provide partial mitigation of warming effects even in high-density redevelopment.

However, it is important to acknowledge that this research includes an important temporal mismatch between satellite observations and energy consumption data. The analysis uses single hourly temperature observations at 11:12 AM with monthly aggregated energy consumption. This limitation indicates that the research captures spatial correlations between UFEs, air temperature, and energy consumption, rather than proving their direct relationships. The R2 values (0.067-0.378) likely represent this temporal mismatch as much as unmeasured variables. Future research should prioritize obtaining hourly energy consumption data and obtaining more frequent satellite observations to better capture temporal scales and conclude clear cascade effects from urban form through temperature to energy consumption. Despite this limitation, the decade-long analysis and multi-scale approach provide valuable insights into the spatial patterns and long-term trends that inform urban planning strategies.

This study advances the understanding of urban environmental relationships by providing empirical evidence from a long-term, multi-scale analysis using complementary analytical methods. While urban form modifications alone cannot mitigate temperature increases or excessive energy consumption, the research demonstrates that evidence-based planning strategies can achieve meaningful improvements in urban environmental conditions. The methodology developed here, combining satellite monitoring, energy analysis, and statistical techniques to handle complex correlations, provides a framework applicable to other dense urban areas facing similar challenges of rapid development and climate change.

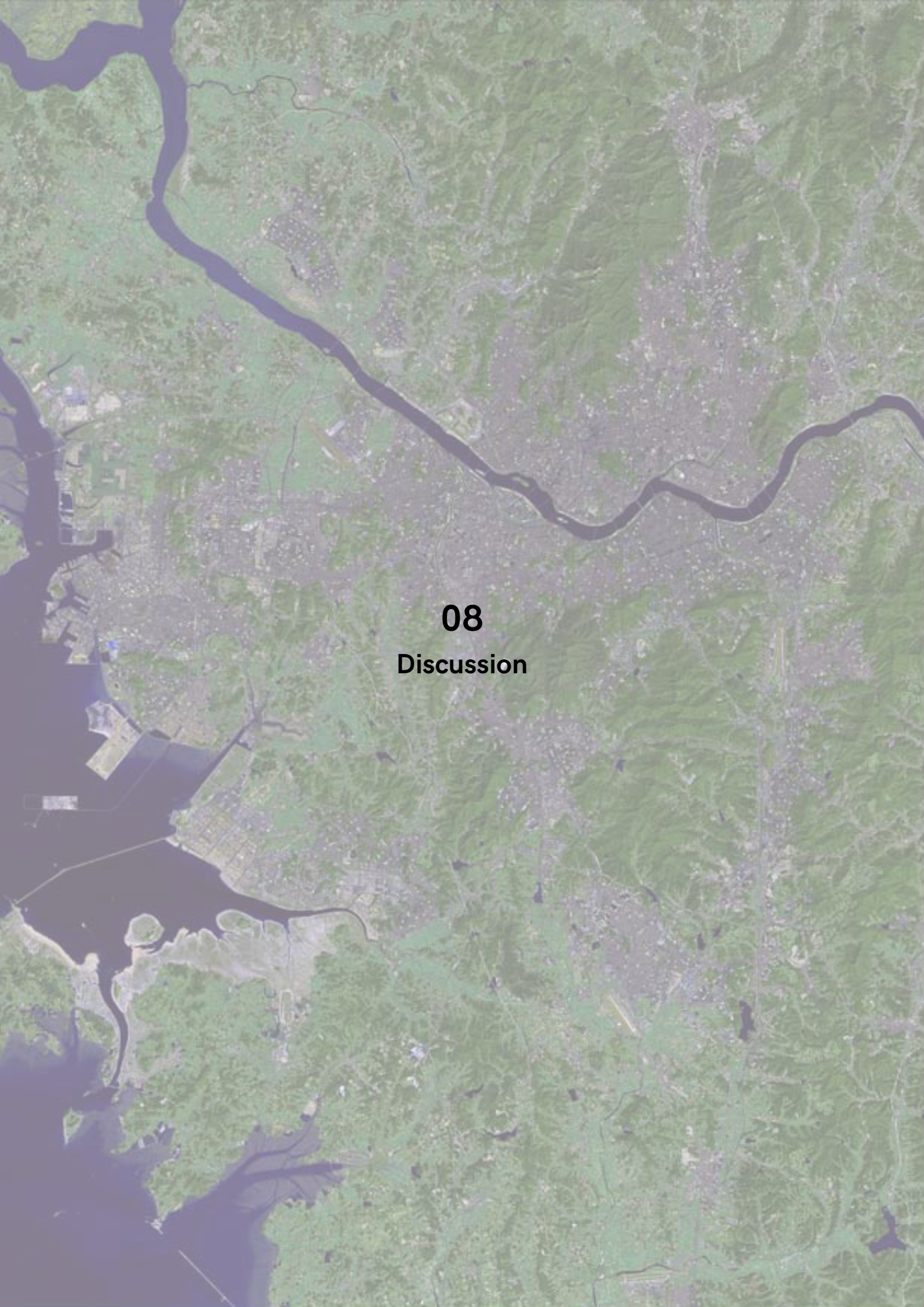

08

Discussion

08 Discussion

8.1 Limitations of the Research

Although this research provides valuable insights into the relationships between UFEs, air temperature, and energy consumption in Heukseok-dong, there are several limitations that must be acknowledged that affect the interpretation and generalizability of the results.

One of the most significant limitations is the **energy consumption data coverage**. The electricity and gas consumption data were not available for all buildings in Heukseok-dong, but primarily for low-rise residential buildings. High-rise apartments, commercial buildings, and university buildings were largely absent from the energy dataset. This limited data availability creates a bias toward older, smaller residential buildings and may not accurately represent the energy consumption patterns of the entire buildings in Heukseok-dong. The positive correlation between building volume and EUI, despite normalization, might be influenced by this sampling bias, as larger buildings with potentially different use types and energy systems were underrepresented in the analysis.

The low R^2 values throughout the analysis from the Genizi method, ranging from 0.067 to 0.378, indicate that 6 UFEs explain only a **small portion of the variance** in both air temperature and energy consumption. This suggests that many variables that are not considered have substantial roles. For energy consumption specifically, many research papers have shown that occupant behavior has been widely considered as one of the key influencing factors on building energy consumption. The absence of occupancy data in this research represents a critical limitation, as building use patterns, occupant density, and behavioral differences significantly affect energy consumption beyond what physical form can predict.

The most critical limitation of this research is the **temporal mismatch** between satellite observations and energy consumption data. Landsat provides only 1-2 images per month at a fixed time of 11:12 AM, meaning each monthly analysis **relies on a single-hour observation**, yet these snapshot observations are correlated with monthly aggregated energy consumption totals. Thus, this research assumes that the air temperature at 11:12 AM on one specific day can represent the entire month's air temperature patterns and energy consumption. This is a significant assumption that likely contributes to the moderate R2 values (0.067-0.378) found in this study.

Furthermore, the 11:12 AM timing may **miss energy demand periods**, with peak cooling typically occurring between 2 and 4 PM, while peak heating occurs in the early morning hours and evenings. Building energy consumption is highly affected by **occupancy patterns** that vary throughout the day. Residential buildings show morning and evening peaks, while commercial buildings peak during business hours. The single snapshot cannot capture these diurnal variations that fundamentally affect the energy demand of the buildings. This temporal mismatch is more severe than the monthly aggregation of energy data because monthly aggregations integrate full consumption patterns, while the satellite data represents an instantaneous moment that may not correlate with when the energy is actually consumed. The moderate correlations found between UFEs and energy consumption may therefore reflect coincidental spatial associations rather than causal relationships mediated by temperature. While the changes in the 10-year analysis provide some compensation through **long-term trends** and explicitly focus on relationships at the satellite overpass time, these approaches do not resolve the fundamental issue with temporally aggregated energy data.

Many building-specific characteristics that were not measured also contribute to the **unexplained variance**. The age of buildings, which varies considerably in Heukseok-dong with many structures dating from the 1950s to the 1970s, affects insulation quality, HVAC system presence, and overall energy efficiency. Building use types have different energy use patterns and operational schedules. Construction materials, window types, and other factors also influence thermal performance, but they were not included in the analysis. These unmeasured factors likely explain the 62-86% unexplained variance in energy consumption models.

Temporal limitations also affect the research findings. The satellite-based air temperature data captured only the 11:12 AM overpass time, missing important diurnal temperature variations. Peak cooling loads typically occur in mid-afternoon, while heating demands peak in early morning hours. The monthly aggregation of energy consumption data masks daily and weekly usage patterns that could provide deeper insights into the relationship between urban form and energy use. Seasonal variations in occupancy, such as vacation periods or academic schedules, were not captured but likely influence energy consumption patterns significantly.

These limitations do not invalidate the research findings but rather provide context for interpretation. The result of significant relationships between UFEs, air temperature, and energy consumption, despite these limitations, suggests that the actual relationships may be even more complex than captured in this analysis. Future research addressing these limitations could provide a more comprehensive understanding of how urban form shapes environmental conditions and energy consumption patterns in dense urban areas.

8.2 Benefits of the Research

This research makes several unique contributions that differentiate it from existing studies on urban environmental conditions and energy consumption. These contributions enhance methodological approaches and provide new insights into the complex relationships between urban form, temperature, and energy use.

The **successful conversion of satellite-based LST to air temperature** with independent testing with S-DoT sensors confirms a significant improvement over prior studies. While many researchers have tried to use satellite imagery for urban temperature analysis, few have validated their models with an independent sensor network. The testing using S-DoT sensors, which achieved an R^2 of 0.807 despite known systematic bias between sensor types, confirms that satellite imagery offers a reliable method for estimating air temperature in urban heat island studies. This independent testing, based on over 23,000 data points from a dense sensor network, shows that satellite-based approaches can accurately convert data to air temperature.

Unlike most urban studies that analyze data over a short period, this research examines a full decade of data from 2015 to 2024. This **long-term analysis** captures not only seasonal variations but also the entire transformation of urban districts through redevelopment. The 10-year span allows for the detection of gradual changes in urban form and their cumulative effects on air temperature and energy consumption, revealing insights often missed in shorter studies. The analysis of District 3 from pre-redevelopment through construction to completion provides empirical evidence of how urban transformations influence environmental conditions over time.

A key innovation in this research is the examination of **cascade effects** linking air temperature, UFEs, and energy consumption as an interconnected system. While many studies have explored the relationship between air temperature and energy consumption or between urban form and energy use separately, few have investigated how all three elements relate to each other. This study demonstrates how UFEs influence air temperature, which in turn affects energy consumption patterns, creating a cascade of effects.

The **combined use of the Genizi method and partial correlation** analysis offers more comprehensive insights than either method alone. While the Genizi method reveals the relative importance of variables despite multicollinearity, partial correlation provides essential directional information. Few studies have employed both methods concurrently, missing either the importance rankings or the directional relationships that together give a complete understanding.

The validation of statistical results through **real-world redevelopment** enhances practical credibility often absent in purely theoretical studies. District 3's transformation, with a 94% reduction in building count but a 2,112.6% increase in building volume, serves as a natural experiment to test whether statistical relationships hold in practice. The observation that, despite significant NDVI improvements (up to 168%), temperatures still increased but less than the district average confirms both the potential and limitations of urban design interventions.

8.3 Implementations of the Research

The findings from this research provide specific, quantitative guidance for urban planning policies aimed at mitigating air temperature and managing energy consumption in dense residential districts. These recommendations are based on the identified relationships between UFEs, air temperature, and energy use patterns observed over a decade in Heukseok-dong.

For air temperature mitigation, urban planning policies should adopt **seasonally differentiated strategies**. During summer months, when building ratio dominates temperature variance (71.8% importance), policies should prioritize reducing ground coverage and building density. The statistical analysis across Heukseok-dong suggests that lower GSI and building ratios correlate with reduced temperatures, while District 3's case demonstrates that even with significant reductions in ground coverage (GSI decreased by 66.9%), temperature increases cannot be completely prevented. While NDVI shows reduced importance in summer (-1.2%), it remains crucial for other seasons, contributing up to 79.3% of temperature variance in spring. Therefore, green space requirements should exceed current standards, with enhanced vegetation coverage throughout redevelopment projects.

The scale-dependent findings indicate that temperature mitigation requires **neighborhood-level interventions**. Since temperature patterns emerge more clearly at a 300m scale, policies should mandate green corridors and open spaces that connect across multiple building blocks. Building height, showing cooling effects through partial correlation from -0.045 to -0.223, suggests that vertical development with reduced ground coverage can provide better natural ventilation and avoid heat accumulation.

For energy consumption management, the research finds that building-level interventions are most effective, as energy patterns are best captured at a smaller scale. The positive correlation between building volume and EUI, despite normalization, indicates that larger buildings require more intensive energy management strategies. Policies should mandate **enhanced energy efficiency standards for buildings with high volume**, such as advanced HVAC systems. The seasonal energy patterns demand different policy approaches for electricity and gas consumption. Since air temperature drives 54.3% of electricity variance in summer, cooling demand reduction through passive design becomes critical. Regulation should require external shading, high-performance glazing, and natural ventilation options, particularly for redevelopments replacing older buildings that currently lack air conditioning. For winter heating, where building volume explains up to 41.3% of gas consumption, policies should prioritize thermal envelope improvements and district heating systems that leverage the efficiency of compact development patterns.

The substantial unexplained variance in energy consumption (62-86%) highlights the importance of addressing factors beyond urban form. Policies should **monitor energy performance** and disclosure for all buildings, not just new construction, to better understand consumption patterns across different building ages and types. Given the significant role of **occupancy behaviors** identified in the other papers, mixed-use development that balances residential and commercial activities could optimize energy use throughout the day.

09
Reference

68% of the world population projected to live in urban areas by 2050, says UN. (2018). United Nations. https://www.un.org/development/desa/en/news/population/2018-revision-of-world-urbanization-prospects.html
Analysis of temperature distribution in Seoul using urban data sensors. (n.d.). The Seoul Research Data Service. Retrieved September 11, 2025, from https://data.si.re.kr/data-insight-report/55616
Bäcklund, K., Molinari, M., Lundqvist, P., & Palm, B. (2023). Building Occupants, Their Behavior and the Resulting Impact on Energy Use in Campus Buildings: A Literature Review with Focus on Smart Building Systems. Energies, 16(17), 6104. https://doi.org/10.3390/en16176104
Bengio, Y. (2012). Practical recommendations for gradient-based training of deep architectures. arXiv (Cornell University). https://doi.org/10.48550/arxiv.1206.5533
Bhattarai, S., Banjara, P., Pandey, V. P., Aryal, A., Pradhan, P., Al-Douri, F., Pradhan, N. R., & Talchabhadel, R. (2025). Quantifying the cooling effects of blue-green spaces across urban landscapes: A case study of Kathmandu Valley, Nepal. Urban Climate, 61, 102493. https://doi.org/10.1016/j.uclim.2025.102493
Cai, X., Yang, J., Zhang, Y., Xiao, X., & Xia, J. (2023). Cooling island effect in urban parks from the perspective of internal park landscape. Humanities and Social Sciences Communications, 10(1). https://doi.org/10.1057/s41599-023-02209-5
Chan, K. Y., Abu-Salih, B., Qaddoura, R., Al-Zoubi, A. M., Palade, V., Pham, D., Del Ser, J., & Muhammad, K. (2023). Deep neural networks in the cloud: Review, applications, challenges and research directions. Neurocomputing, 545, 126327. https://doi.org/10.1016/j.neucom.2023.126327
Chaudhary, V., Bhadola, P., Kaushik, A., Khalid, M., Furukawa, H., & Khosla, A. (2022). Assessing temporal correlation in environmental risk factors to design efficient area-specific COVID-19 regulations: Delhi based case study. Scientific Reports, 12(1). https://doi.org/10.1038/s41598-022-16781-4
Chen, H., Han, Q., & De Vries, B. (2019). Urban morphology indicator analyzes for urban energy modeling. Sustainable Cities and Society, 52, 101863. https://doi.org/10.1016/j.scs.2019.101863
Chen, Y., Quan, J., Zhan, W., & Guo, Z. (2016). Enhanced statistical estimation of air temperature incorporating nighttime light data. Remote Sensing, 8(8), 656. https://doi.org/10.3390/rs8080656
Choi, J., & Kim, G. (2022). History of Seoul's Parks and Green Space Policies: Focusing on policy changes in urban development. Land, 11(4), 474. https://doi.org/10.3390/land11040474
Choi, S., Jin, D., Seong, N., Jung, D., Sim, S., Woo, J., Jeon, U., Byeon, Y., & Han, K. (2021). Near-Surface Air Temperature Retrieval Using a Deep Neural Network from Satellite Observations over South Korea. Remote Sensing, 13(21), 4334. https://doi.org/10.3390/rs13214334
Cui, P., Lu, J., Wu, Y., Tang, J., & Jiang, J. (2024). Effect of urban morphology on microclimate and building cluster energy consumption in cold regions of China. Sustainable Cities and Society, 105838. https://doi.org/10.1016/j.scs.2024.105838
Cybenko, G. (1989). Approximation by superpositions of a sigmoidal function. Mathematics of Control Signals and Systems, 2(4), 303–314. https://doi.org/10.1007/bf02551274
De Almeida, C. R., Teodoro, A. C., & Gonçalves, A. (2021). Study of the Urban Heat Island (UHI) Using Remote Sensing Data/Techniques: A Systematic Review. Environments, 8(10), 105. https://doi.org/10.3390/environments8100105
Delzendeh, E., Wu, S., Lee, A., & Zhou, Y. (2017). The impact of occupants' behaviours on building energy analysis: A research review. Renewable and Sustainable Energy Reviews, 80, 1061–1071. https://doi.org/10.1016/j.rser.2017.05.264
Ding, X., Zhao, Y., Fan, Y., Li, Y., & Ge, J. (2023). Machine learning-assisted mapping of city-scale air temperature: Using sparse meteorological data for urban climate modeling and adaptation. Building and Environment, 234, 110211. https://doi.org/10.1016/j.buildenv.2023.110211
Dong, J., Lin, M., Zuo, J., Lin, T., Liu, J., Sun, C., & Luo, J. (2020). Quantitative study on the cooling effect of green roofs in a high-density urban Area—A case study of Xiamen, China. Journal of Cleaner Production, 255, 120152. https://doi.org/10.1016/j.jclepro.2020.120152
Fan, J., Chen, X., Xie, S., & Zhang, Y. (2023). Study on the response of the summer land surface temperature to urban morphology in Urumqi, China. Sustainability, 15(21), 15255. https://doi.org/10.3390/su152115255
Fikru, M. G., & Gautier, L. (2015). The impact of weather variation on energy consumption in residential houses. Applied Energy, 144, 19–30. https://doi.org/10.1016/j.apenergy.2015.01.040
Gao, S., Zhan, Q., Yang, C., & Liu, H. (2020). The Diversified Impacts of Urban Morphology on Land Surface Temperature among Urban Functional Zones. International Journal of Environmental Research and Public Health, 17(24), 9578. https://doi.org/10.3390/ijerph17249578
Gardner, M., & Dorling, S. (1998). Artificial neural networks (the multilayer perceptron)—a review of applications in the atmospheric sciences. Atmospheric Environment, 32(14–15), 2627–2636. https://doi.org/10.1016/s1352-2310(97)00447-0
Glorot, X., Bordes, A., Bengio, Y., DIRO, Universit´e de Montr´eal, Heudiasyc, UMR CNRS 6599, & UTC, Compi`egne, France. (2011). Deep sparse rectifier neural networks. In Proceedings of the 14th International Conference on Artificial Intelligence and Statistics (AISTATS) 2011. http://proceedings.mlr.press/v15/glorot11a/glorot11a.pdf
Godoy-Shimizu, D., Steadman, P., & Evans, S. (2021). Density and morphology: from the building scale to the city scale. Buildings and Cities, 2(1), 92–113. https://doi.org/10.5334/bc.83
Good, E. J., Ghent, D. J., Bulgin, C. E., & Remedios, J. J. (2017). A spatiotemporal analysis of the relationship between near surface air temperature and satellite land surface temperatures using 17 years of data from the ATSR series. Journal of Geophysical Research Atmospheres, 122(17), 9185–9210. https://doi.org/10.1002/2017jd026880
Hastie, T., Tibshirani, R., & Friedman, J. (2009). The elements of statistical learning. In Springer series in statistics. https://doi.org/10.1007/b94608
Hong, J., Hong, J., Kwon, E. E., & Yoon, D. (2019). Temporal dynamics of urban heat island correlated with the socio-economic development over the past half-century in Seoul, Korea. Environmental Pollution, 254, 112934. https://doi.org/10.1016/j.envpol.2019.07.102
Hu, Y., Dai, Z., & Guldmann, J. (2020). Modeling the impact of 2D/3D urban indicators on the urban heat island over different seasons: A boosted regression tree approach. Journal of Environmental Management, 266, 110424. https://doi.org/10.1016/j.jenvman.2020.110424
Imhoff, M. L., Zhang, P., Wolfe, R. E., & Bounoua, L. (2009). Remote sensing of the urban heat island effect across biomes in the continental USA. Remote Sensing of Environment, 114(3), 504–513. https://doi.org/10.1016/j.rse.2009.10.008
Jamei, E., & Tapper, N. (2018). WSUD and urban Heat island effect mitigation. In Elsevier eBooks (pp. 381–407). https://doi.

org/10.1016/b978-0-12-812843-5.00019-8
Kingma, D. P., & Ba, J. L. (2014). Adam: A method for stochastic optimization. arXiv (Cornell University). https://doi.org/10.48550/arxiv.1412.6980
Korea Architecture Hub. (2024, May). Retrieved September 10, 2025, from https://www.hub.go.kr/portal/opn/tyb/idx-nbem-elcty.do
Korea Meteorological Administration. (n.d.). Retrieved September 11, 2025, from https://data.kma.go.kr/cmmn/main.do
Korean Architecture Hub - Building energy. (2025). Retrieved September 11, 2025, from https://www.hub.go.kr/portal/opn/tyb/idx-nbem-elcty.do
Kotsiopoulos, T., Sarigiannidis, P., Ioannidis, D., & Tzovaras, D. (2021). Machine Learning and Deep Learning in smart manufacturing: The Smart Grid paradigm. Computer Science Review, 40, 100341. https://doi.org/10.1016/j.cosrev.2020.100341
Led, R. (2023). Buildings. In Cambridge University Press eBooks (pp. 953–1048). https://doi.org/10.1017/9781009157926.011
Li, M., Allinson, D., & He, M. (2018). Seasonal variation in household electricity demand: A comparison of monitored and synthetic daily load profiles. Energy and Buildings, 179, 292–300. https://doi.org/10.1016/j.enbuild.2018.09.018
Li, X., Zhou, Y., Yu, S., Jia, G., Li, H., & Li, W. (2019). Urban heat island impacts on building energy consumption: A review of approaches and findings. Energy, 174, 407–419. https://doi.org/10.1016/j.energy.2019.02.183
Li, Y., Schubert, S., Kropp, J. P., & Rybski, D. (2020). On the influence of density and morphology on the Urban Heat Island intensity. Nature Communications, 11(1). https://doi.org/10.1038/s41467-020-16461-9
Li, Z., Tang, B., Wu, H., Ren, H., Yan, G., Wan, Z., Trigo, I. F., & Sobrino, J. A. (2013). Satellite-derived land surface temperature: Current status and perspectives. Remote Sensing of Environment, 131, 14–37. https://doi.org/10.1016/j.rse.2012.12.008
Li, Z., Wu, H., Duan, S., Zhao, W., Ren, H., Liu, X., Leng, P., Tang, R., Ye, X., Zhu, J., Sun, Y., Si, M., Liu, M., Li, J., Zhang, X., Shang, G., Tang, B., Yan, G., & Zhou, C. (2022). Satellite Remote sensing of global land surface temperature: definition, methods, products, and applications. Reviews of Geophysics, 61(1). https://doi.org/10.1029/2022rg000777
Liao, W., Hong, T., & Heo, Y. (2021). The effect of spatial heterogeneity in urban morphology on surface urban heat islands. Energy and Buildings, 244, 111027. https://doi.org/10.1016/j.enbuild.2021.111027
Masters, D., & Luschi, C. (2018). Revisiting small batch training for deep neural networks. arXiv (Cornell University). https://doi.org/10.48550/arxiv.1804.07612
Measuring heat islands | US EPA. (2025, March 18). US EPA. https://www.epa.gov/heatislands/measuring-heat-islands
Meyer, H., Katurji, M., Appelhans, T., Müller, M., Nauss, T., Roudier, P., & Zawar-Reza, P. (2016). Mapping daily air temperature for Antarctica based on MODIS LST. Remote Sensing, 8(9), 732. https://doi.org/10.3390/rs8090732
Mildrexler, D. J., Zhao, M., & Running, S. W. (2011). A global comparison between station air temperatures and MODIS land surface temperatures reveals the cooling role of forests. Journal of Geophysical Research Atmospheres, 116(G3). https://doi.org/10.1029/2010jg001486
Mostafavi, N., Heris, M., Gándara, F., & Hoque, S. (2021). The Relationship between Urban Density and Building Energy Consumption. Buildings, 11(10), 455. https://doi.org/10.3390/buildings11100455
Muller, C. L., Chapman, L., Grimmond, C. S. B., Young, D. T., & Cai, X. (2013). Sensors and the city: a review of urban meteorological networks. International Journal of Climatology, 33(7), 1585–1600. https://doi.org/10.1002/joc.3678
Na, N., Lou, D., Xu, D., Ni, X., Liu, Y., & Wang, H. (2024). Measuring the cooling effects of green cover on urban heat island effects using Landsat satellite imagery. International Journal of Digital Earth, 17(1). https://doi.org/10.1080/17538947.2024.2358867
Naserikia, M., Hart, M. A., Nazarian, N., Bechtel, B., Lipson, M., & Nice, K. A. (2023). Land surface and air temperature dynamics: The role of urban form and seasonality. The Science of the Total Environment, 905, 167306. https://doi.org/10.1016/j.scitotenv.2023.167306
Ngarambe, J., Oh, J. W., Su, M. A., Santamouris, M., & Yun, G. Y. (2021). Influences of wind speed, sky conditions, land use and land cover characteristics on the magnitude of the urban heat island in Seoul: An exploratory analysis. Sustainable Cities and Society, 71, 102953. https://doi.org/10.1016/j.scs.2021.102953
Noi, P., Degener, J., & Kappas, M. (2017). Comparison of Multiple Linear Regression, Cubist Regression, and Random Forest Algorithms to Estimate Daily Air Surface Temperature from Dynamic Combinations of MODIS LST Data. Remote Sensing, 9(5), 398. https://doi.org/10.3390/rs9050398
Oh, J. W., Ngarambe, J., Duhirwe, P. N., Yun, G. Y., & Santamouris, M. (2020). Using deep-learning to forecast the magnitude and characteristics of urban heat island in Seoul Korea. Scientific Reports, 10(1). https://doi.org/10.1038/s41598-020-60632-z
Oke, T. R. (1982). The energetic basis of the urban heat island. Quarterly Journal of the Royal Meteorological Society, 108(455), 1–24. https://doi.org/10.1002/qj.49710845502
Park, J., Kim, J., Lee, D. K., Park, C. Y., & Jeong, S. G. (2016). The influence of small green space type and structure at the street level on urban heat island mitigation. Urban Forestry & Urban Greening, 21, 203–212. https://doi.org/10.1016/j.ufug.2016.12.005
Park, M., & Baek, K. (2023). Quality Management System for an IoT Meteorological Sensor Network—Application to Smart Seoul Data of Things (S-DOT). Sensors, 23(5), 2384. https://doi.org/10.3390/s23052384
Peng, M., & Huang, H. (2022). The synergistic effect of urban canyon geometries and greenery on outdoor thermal comfort in humid subtropical climates. Frontiers in Environmental Science, 10. https://doi.org/10.3389/fenvs.2022.851810
Peng, S., Piao, S., Ciais, P., Friedlingstein, P., Ottle, C., Bréon, F., Nan, H., Zhou, L., & Myneni, R. B. (2011). Surface Urban Heat Island across 419 global big cities. Environmental Science & Technology, 46(2), 696–703. https://doi.org/10.1021/es2030438
Pont, M. B., & Haupt, P. (2023). SpaceMatrix: Space, Density and Urban form. https://doi.org/10.59490/mg.38
Prechelt, L. (2012). Early stopping — but when? In Lecture notes in computer science (pp. 53–67). https://doi.org/10.1007/978-3-642-35289-8_5
Raj, S., & Yun, G. Y. (2024). Exploring the role of strategic urban planning and greening in decreasing surface urban heat island intensity. Journal of Asian Architecture and Building Engineering, 1–14. https://doi.org/10.1080/13467581.2024.2308592
Rasp, S., Pritchard, M. S., & Gentine, P. (2018). Deep learning to represent subgrid processes in climate models. Proceedings of the National Academy of Sciences, 115(39), 9684–9689. https://doi.org/10.1073/pnas.1810286115
Sahani, N. (2021). Assessment of spatio-temporal changes of land surface temperature (LST) in Kanchenjunga Biosphere Reserve (KBR), India using Landsat satellite image and single channel algorithm. Remote Sensing Applications Society and Environment, 24, 100659. https://doi.org/10.1016/j.rsase.2021.100659
Salehin, I., & Kang, D. (2023). A Review on Dropout Regularization Approaches for Deep Neural Networks within the Scholarly Domain. Electronics, 12(14), 3106. https://doi.org/10.3390/electronics12143106

Salih, W., Khalki, E. M. E., Ongoma, V., Lguensat, R., Aithssaine, B., Ouatiki, H., Driouech, F., Sebbar, B., Achli, S., & Chehbouni, A. (2025). TEMLI: A High-Resolution air temperature estimation using machine learning and land surface data across Morocco. Earth Systems and Environment. https://doi.org/10.1007/s41748-025-00629-8
Santamouris, M. (2015). Analyzing the heat island magnitude and characteristics in one hundred Asian and Australian cities and regions. The Science of the Total Environment, 512–513, 582–598. https://doi.org/10.1016/j.scitotenv.2015.01.060
Santamouris, M. (2019). Recent progress on urban overheating and heat island research. Integrated assessment of the energy, environmental, vulnerability and health impact. Synergies with the global climate change. Energy and Buildings, 207, 109482. https://doi.org/10.1016/j.enbuild.2019.109482
Santamouris, M., Cartalis, C., Synnefa, A., & Kolokotsa, D. (2014). On the impact of urban heat island and global warming on the power demand and electricity consumption of buildings—A review. Energy and Buildings, 98, 119–124. https://doi.org/10.1016/j.enbuild.2014.09.052
Schatz, J., & Kucharik, C. J. (2015). Urban climate effects on extreme temperatures in Madison, Wisconsin, USA. Environmental Research Letters, 10(9), 094024. https://doi.org/10.1088/1748-9326/10/9/094024
Schultz, J. M., & Svendsen, S. (1998). WinSim: A simple simulation program for evaluating the influence of windows on heating demand and risk of overheating. Solar Energy, 63(4), 251–258. https://doi.org/10.1016/s0038-092x(98)00062-0
Smart Seoul Data of Things(S-DOT). (2024, July 25). Seoul Metropolitan Government. https://news.seoul.go.kr/gov/archives/539344
Sobrino, J. A., Jiménez-Muñoz, J. C., & Paolini, L. (2004). Land surface temperature retrieval from LANDSAT TM 5. Remote Sensing of Environment, 90(4), 434–440. https://doi.org/10.1016/j.rse.2004.02.003
Song, S., Leng, H., Xu, H., Guo, R., & Zhao, Y. (2020). Impact of urban morphology and climate on heating energy consumption of buildings in severe cold regions. International Journal of Environmental Research and Public Health, 17(22), 8354. https://doi.org/10.3390/ijerph17228354
Stewart, I. D., Krayenhoff, E. S., Voogt, J. A., Lachapelle, J. A., Allen, M. A., & Broadbent, A. M. (2021). Time evolution of the surface urban Heat Island. Earth S Future, 9(10). https://doi.org/10.1029/2021ef002178
Su, M. A., Ngarambe, J., Santamouris, M., & Yun, G. Y. (2021). Empirical evidence on the impact of urban overheating on building cooling and heating energy consumption. iScience, 24(5), 102495. https://doi.org/10.1016/j.isci.2021.102495
Su, Y., Foody, G. M., & Cheng, K. (2012). Spatial non-stationarity in the relationships between land cover and surface temperature in an urban heat island and its impacts on thermally sensitive populations. Landscape and Urban Planning, 107(2), 172–180. https://doi.org/10.1016/j.landurbplan.2012.05.016
Tang, K., Zhu, H., & Ni, P. (2021). Spatial Downscaling of Land Surface Temperature over Heterogeneous Regions Using Random Forest Regression Considering Spatial Features. Remote Sensing, 13(18), 3645. https://doi.org/10.3390/rs13183645
Tian, L., Li, Y., Lu, J., & Wang, J. (2021). Review on Urban Heat Island in China: methods, its impact on buildings energy demand and mitigation strategies. Sustainability, 13(2), 762. https://doi.org/10.3390/su13020762
Tong, S., Wong, N. H., Jusuf, S. K., Tan, C. L., Wong, H. F., Ignatius, M., & Tan, E. (2017). Study on correlation between air temperature and urban morphology parameters in built environment in northern China. Building and Environment, 127, 239–249. https://doi.org/10.1016/j.buildenv.2017.11.013
USGS: What are the acquisition schedules for the Landsat satellites? (2025, February 14). https://www.usgs.gov/faqs/what-are-acquisition-schedules-landsat-satellites
Voogt, J., & Oke, T. (2003). Thermal remote sensing of urban climates. Remote Sensing of Environment, 86(3), 370–384. https://doi.org/10.1016/s0034-4257(03)00079-8
Vujovic, S., Haddad, B., Karaky, H., Sebaibi, N., & Boutouil, M. (2021). Urban Heat Island: Causes, Consequences, and Mitigation Measures with Emphasis on Reflective and Permeable Pavements. CivilEng, 2(2), 459–484. https://doi.org/10.3390/civileng2020026
Wang, C., Song, J., Shi, D., Reyna, J. L., Horsey, H., Feron, S., Zhou, Y., Ouyang, Z., Li, Y., & Jackson, R. B. (2023). Impacts of climate change, population growth, and power sector decarbonization on urban building energy use. Nature Communications, 14(1). https://doi.org/10.1038/s41467-023-41458-5
Wang, D., Zhang, G., Lin, T., Hu, X., Zhao, Z., & Shi, L. (2021). Exploring the Connection between Urban 3D Form and Building Energy Performance and the Influencing Mechanism. ISPRS International Journal of Geo-Information, 10(10), 709. https://doi.org/10.3390/ijgi10100709
Wang, L., Lu, Y., & Yao, Y. (2019). Comparison of Three Algorithms for the Retrieval of Land Surface Temperature from Landsat 8 Images. Sensors, 19(22), 5049. https://doi.org/10.3390/s19225049
Wang, P., Yang, Y., Ji, C., & Huang, L. (2023). Influence of built environment on building energy consumption: a case study in Nanjing, China. Environment Development and Sustainability, 26(2), 5199–5222. https://doi.org/10.1007/s10668-023-02930-w
Weng, Q., Fu, P., & Gao, F. (2014). Generating daily land surface temperature at Landsat resolution by fusing Landsat and MODIS data. Remote Sensing of Environment, 145, 55–67. https://doi.org/10.1016/j.rse.2014.02.003
Wu, W., Yu, Z., Ma, J., & Zhao, B. (2022). Quantifying the influence of 2D and 3D urban morphology on the thermal environment across climatic zones. Landscape and Urban Planning, 226, 104499. https://doi.org/10.1016/j.landurbplan.2022.104499
Xiong, J., Chen, L., & Zhang, Y. (2023). Building energy saving for indoor cooling and heating: Mechanism and comparison on temperature difference. Sustainability, 15(14), 11241. https://doi.org/10.3390/su151411241
Yang, C., Kui, T., Zhou, W., Fan, J., Pan, L., Wu, W., & Liu, M. (2022). Impact of refined 2D/3D urban morphology on hourly air temperature across different spatial scales in a snow climate city. Urban Climate, 47, 101404. https://doi.org/10.1016/j.uclim.2022.101404
Yang, X., Peng, L. L., Jiang, Z., Chen, Y., Yao, L., He, Y., & Xu, T. (2019). Impact of urban heat island on energy demand in buildings: Local climate zones in Nanjing. Applied Energy, 260, 114279. https://doi.org/10.1016/j.apenergy.2019.114279
Yoshino, H., Hong, T., & Nord, N. (2017). IEA EBC annex 53: Total energy use in buildings—Analysis and evaluation methods. Energy and Buildings, 152, 124–136. https://doi.org/10.1016/j.enbuild.2017.07.038
Zhou, D., Zhao, S., Liu, S., Zhang, L., & Zhu, C. (2014). Surface urban heat island in China's 32 major cities: Spatial patterns and drivers. Remote Sensing of Environment, 152, 51–61. https://doi.org/10.1016/j.rse.2014.05.017
Ziter, C. D., Pedersen, E. J., Kucharik, C. J., & Turner, M. G. (2019). Scale-dependent interactions between tree canopy cover and impervious surfaces reduce daytime urban heat during summer. Proceedings of the National Academy of Sciences, 116(15), 7575–7580. https://doi.org/10.1073/pnas.1817561116

10
Appendix

Appendix 1 Information of AWS

Code	Name	Latitude	Longitude	Altitude
400	강남	37.4982	127.0816	12.66
401	서초	37.48462	127.026	33.05
402	강동	37.55556	127.145	55.29
403	송파	37.51151	127.0967	58.26
404	강서	37.5739	126.8295	9.299
405	양천	37.52823	126.8794	22.75
406	도봉	37.66557	127.0304	56.65
407	노원	37.62186	127.0919	25.3
408	동대문	37.58463	127.0604	53.96
409	중랑	37.58551	127.0868	39.09
410	기상청	37.4933	126.9175	41.758
411	마포	37.55165	126.9292	100.67
412	서대문	37.57047	126.9408	103.08
413	광진	37.53344	127.086	29.912
414	성북	37.61134	126.9998	128.62
415	용산	37.51955	126.9763	31.73
416	은평	37.64647	126.9427	55
417	금천	37.46551	126.9002	45
418	한강	37.52489	126.939	10.66

Code	Name	Latitude	Longitude	Altitude
419	중구	37.55236	126.9874	267.05
421	성동	37.54721	127.0389	34.73
422	북악산	37.60344	126.9844	333.8
423	구로	37.49328	126.8263	56.08
424	강북	37.63801	127.0098	69.8
425	남현	37.46347	126.9815	113
509	관악	37.45284	126.9502	141.64
510	영등포	37.52706	126.9071	25.38
889	현충원	37.50036	126.9765	16.23
590	과천	37.44028	127.0025	46.6
541	남양주	37.63405	127.1506	25.36
450	주교	37.59834	126.849	45.34
532	의정부	37.73476	127.0735	89.49
540	고양	37.6373	126.892	44.71
444	하남	37.53794	127.2137	27.68
572	성남	37.42093	127.1248	28.65
649	부평	37.47223	126.7507	25.91
116	관악(레)	37.44526	126.964	624.82
569	구리	37.58224	127.157	27.15

Appendix 2 Landsat 8 Obtained Time

Year	Date	Time
2013	16/Mar	02:12:30.8483140Z
2013	17/May	02:11:11.1128030Z
2013	11/Jun	02:11:06.4518000Z
2013	18/Sep	02:10:50.8580940Z
2013	22/Oct	02:10:21.4068040Z
2013	21/Dec	02:10:29.0925990Z
2014	17/Jan	02:10:40.5742760Z
2014	22/Feb	02:11:11.1177340Z
2014	29/Mar	02:11:07.8291040Z
2014	13/May	02:10:56.9703300Z
2014	16/Jun	02:10:47.4312600Z
2014	19/Aug	02:11:02.4569760Z
2014	21/Sep	02:11:04.9631590Z
2014	22/Oct	02:11:17.2364270Z
2014	13/Dec	02:10:48.0682050Z
2015	19/Jan	02:10:57.8989180Z
2015	17/Mar	02:11:08.6982830Z
2015	19/May	02:12:17.2364270Z
2015	21/Jun	02:12:13.1821710Z
2015	17/Jul	02:10:59.6394180Z
2015	19/Sep	02:12:48.0682050Z
2015	11/Oct	02:12:57.8989180Z
2015	23/Dec	02:11:08.6982830Z
2016	13/Jan	02:12:13.9619269Z
2016	22/Mar	02:11:07.8291040Z
2016	19/Apr	02:10:56.9703300Z
2016	17/May	02:12:47.4312600Z
2016	20/Jul	02:11:02.4569760Z
2016	22/Aug	02:12:04.9631590Z
2016	18/Sep	02:12:17.2364270Z

Year	Date	Time
2016	10/Oct	02:11:48.0682050Z
2016	14/Nov	02:10:57.8938180Z
2016	16/Dec	02:11:01.6982830Z
2017	13/Jan	02:12:17.2364270Z
2017	24/Feb	02:11:04.9631590Z
2017	23/Mar	02:11:17.2364270Z
2017	09/Apr	02:10:48.0682050Z
2017	17/May	02:10:57.8989180Z
2017	24/Jun	02:11:08.6982830Z
2017	28/Aug	02:12:17.2364270Z
2017	11/Oct	02:12:13.1821710Z
2017	18/Nov	02:10:59.6394180Z
2017	24/Dec	02:12:48.0682050Z
2018	25/Jan	02:11:01.6982830Z
2018	22/Feb	02:12:17.2364270Z
2018	14/Mar	02:11:04.9631590Z
2018	18/May	02:11:17.2364270Z
2018	20/Nov	02:10:48.0682050Z
2018	11/Dec	02:12:17.2364270Z
2019	08/Jan	02:12:17.2364270Z
2019	18/Feb	02:12:48.0682050Z
2019	29/May	02:12:57.8989180Z
2019	22/Jun	02:11:08.6982830Z
2019	26/Oct	02:12:17.2364270Z
2019	15/Nov	02:12:13.1821710Z
2019	19/Dec	02:11:04.9631590Z
2020	14/Jan	02:10:57.8389180Z
2020	09/Feb	02:11:08.6102830Z
2020	20/Mar	02:12:17.2114270Z
2020	15/Apr	02:12:13.2021710Z

Year	Date	Time
2020	28/May	02:12:09.2114270Z
2020	23/Dec	02:12:23.2021710Z
2021	23/Feb	02:12:15.6982830Z
2021	29/Mar	02:12:22.2364270Z
2021	11/Apr	02:11:43.9631590Z
2021	25/Jun	02:11:36.2364270Z
2021	19/Aug	02:12:43.0682050Z
2021	20/Sep	02:12:21.8989180Z
2021	11/Oct	02:11:15.6112830Z
2022	08/Jan	02:12:52.2064270Z
2022	27/Apr	02:12:23.1121710Z
2022	25/May	02:10:19.8989180Z
2022	13/Jun	02:11:33.6982830Z
2022	22/Sep	02:12:39.2364270Z
2022	18/Oct	02:12:52.1821710Z
2022	24/Nov	02:10:27.6394180Z
2022	15/Dec	02:12:49.0682050Z
2023	15/Mar	02:11:11.6982830Z
2023	19/May	02:12:25.2364270Z
2023	22/Oct	02:11:11.9631590Z
2023	22/Nov	02:11:10.2364270Z
2023	14/Dec	02:11:12.9631590Z
2024	13/Jan	02:12:30.8989180Z
2024	22/Apr	02:12:01.6283930Z
2024	19/May	02:12:17.2364270Z
2024	24/Jun	02:11:04.9631590Z
2024	29/Aug	02:11:17.2364270Z
2024	02/Oct	02:12:48.0682050Z
2024	14/Dec	02:12:57.8989180Z

Obtained Time is in UTC (+9)

Appendix 3 Genizi Method Result

Air Temperature

Air Temperature Genizi Method				Pixel Scale
UFE	**Spring (R^2=0.137)**	**Summer (R^2=0.195)**	**Fall (R^2=0.098)**	**Winter (R^2=0.067)**
NDVI	59.2	-1.2	63.8	60.1
Building Ratio	6.3	71.8	4.3	3.2
Weighted Height	5.8	7.8	3.1	13.5
GSI	1.5	19.5	0.9	1.8
Volume Density	0.8	3.2	0.6	1.2
FSI	-0.3	-1.1	-0.1	0.2
Air Temperature Genizi Method				**100m Scale**
UFE	**Spring (R^2=0.218)**	**Summer (R^2=0.281)**	**Fall (R^2=0.186)**	**Winter (R^2=0.144)**
NDVI	79.3	-4.8	64.7	71.6
Building Ratio	11.2	62.3	7.8	5.4
Weighted Height	9.7	13.5	6.9	19.8
GSI	3.5	21.7	2.4	6.2
Volume Density	-2.8	8.9	-1.3	-1.8
FSI	-0.9	-2.6	-0.5	-1.2
Air Temperature Genizi Method				**300m Scale**
UFE	**Spring (R^2=0.304)**	**Summer (R^2=0.407)**	**Fall (R^2=0.328)**	**Winter (R^2=0.228)**
NDVI	83.9	43.7	73.4	77.3
Building Ratio	-3.6	-3.3	-1.7	-4.3
Weighted Height	23.5	28.3	19.8	34.7
GSI	5.4	36.8	-8.4	-14.8
Volume Density	15.8	-17.9	12.7	23.5
FSI	-10.3	12.4	4.2	8.6

Electricity EUI

Electricity EUI Genizi Method - 100m Scale				100m Scale
UFE	**Spring (R^2=0.256)**	**Summer (R^2=0.378)**	**Fall (R^2=0.271)**	**Winter (R^2=0.238)**
Air Temperature	41.2	54.3	36.8	14.8
NDVI	2.8	1.3	7.6	1.3
Building Ratio	8.2	13.5	7.3	16.9
Building Height	-11.3	-6.8	-9.4	-4.3
GSI	14.6	9.2	13.8	11.3
Building Volume	25.8	15.8	23.7	33.8
FSI	18.7	12.7	20.2	27.2
Electricity EUI Genizi Method - 300m Scale				**300m Scale**
UFE	**Spring (R^2=0.194)**	**Summer (R^2=0.262)**	**Fall (R^2=0.172)**	**Winter (R^2=0.152)**
Air Temperature	32.4	39.8	23.2	8.5
NDVI	28.7	34.6	25.6	20.8
Building Ratio	6.7	-24.7	-14.8	-10.3
Building Height	12.7	6.0	13.6	3.8
GSI	-18.3	21.3	-13.2	-19.7
Building Volume	21.3	13.2	28.3	31.2
FSI	16.5	9.8	17.3	25.7

Gas EUI

Gas EUI Genizi Method - 100m Scale				100m Scale
UFE	**Spring (R^2=0.312)**	**Summer (R^2=0.236)**	**Fall (R^2=0.337)**	**Winter (R^2=0.382)**
Air Temperature	24.8	6.8	27.6	31.3
NDVI	2.8	0.6	1.2	-1.3
Building Ratio	7.8	3.5	5.1	3.8
Building Height	-14.2	-13.2	-12.8	-11.7
GSI	16.8	19.4	15.2	12.8
Building Volume	26.3	41.3	28.9	35.2
FSI	21.7	31.8	23.4	20.1
Gas EUI Genizi Method - 300m Scale				**300m Scale**
UFE	**Spring (R^2=0.228)**	**Summer (R^2=0.164)**	**Fall (R^2=0.243)**	**Winter (R^2=0.252)**
Air Temperature	17.8	3.2	21.3	23.7
NDVI	25.8	18.7	28.3	31.4
Building Ratio	-12.7	-8.7	-13.5	-14.2
Building Height	4.2	2.3	3.8	2.3
GSI	-18.6	-23.8	-15.4	-12.8
Building Volume	23.8	38.6	26.8	32.6
FSI	19.3	29.3	20.7	17.8

Appendix 4 10-Year Change in Heukseok-dong

Year 2015

Year 2016

Year 2017

Year 2018

Year 2019

Year 2020

Year 2021

Year 2022

Year 2023

Year 2024

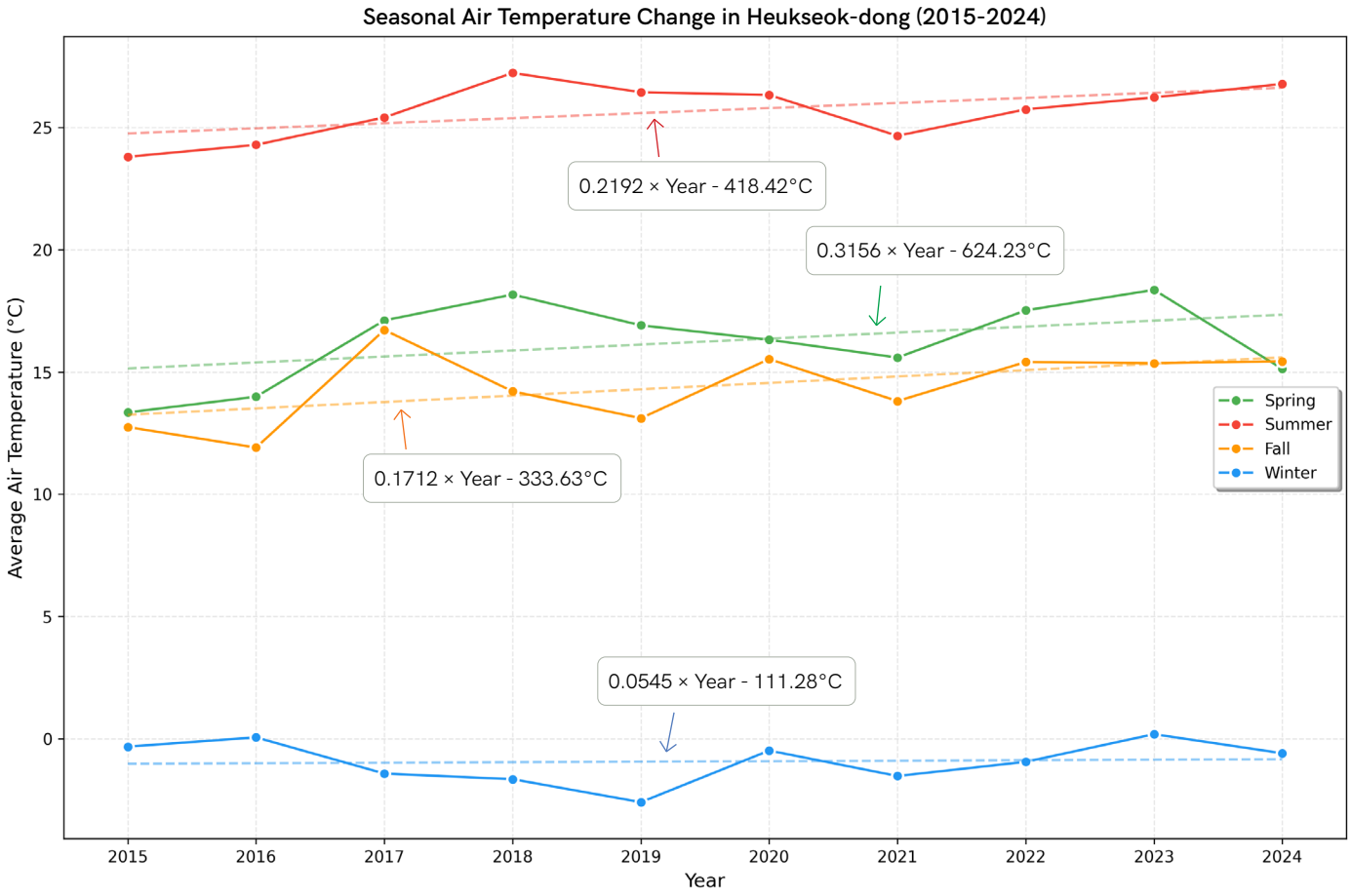
Seasonal Air Temperature Change in Heukseok-dong (2015-2024)
Average Air Temperature (°C)
Year
0.2192 × Year - 418.42°C
0.3156 × Year - 624.23°C
0.1712 × Year - 333.63°C
0.0545 × Year - 111.28°C
Spring
Summer
Fall
Winter

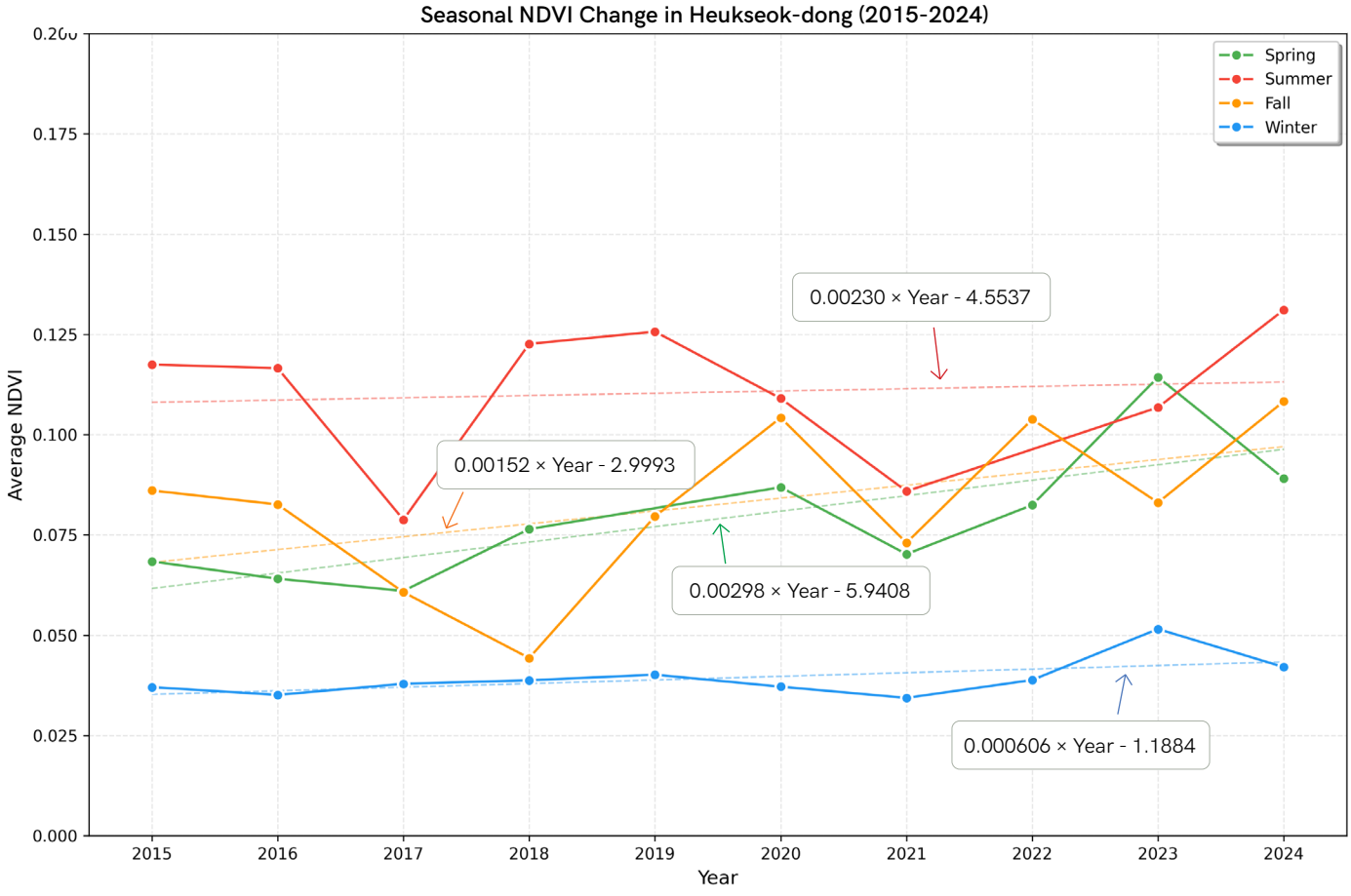
Seasonal NDVI Change in Heukseok-dong (2015-2024)
Average NDVI
Year
0.00230 × Year - 4.5537
0.00152 × Year - 2.9993
0.00298 × Year - 5.9408
0.000606 × Year - 1.1884
Spring
Summer
Fall
Winter

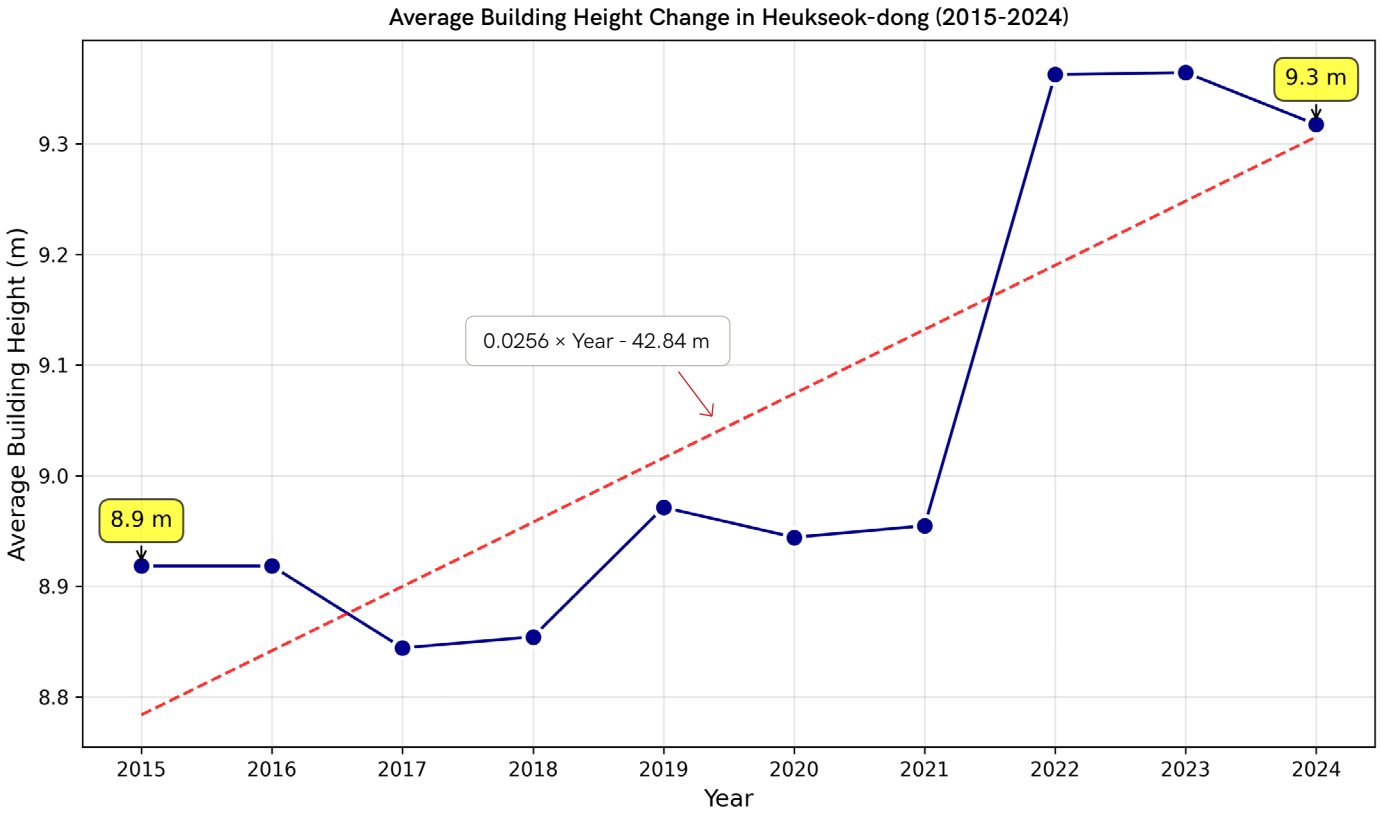
Average Building Height Change in Heukseok-dong (2015-2024)
Average Building Height (m)
Year
0.0256 × Year - 42.84 m
8.9 m
9.3 m
9.3
9.2
9.1
9.0
8.9
8.8
2015
2016
2017
2018
2019
2020
2021
2022
2023
2024

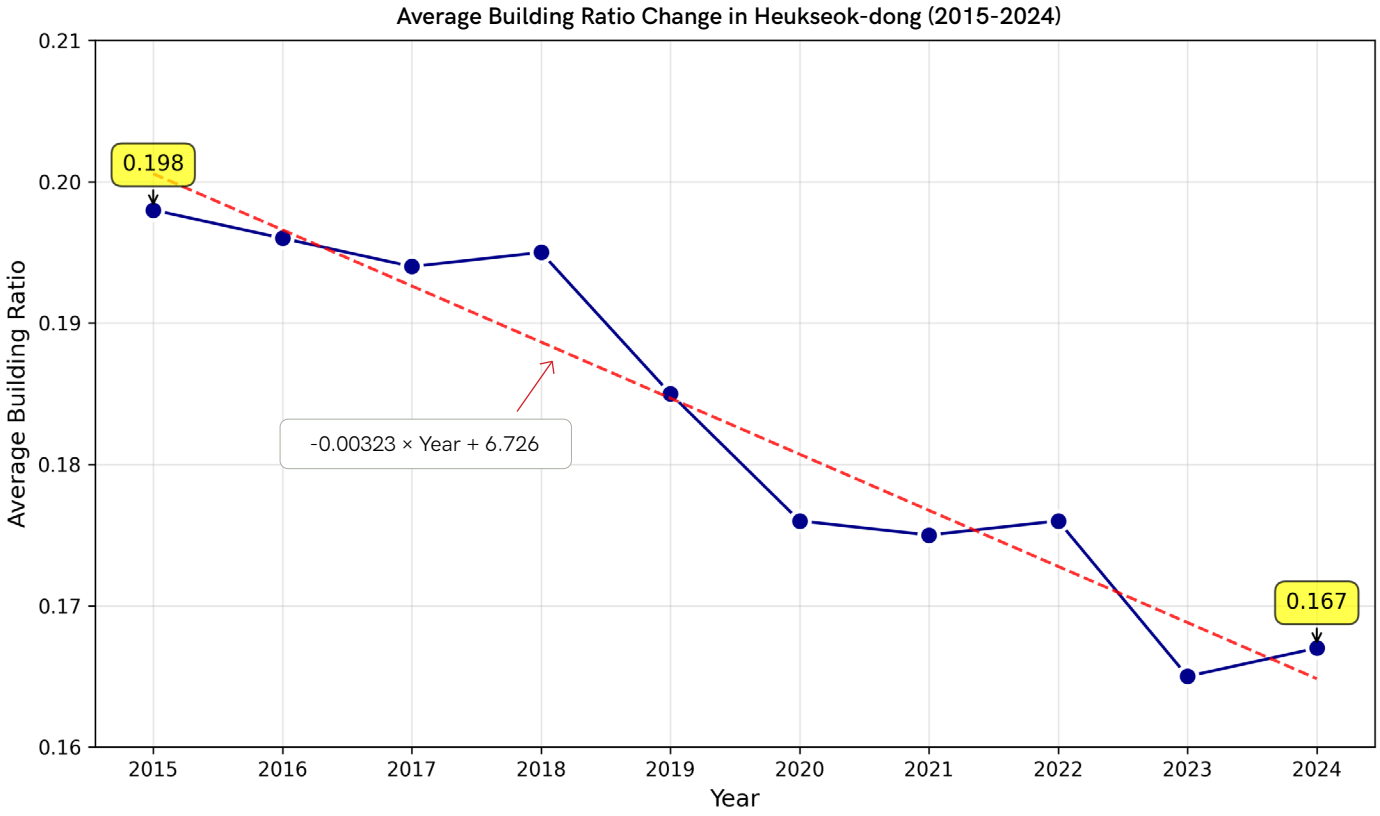
Average Building Ratio Change in Heukseok-dong (2015-2024)
Average Building Ratio
Year
-0.00323 × Year + 6.726
0.198
0.167
0.21
0.20
0.19
0.18
0.17
0.16
2015
2016
2017
2018
2019
2020
2021
2022
2023
2024

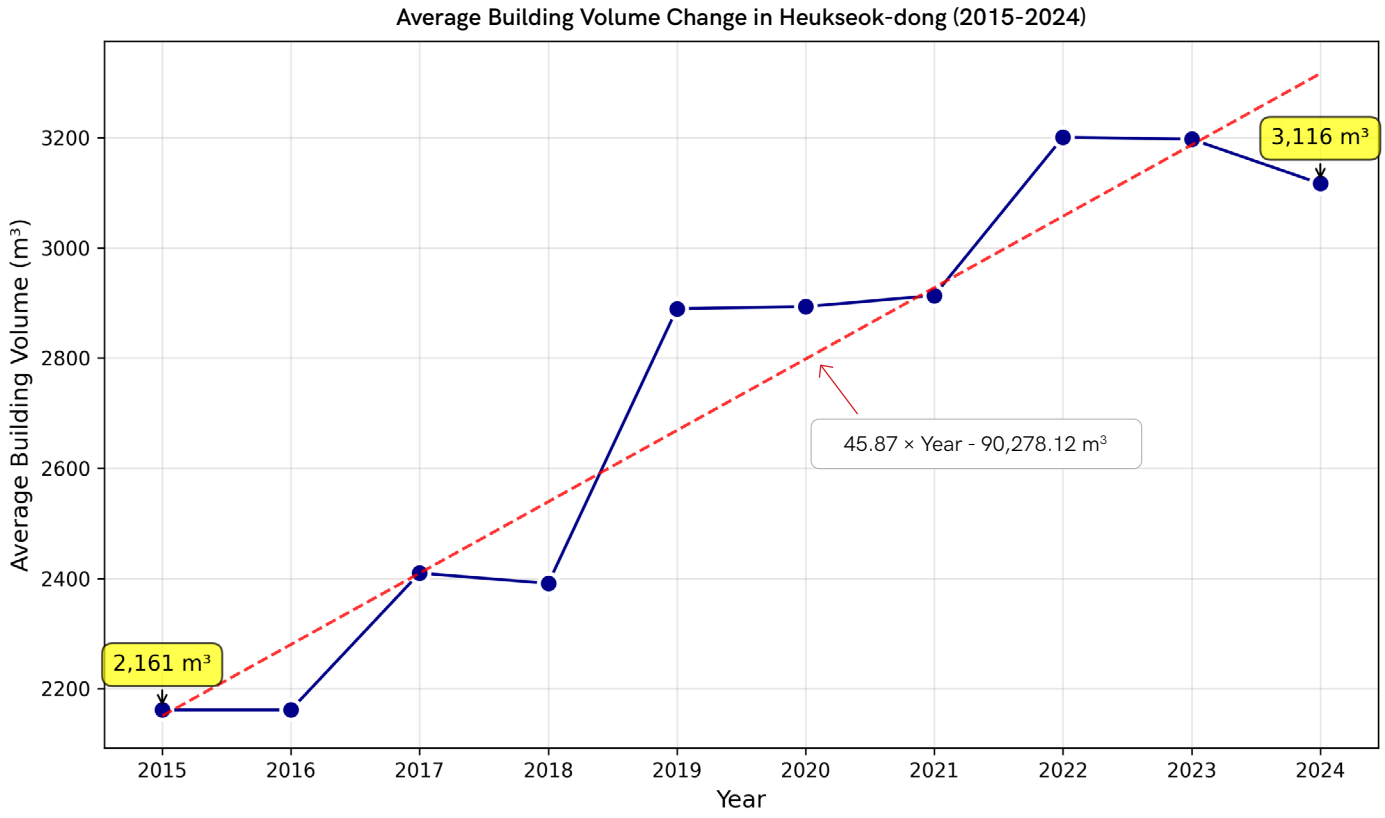
Average Building Volume Change in Heukseok-dong (2015-2024)
Average Building Volume (m³)
Year
2,161 m³
3,116 m³
45.87 × Year - 90,278.12 m³

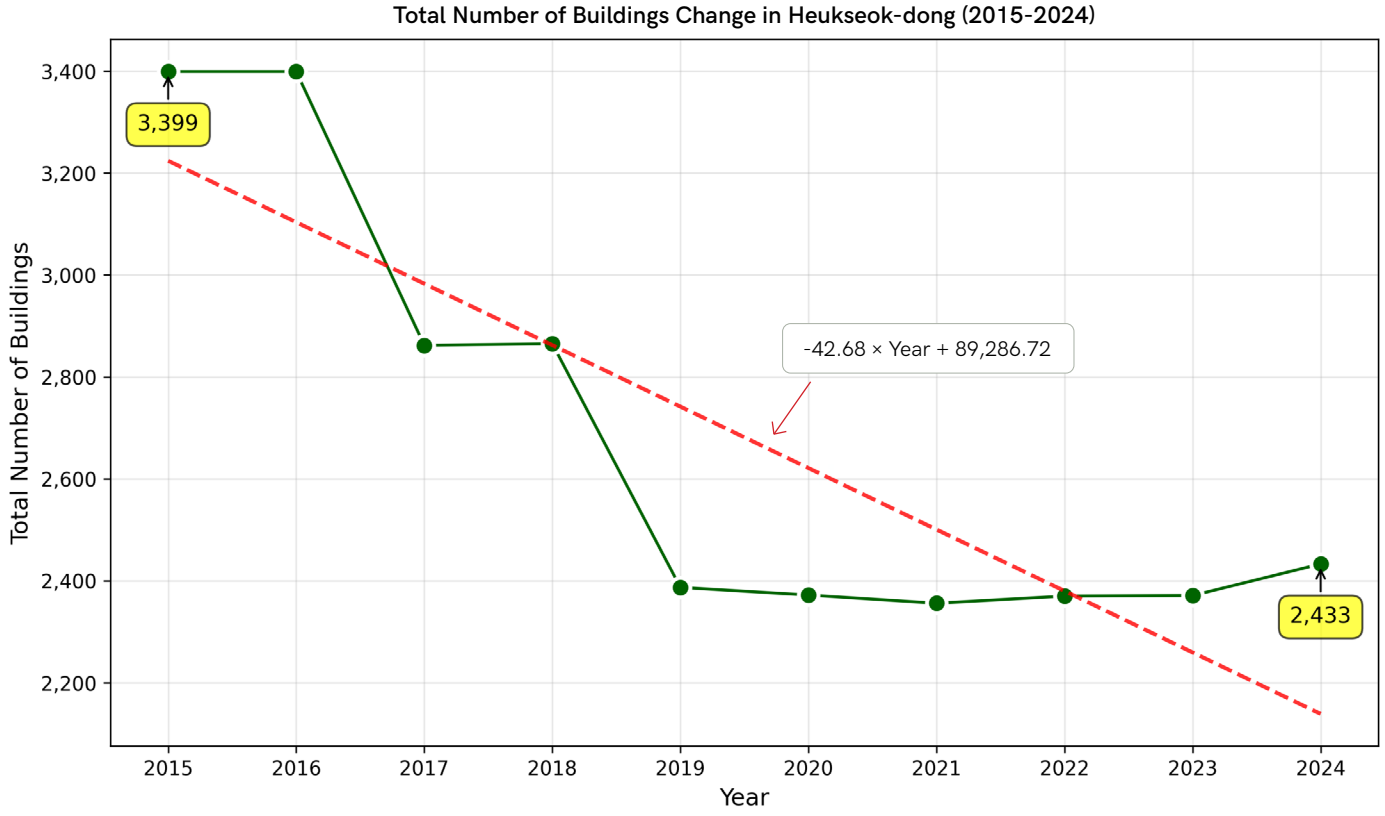
Total Number of Buildings Change in Heukseok-dong (2015-2024)
Total Number of Buildings
Year
3,399
2,433
-42.68 × Year + 89,286.72

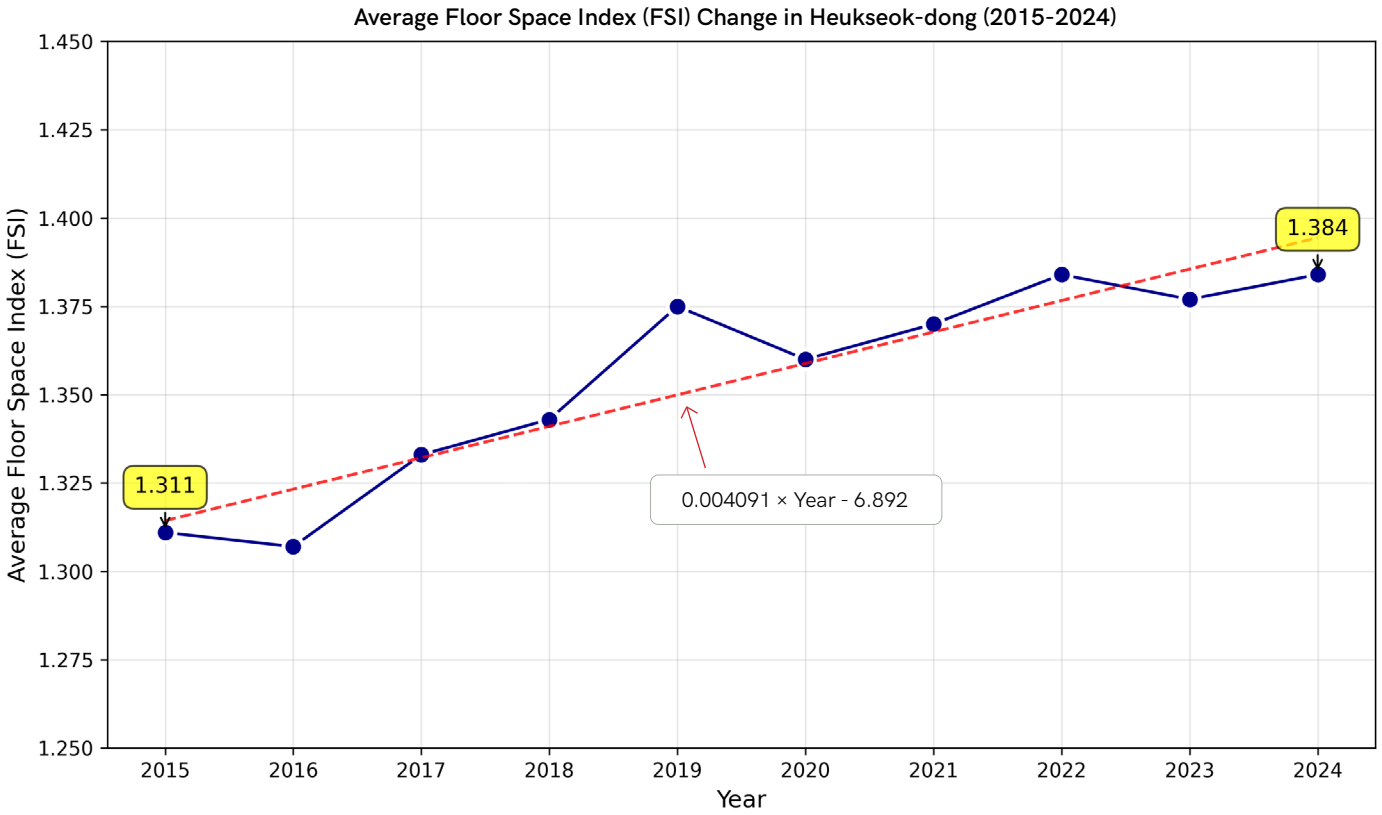
Average Floor Space Index (FSI) Change in Heukseok-dong (2015-2024)
Average Floor Space Index (FSI)
Year
1.311
1.384
0.004091 × Year - 6.892
1.450
1.425
1.400
1.375
1.350
1.325
1.300
1.275
1.250
2015
2016
2017
2018
2019
2020
2021
2022
2023
2024

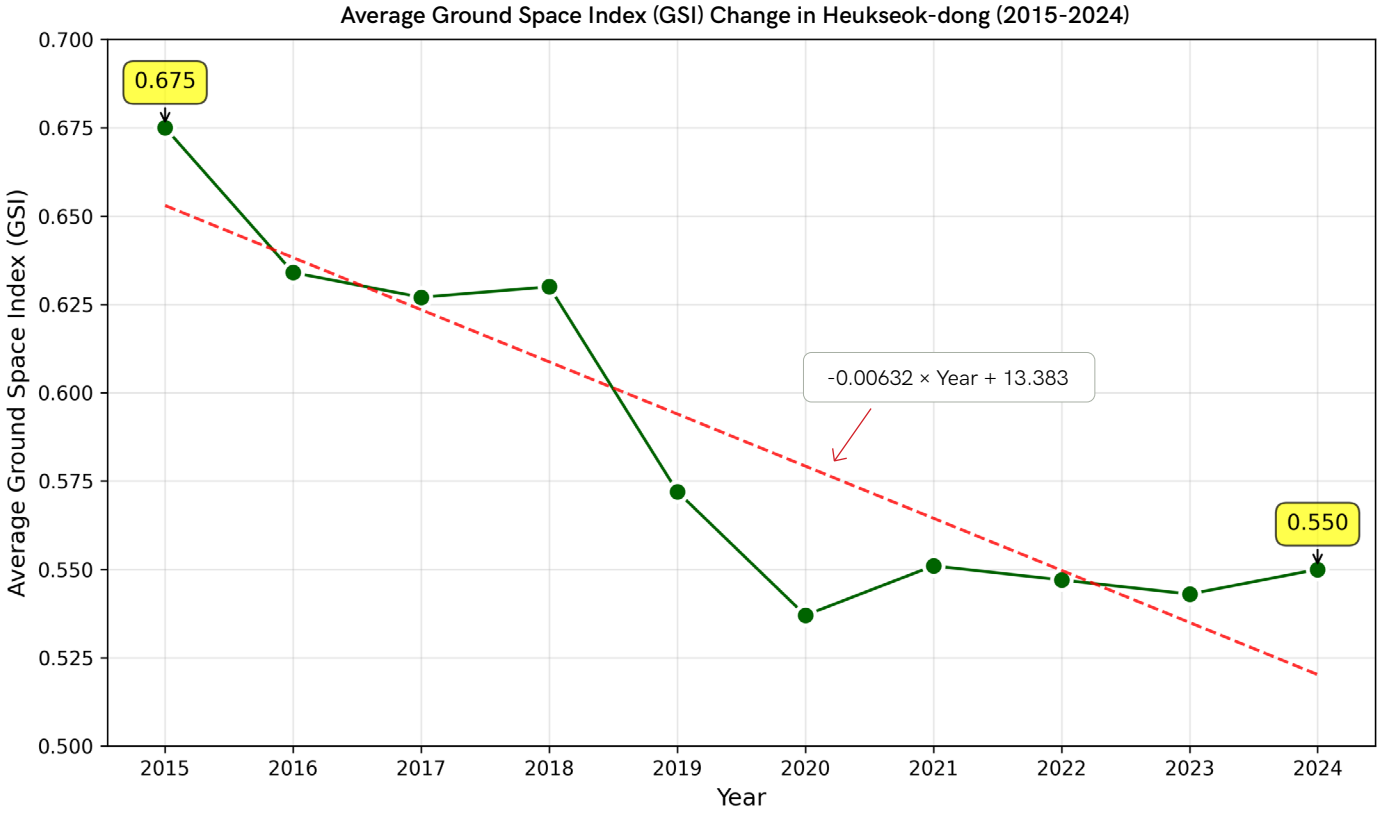
Average Ground Space Index (GSI) Change in Heukseok-dong (2015-2024)
Average Ground Space Index (GSI)
Year
0.675
0.550
-0.00632 × Year + 13.383
0.700
0.675
0.650
0.625
0.600
0.575
0.550
0.525
0.500
2015
2016
2017
2018
2019
2020
2021
2022
2023
2024

Appendix 5 10-Year Change in District 3

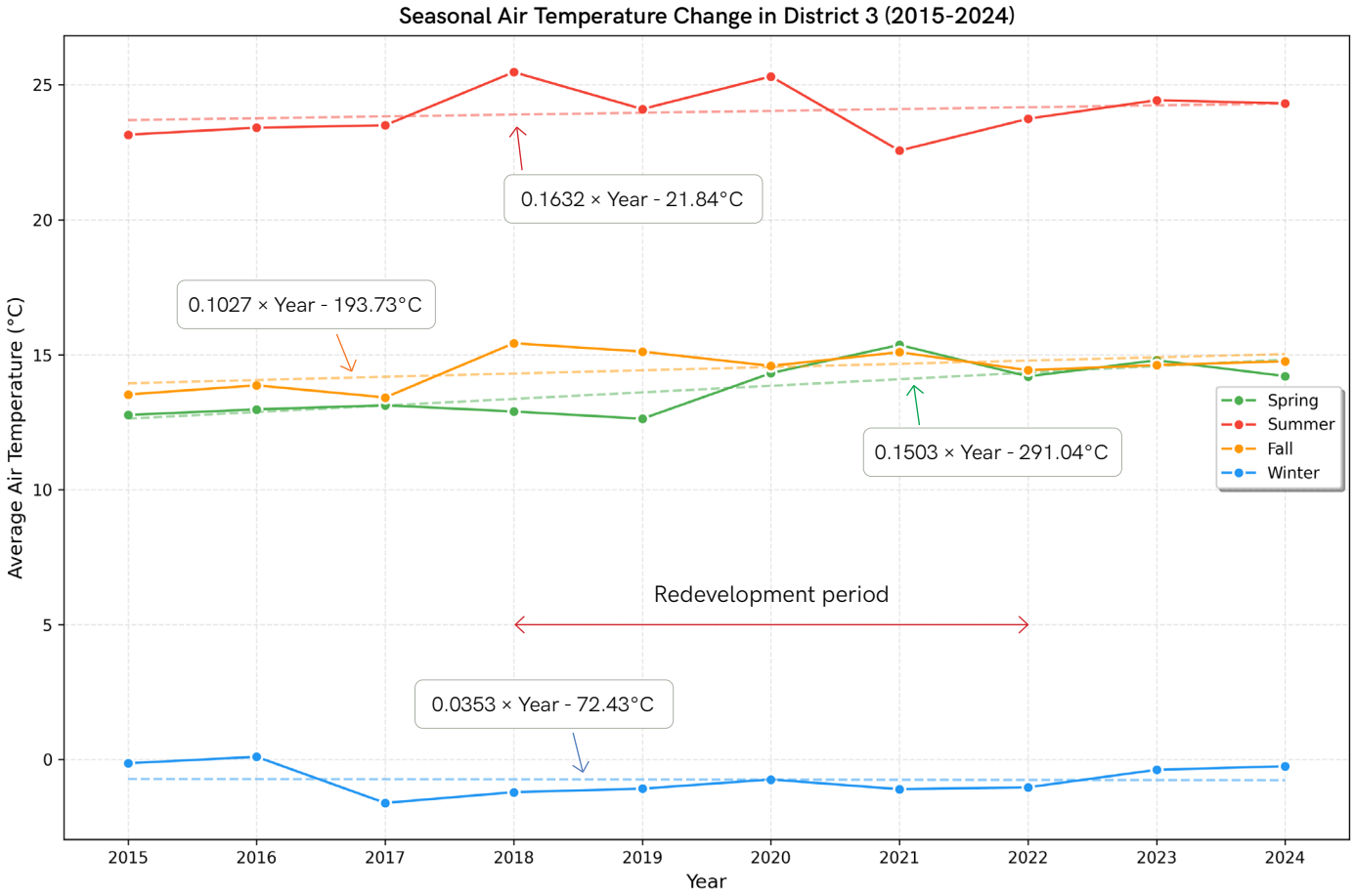

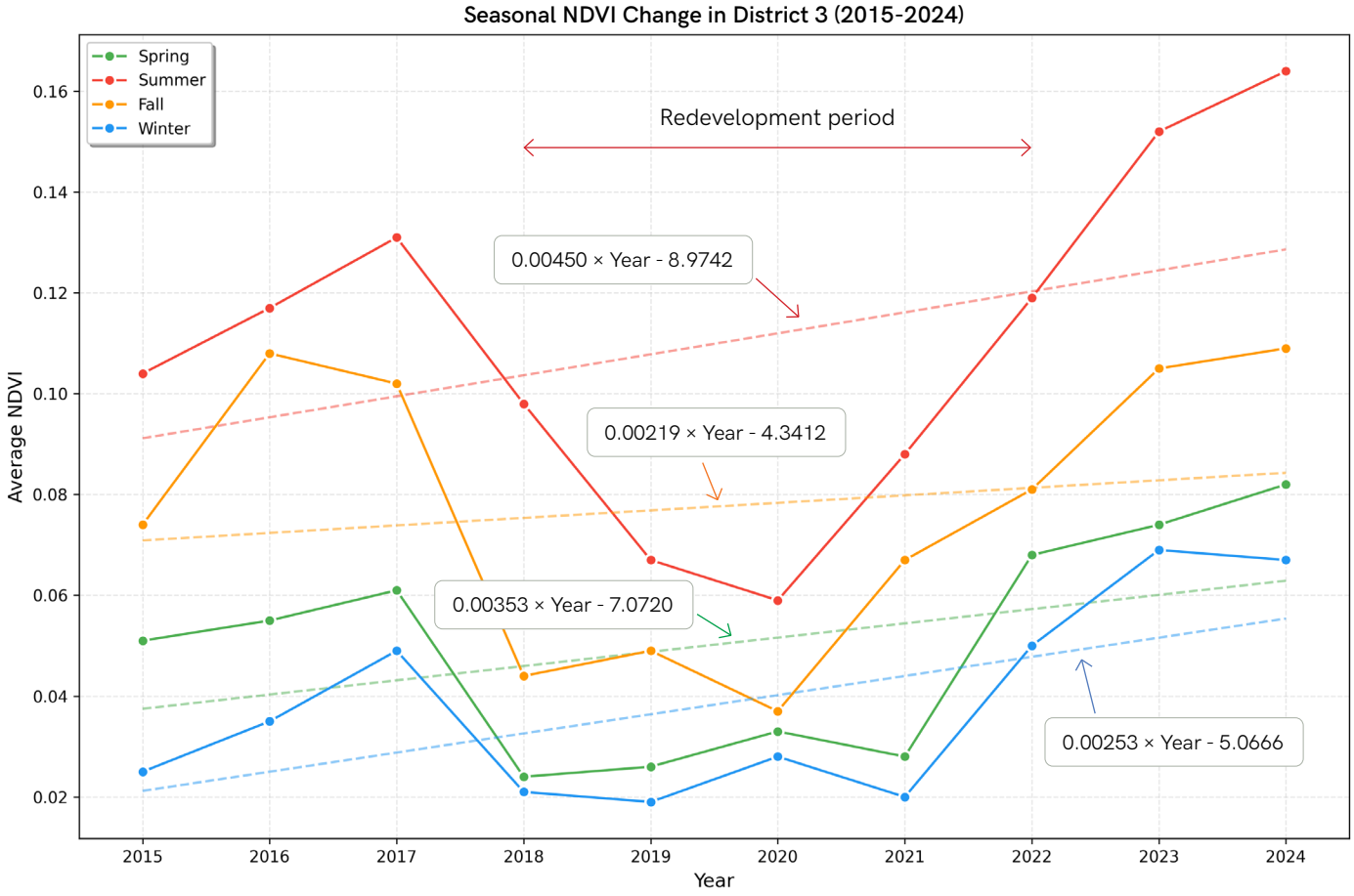

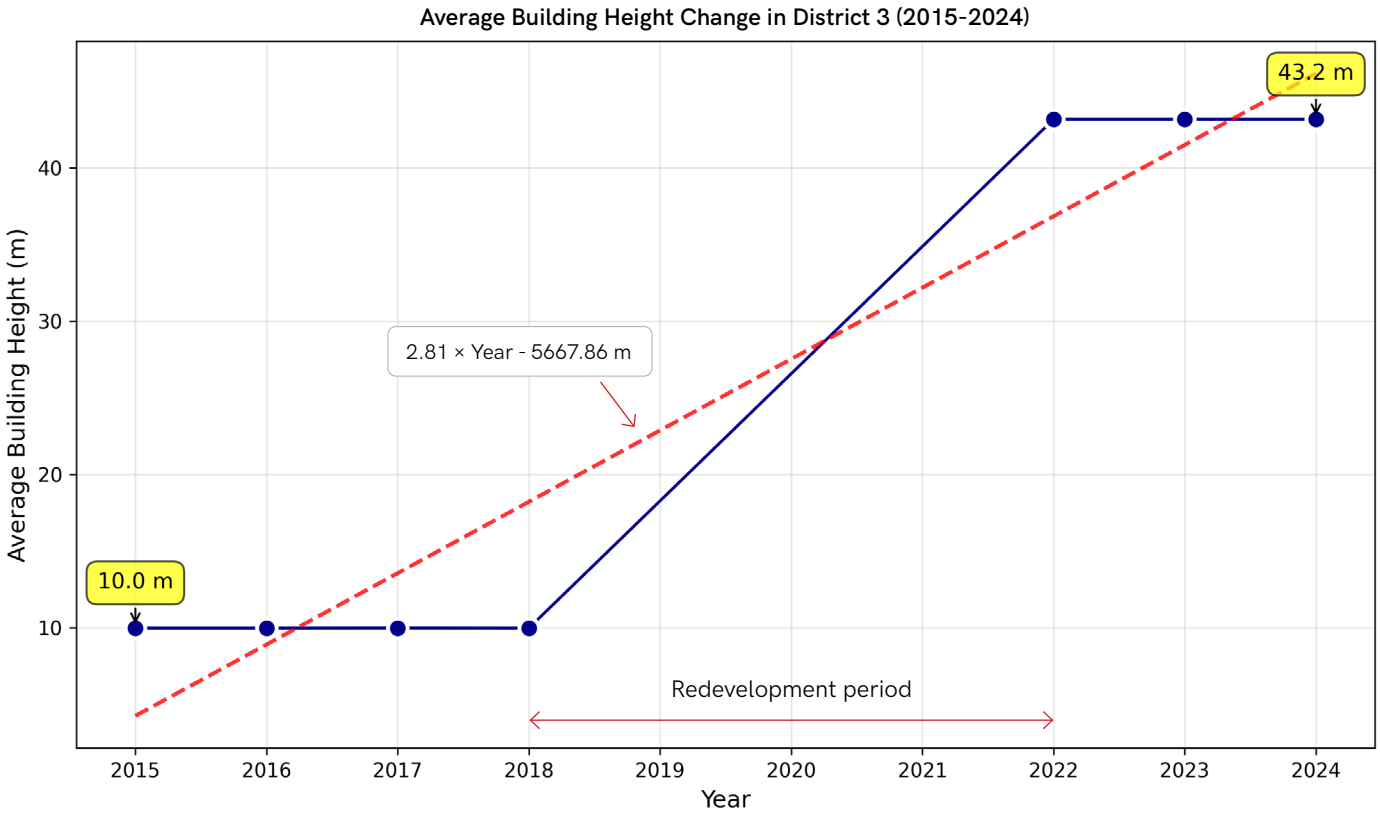
Average Building Height Change in District 3 (2015-2024)
Average Building Height (m)
Year
43.2 m
10.0 m
2.81 × Year - 5667.86 m
Redevelopment period
40
30
20
10
2015
2016
2017
2018
2019
2020
2021
2022
2023
2024

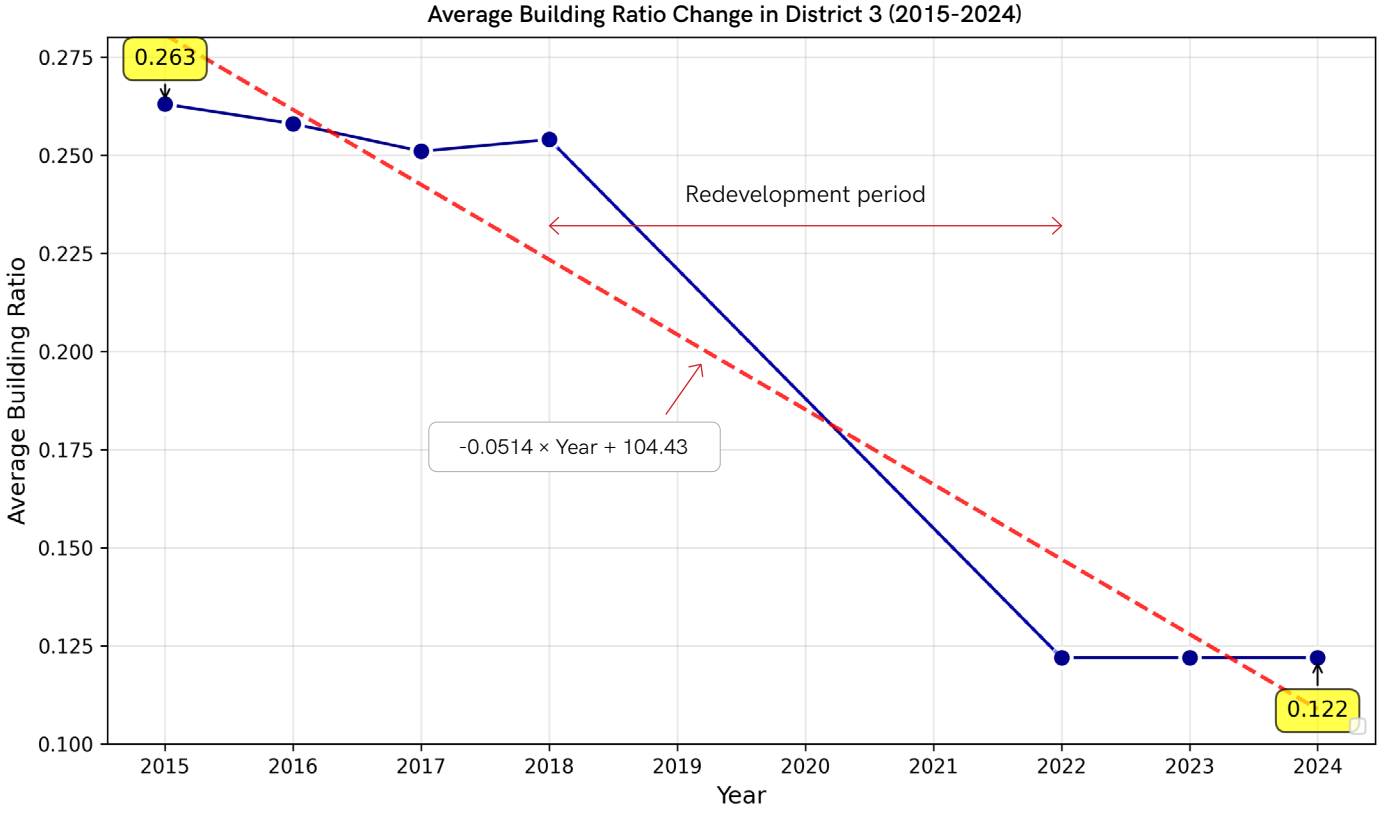
Average Building Ratio Change in District 3 (2015-2024)
Average Building Ratio
Year
0.263
0.122
Redevelopment period
-0.0514 × Year + 104.43
0.275
0.250
0.225
0.200
0.175
0.150
0.125
0.100
2015
2016
2017
2018
2019
2020
2021
2022
2023
2024

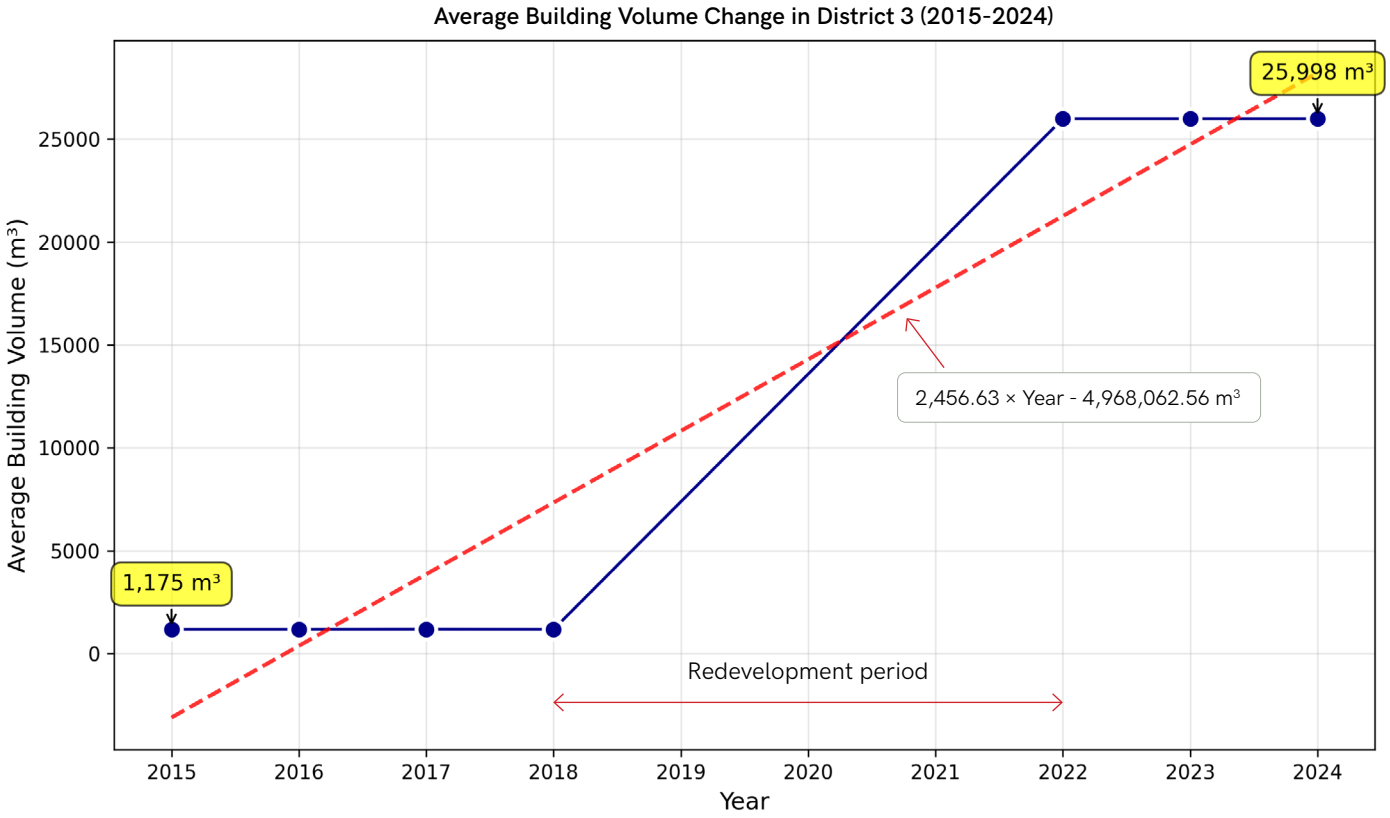
Average Building Volume Change in District 3 (2015-2024)
Average Building Volume (m³)
Year
25,998 m³
1,175 m³
2,456.63 × Year - 4,968,062.56 m³
Redevelopment period
0
5000
10000
15000
20000
25000
2015
2016
2017
2018
2019
2020
2021
2022
2023
2024

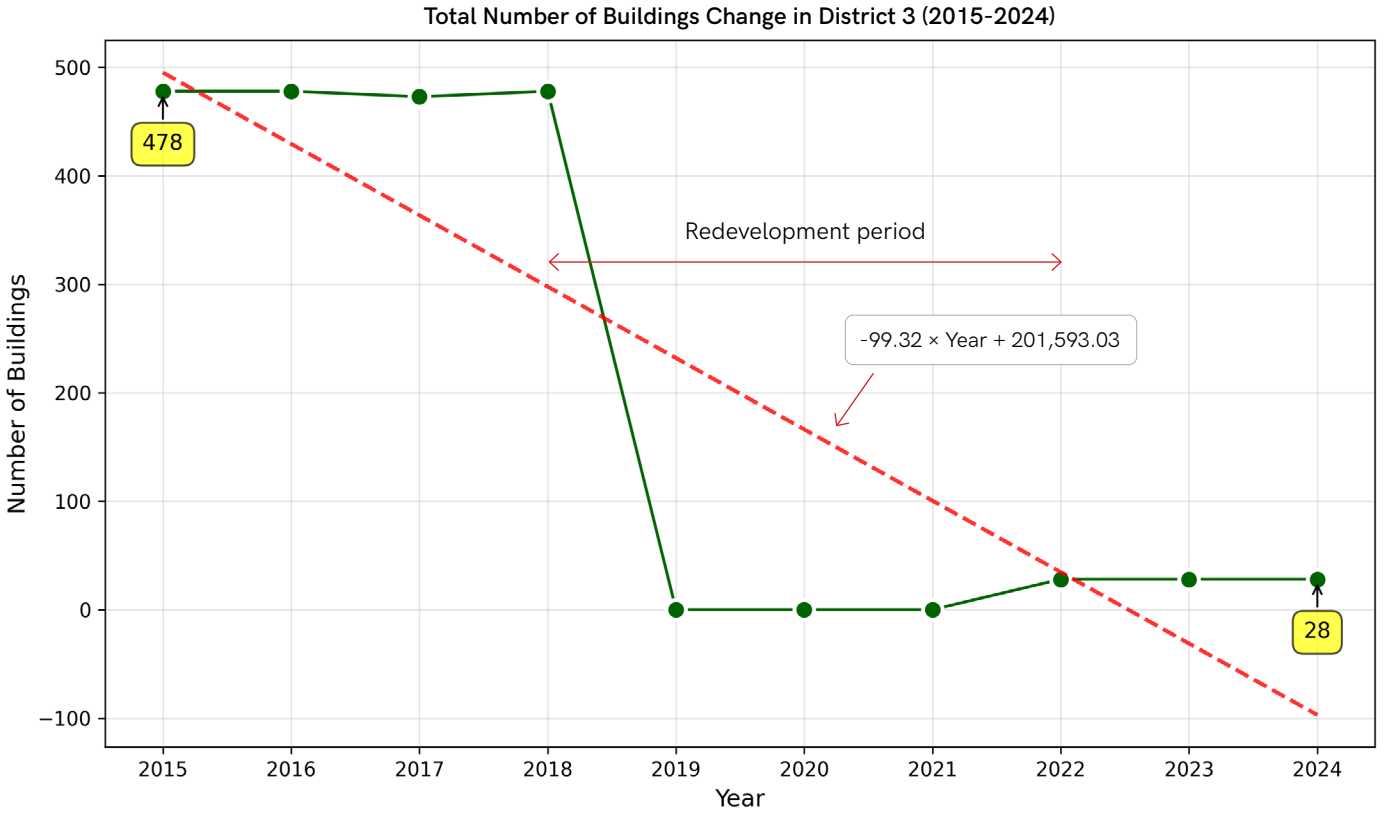
Total Number of Buildings Change in District 3 (2015-2024)
Number of Buildings
Year
478
28
Redevelopment period
-99.32 × Year + 201,593.03
−100
0
100
200
300
400
500
2015
2016
2017
2018
2019
2020
2021
2022
2023
2024

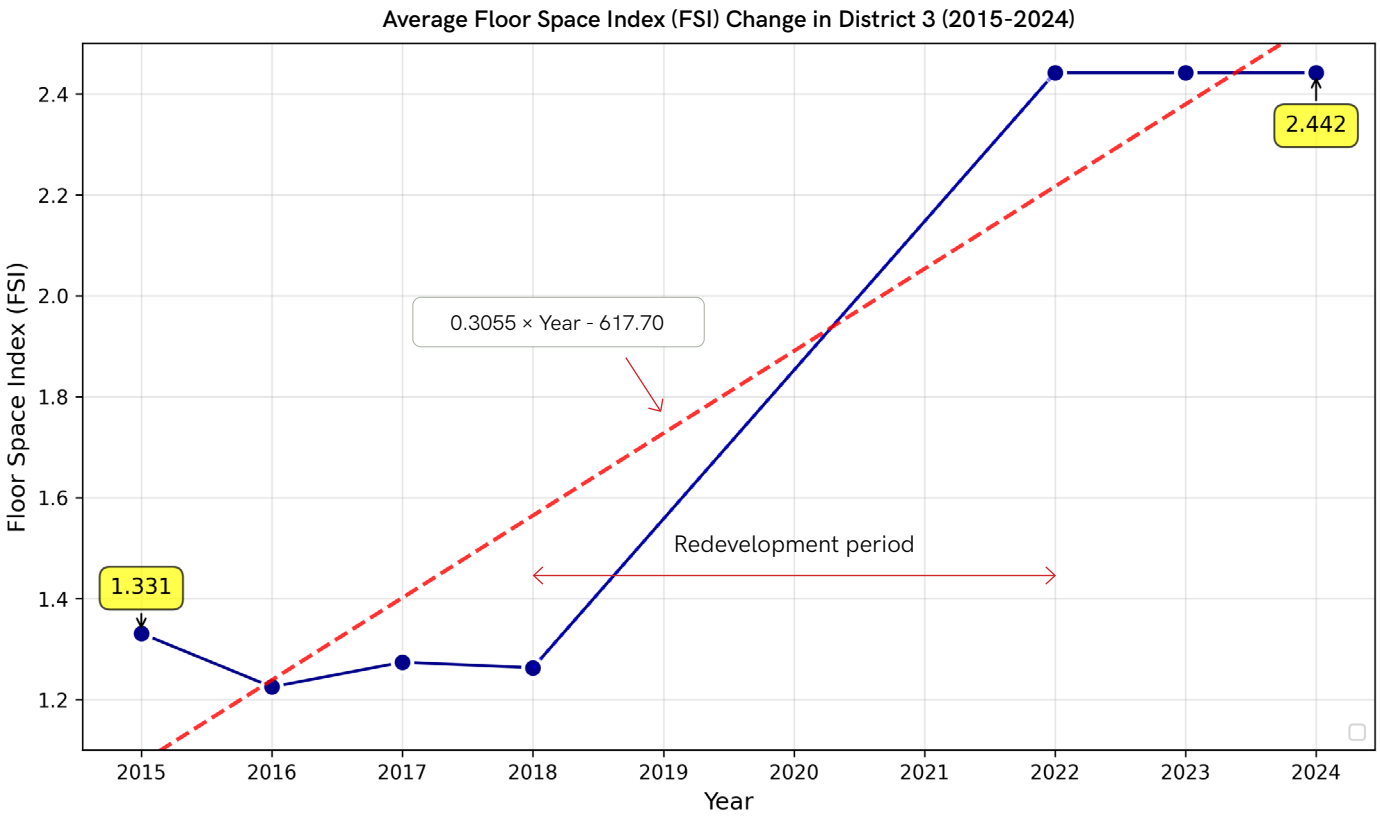
Average Floor Space Index (FSI) Change in District 3 (2015-2024)
Floor Space Index (FSI)
Year
0.3055 × Year - 617.70
Redevelopment period
1.331
2.442
2.4
2.2
2.0
1.8
1.6
1.4
1.2
2015
2016
2017
2018
2019
2020
2021
2022
2023
2024

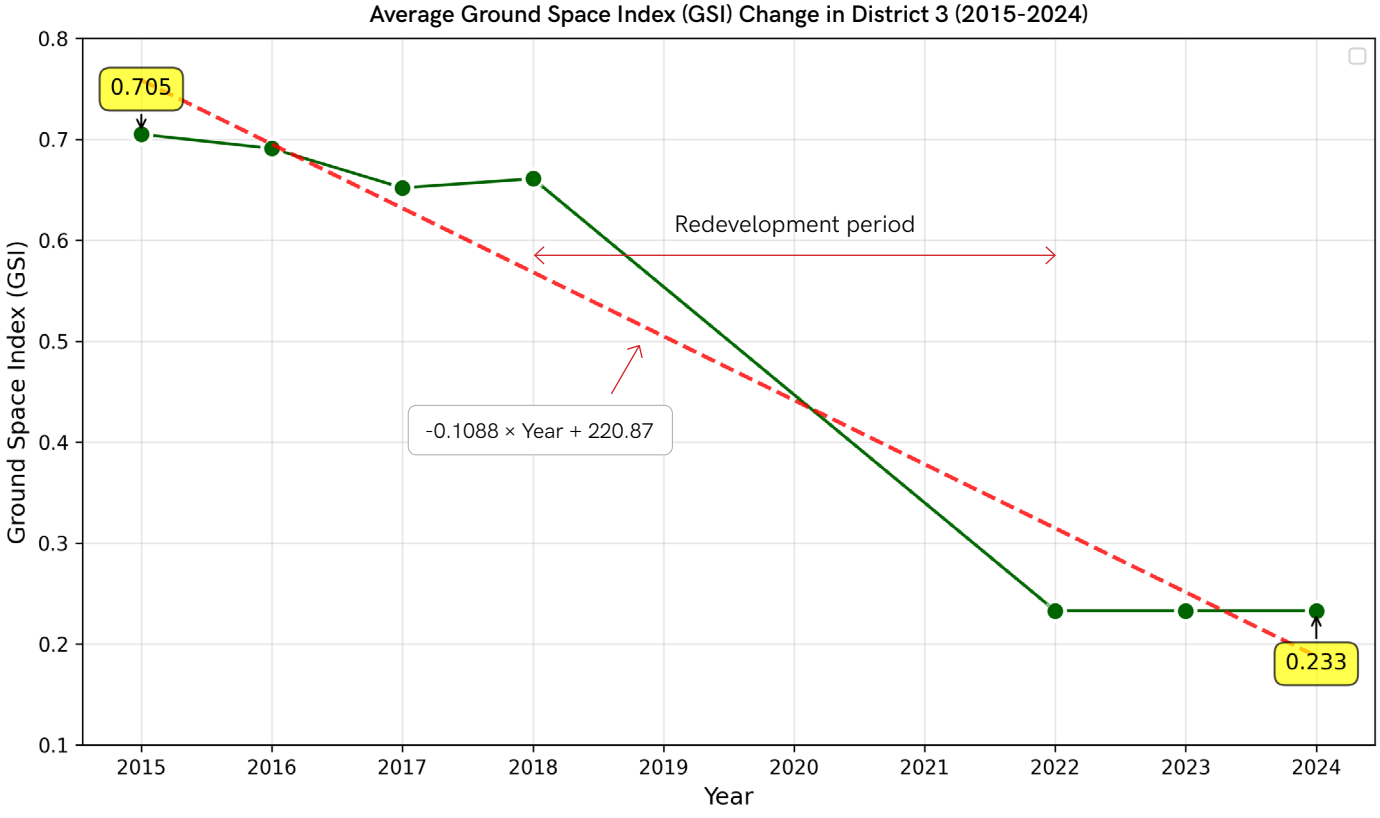
Average Ground Space Index (GSI) Change in District 3 (2015-2024)
Ground Space Index (GSI)
Year
0.705
Redevelopment period
-0.1088 × Year + 220.87
0.233
0.8
0.7
0.6
0.5
0.4
0.3
0.2
0.1
2015
2016
2017
2018
2019
2020
2021
2022
2023
2024